Dissertations (2009 -)   Dissertations, Theses, and Professional Projects

Analysis of the Detection of Organophosphate Pesticides in Aqueous Solutions Using Polymer-Coated SH-SAW Devices

Arnold Kweku Mensah-Brown
Marquette University

ANALYSIS OF THE DETECTION OF ORGANOPHOSPHATE PESTICIDES IN AQUEOUS SOLUTIONSUSING POLYMER-COATED SH-SAW DEVICES

by

ARNOLD K. MENSAH-BROWN, B.SC., M.S.

A Dissertation submitted to the Faculty of the Graduate School,
Marquette University,
in Partial Fulfillment of the Requirements for
the Degree of Doctor of Philosophy

Milwaukee, Wisconsin

December 2010

ABSTRACT
ANALYSIS OF THE DETECTION OF ORGANOPHOSPHATE
PESTICIDES IN AQUEOUS SOLUTIONS USING
POLYMER-COATED SH-SAW DEVICES

Arnold K. Mensah-Brown, B.Sc., M.S

Marquette University, 2010

Organophosphate pesticides (OPs) have been found as contaminants in surface and ground waters, soil, and agricultural products. Because OPs are toxic compounds, rapid detection/monitoring of OPs in groundwater is necessary to allow for real-time remediation. Detection of OPs in water has already been demonstrated using poly(epichlorohydrin) [PECH] and polyurethane as the sensing layers. However, the response times were relatively long, hindering real-time monitoring. In this work, a hybrid organic/inorganic chemically sensitive layer [bisphenol A-hexamethyltrisiloxane (BPA-HMTS)] that shows a high degree of partial selectivity for OPs is synthesized, characterized (in terms of the glass transition temperature, T_g, water stability, sensitivity, selectivity, detection limit, and absorption/response time) for the rapid detection of organophosphate pesticides. Direct chemical sensing in aqueous solutions is performed using guided shear horizontal surface acoustic wave sensor platforms on 36° rotated Y-cut LiTaO$_3$ and 42.75° rotated Y-cut Quartz, respectively. It is shown that, for the same coating thickness, a 60% reduction in sensor response time is achieved without reduction in sensitivity compared to PECH. Considering the T_g, for the polymers, it is seen that the faster response shown by BPA-HMTS is due to the porous siloxane backbone, HMTS. Kinetic studies for the absorption of OPs (parathion-methyl, parathion, and paraoxon) from aqueous solutions into the BPA-HMTS coating are conducted. The data are analyzed within the context of two absorption models: penetration-limited and diffusion-limited absorptions. It is shown that the absorption process is rate limited by penetration with a concentration independent absorption time constant or mass transfer coefficient. The absorption time constants for parathion-methyl, parathion, and paraoxon are calculated. A limit of detection of 60, 20 and 100 μg/L (ppb) for parathion-methyl, parathion, and paraoxon, respectively, is calculated for the present non-optimized sensor. Concentrations as low as 500 μg/L (ppb) parathion are actually measured. This is much lower than the typical concentrations found on agricultural produce ($\geq$ 10 ppm). Furthermore, sensor signal analysis in the form of the extended Kalman filter (EKF) is employed on-line during the detection process. The sensor response was first represented by a state-space model which includes all relevant contributions to the polymer-coated device response. This allows for the steady-state response and absorption time constant to be extracted on-line well before the steady-state is reached, thus further reducing the time for analyte identification and quantification. It is noted the absorption time constant, often unique to a class of analyte-coating pairs, can be used to improve analyte recognition.

ACKNOWLEDGMENTS

ARNOLD K. MENSAH-BROWN, B.SC., M.S

This is arguably the most challenging endeavor I have undertaken. It has not been easy and I know that it is by God's grace that I am what I am, and the grace that He has given me was not without effect. On the contrary, I have worked hard, although it was not really my own doing. This grace includes my faith, the opportunity to use my energy and talents to do this work, and the people He has put in my life to help me on my journey.

I would like to express my gratitude to my advisor and mentor, Dr. Fabien Josse; the countless hours of discussions, suggestions, and review of this dissertation helped me complete this work in a timely manner. I am also thankful to him for exposing me to the international sensor community and helping me develop my writing and presentation skills. I would also like to thank Dr. Edwin Yaz for sharing his expertise in control systems and estimation theory, which were a great help in developing the state-space models used in this work. My sincere gratitude also goes to my entire research committee: Dr. Yaz, Dr. Schneider, Dr. Cernosek, and Dr. Lee. Thank you for reviewing my work and making suggestions on how to improve this dissertation. I would also like to thank Dr. Henry Mensah-Brown for countless valuable discussions and introducing me to experimental design concepts. I also thank Dr. Michael Wenzel, a former fellow student and friend, for helpful discussions on signal processing and estimation theory.

In addition, I would like to thank my former and present fellow students (Michael Wenzel, Greg Novak, Ryan Kabacinski, Meetalee Dalal, Tao Cai, Jinjin Zhang, Russell Cox, Tian Newman, Michael McCarthy, and Ashley Milner) in the Microsensor Research Laboratory at Marquette University. Special thanks also to Dave Gibas, Ray Hamilton, and Tom Silman in the Discovery Learning Center at Marquette University, for their assistance in machining parts for this project and our lab. My sincere appreciation to Darlington Mlambo, a doctoral student in the Chemistry Department at Marquette University, for his help in synthesizing and characterizing the polymer used in this work and for sharing relevant references; your commitment and friendship was a source of moral support. I would also like to thank Dr. Hossenlopp for granting me access to her laboratory, without which the polymer used in this work could not have been synthesized. I would also like to thank Drs. Bender, Schneider, and Lee for helpful discussions.

Finally, I sincerely thank my parents, Henry and Christabel, for all their sacrifices, wisdom, patience, prayers, love, care, and encouragement over the years; my sisters, Shirley and Henrietta, as well as members of my extended family, especially Grandma Christina; my uncles, Dr. Sannichie Quaicoe and family, Mr. Papa Yorke and family, Dr. Ernest Hinson and family, and Mr. Ato Coleman and family, for their support and giving me a home away from home; and many of my friends for your prayers, patience, love and support. Special thanks to Melissa Lemke for proofing initial chapters of this dissertation, helpful discussions, prayers, patience, love, listening, encouragement, and sharing in my humanity.

Prayer for Generosity

"Lord, teach me to be generous.

Teach me to serve you as you deserve;

To give and not to count the cost,

To fight and not to heed the wounds,

To toil and not to seek for rest,

To labor and not to ask for reward,

Save that of knowing that I do your will."

-ST. IGNATIUS OF LOYOLA

FOUNDER OF THE SOCIETY OF JESUS

TABLE OF CONTENTS

LIST OF TABLES

LIST OF FIGURES

1 INTRODUCTION

1.1 The Pesticide Problem

The US Environmental Protection Agency (EPA) defines the term pesticide as any substance or mixture of substances intended for preventing, destroying, repelling, or mitigating any pest [1]. The Food and Agriculture Organization of the United Nations (FAO) defines the term pesticide as any substance or mixture of substances intended for preventing, destroying or controlling any pest, including vectors of human or animal disease, unwanted species of plants or animals causing harm during or otherwise interfering with the production, processing, storage, transport or marketing of food, agricultural commodities, wood and wood products or animal feedstuffs, or substances which may be administered to animals for the control of insects, arachnids or other pests in or on their bodies [2]. The term includes substances intended for use as a plant growth regulator, defoliant, desiccant or agent for thinning fruit or preventing the premature fall of fruit, and substances applied to crops either before or after harvest to protect the commodity from deterioration during storage and transport [2]. From these definitions, it is clear that the term "pesticide" not only refers to insecticides, but it also applies to herbicides, fungicides, and various other substances used to control pests.

Pesticides are widely used in our environments (e.g., agriculture, homes, gardens, and veterinary medicine) to control pests. While their application is beneficial, there are serious risks, to both human health and the environmental, associated with their use. The next subsections will give a brief review of pesticides and discuss why there is growing public health concern regarding pesticide exposure.

1.1.1 History

The use of pesticides began in the nineteenth century when sulfur compounds were developed as fungicides [3]. During the late nineteenth century, arsenic compounds were introduced to control insects that attacked fruit and vegetable crops; for example, lead arsenate was used widely on apples and grapes [3]. Even though these compounds are very toxic, they were used extensively until the 1940s when chlorinated hydrocarbon pesticides or organochlorines, most notably dichlorodiphenyltrichloroethane (DDT), were introduced. This class of pesticides was considered safer than arsenic-based pesticides because they had little or no immediate toxicity [3-5].

After World War II, the US began using synthetic pesticides extensively. This was due in part to the fact that many of the ingredients used in today's pesticides were created as chemical weapons for war (e.g., nerve gases tabun, sarin, and soman) [3;6]. The widespread use of these pesticides in agriculture over the last five decades contributed to increased crop production in many parts of the world [3;7]. Furthermore, in the late 1940s, chemicals such as DDT were sprayed in urban communities in an effort to eradicate the female anopheles mosquitoes, fire ants, gypsy moths, and other harmful insects. To some degree, the health benefits were realized.

However, in 1962, Rachel Carson published a book, *Silent Spring*, that exposed the hazards associated with the use of synthetic pesticides and drew public attention to environmental issues that had never been addressed before [3;5;7]. Carson's work showed, for example, that DDT caused reproductive failure in eagles and ospreys, species that had accumulated large doses of DDT because of their position high in the food chain. As a result, in 1972 and 1985 the EPA in the US and Ghana, respectively, banned the use

of DDT. However, in 2006 the World Health Organization (WHO) recommended the re-introduction of DDT to prevent malaria in developing countries. Consequently, it is currently being used in some developing nations to prevent malaria and other tropical diseases by spraying on interior walls to kill or repel mosquitoes [8].

In recent times, the principal classes of insecticides in use in the United States and in most industrialized countries are the organophosphates, carbamates, and pyrethroids [5]. Ethyl parathion or parathion (for short) was the first organophosphate to be marketed commercially [9]. It was formulated in 1946 as a broad-spectrum, nonsystemic insecticide and is now approved for nine crops: alfalfa, barley, corn, cotton, canola, sorghum, soybean, sunflower, and wheat. In the environment, it breaks down to its more potent form, paraoxon. Other organophosphates that are frequently used include phosmet (apples, fruit crops, and vines), methyl parathion (almonds, cabbage, onions, rice, and sweet potatoes), and chlorpyrifos (orchards, row crops, and residential pesticides).

1.1.2 Classification

There are six major classes of pesticides [10]. The first group consists of organic phosphates that are known as organophosphate pesticides (OPs). OPs are the focus of this work as they are known to affect the nervous system by disrupting the enzyme that regulates the neurotransmitter acetylcholine. Most organophosphates are insecticides, and their toxicological effects on insects are similar to their effects on humans. This has been exploited to develop weapons of mass destruction (used in World War II as nerve agents and most recently in the Tokyo subway attack in 1995) [3;11]. They include diazinon, parathion, methyl parathion, and phosmet [10;12]. The second group is the carbamates. They also affect the nervous system by disrupting the enzyme that regulates

acetylcholine. Carbaryl, carbofuran, and methomyl are examples of carbamates [3;10;13]. The third group consists of chlorinated hydrocarbons or organochlorines. These pesticides generally persist in the environment for long periods of time. They include DDT, chlordane, and heptachlor [3;11]. The fourth group is the pyrethroid. These pesticides were developed as a synthetic version of the naturally occurring pesticide pyrethrin, which is found in chrysanthemums. They have been modified to increase their stability in the environment [11]. Allethrin and fenvalerate are examples of pyrethroid [10]. The last two groups are metal and organometal pesticides e.g., tributyl tin (TBT), dimethylarsinic acid, and arsenic [10;14].

1.1.3   Environmental and Health Effects of Pesticides

Among the class of pesticides, organophosphate pesticides (OPs) such as parathion and malathion are the most widely used chemical pesticides in the US and throughout the world [15]. According to the US EPA, over 1,100 million pounds of pesticides are produced each year [16;17] and are approved for use in various sectors including residential and urban settings [5;18-20] with the agro-industry being the number one consumer [3]. The widespread use of OPs is due to their high insecticidal activity and perceived rapid degradation in the environment [10;21-23]. However, recent research shows that these pesticides persist variably under different environmental conditions [10;24].

Pesticides play a vital role in controlling agricultural, industrial, home/garden, and public health pests. As a result, goods and services can be supplied at reasonable cost and high quality. However, the economic benefits from pesticide use cannot be achieved without associated risk to the environment and human health. This is due to the fact that

pesticides are toxic chemicals and move from their target sites as a result of pesticide spray drift, erosion, and contaminated soils particles being blown by winds [3;25]. OPs are toxic because they act as inhibitors of acetylcholinesterase, an enzyme that catalyzes the hydrolysis of the neurotransmitter acetylcholine [26]. The inhibition of this enzyme disrupts the transmission of nerve impulses [24]. As mentioned earlier, pesticides move to non target sites, and the amount of pesticides that migrates from the intended application site depends on several factors including its chemical properties (i.e., water solubility, vapor pressure, ability to bind to soil and plant tissue), the weather, soil properties, type of plant tissues on which they are adsorbed, and the way they are applied.

In the agricultural sector, OPs (solid granules or liquids) are often dissolved in organic solvents and applied to fields by hand-sprayers, motorized blowers and dusters, and by aircraft [10]. When pesticide solutions are sprayed, the nozzles on the equipments produce droplets. Some of these droplets are very small. Therefore, they remain suspended in air and are carried by air currents to other locations, potentially contaminating areas beyond the intended application sites. Furthermore, pesticides may threaten nearby wildlife when they are applied to crops by escaping into the atmosphere and being blown by winds to nearby areas. In certain situations, atomized or volatized pesticide can be blown to areas where they adhere poorly to surfaces (e.g. soil, plant tissue, and ground).

The presence of pesticides in the soil is a source of soil pollution since they negatively affect soil conservation by destroying organisms such as earthworms. In turn, this reduces the soil quality and decreases the amount of organic matter (e.g., earthworm casts) in the soil, which also decreases the ability of the soil to retain water.

Consequently, rain and other water can easily carry pesticide particles to off-target sites. This is known as runoff. Runoffs in agricultural regions enter water sources (groundwater and surface water) by seeping through the soil and leaching [25]. Pesticides may also enter water sources through spray drift, spillage (accidental or intentional), and soil erosion. The polluted water then enter aquifers, source of drinking water in many communities [3;27]. Once OPs enter water, they pose potential risk to human health and aquatic environment.

In the aquatic environment, the exposure of organisms to OPs affects the balance of aquatic ecosystems. Adverse health effects from OPs that may occur in drinking water include acute effects (caused by exposure to high concentrations during short times) and chronic effects (caused by exposure to low concentrations over many years) [28]. The primary effects of OP acute exposure are on the parasympathetic, sympathetic, and central nervous systems, with symptoms including fatigue, muscle cramps, and diarrhea [29]. Chronic effects are usually neuropsychological, including poor concentration and suicidal thoughts [7;29;30]. Most recently, exposure to OPs has also been linked to asthma [15].

Groundwater is an important natural resource. It constitutes about 4% of the total hydrologic cycle and is often used as drinking water. In many countries, groundwater is a substantial strategic resource in the public water supply (50% in the US, 35% in England, and 70% in the Netherlands) [3;25].Therefore, it is critical that groundwater aquifers are managed to meet drinking water standards, which are set by the "Safe Drinking Water Act" and mandates the EPA to set Maximum Contamination Levels (MCLs) for a number of pesticides including alachlor (2 ppb) and atrazine (3 ppb) [31]. WHO and

European Union (EU) maximum residue level (MRL) of pesticides is 10 ppm for most

foods and 0.1 ppb for drinking water [10]. It is noted that these levels were determined

using laboratory analytical instruments and agricultural produce typically have high

residue levels (>10 ppm) of OPs [10;32;33].

Managing aquifers to meet drinking water standards is a major challenge because

it is difficult to monitor the movement of groundwater and there is a significant time

difference between emissions and detection of chemical residues [3]. Furthermore, it is

very expensive to treat contaminated aquifers; as a result, the best approach for protecting

ground water is to control contamination at its source. The major problem policy makers

face is establishing the relationship between on-site emissions and groundwater

contaminant concentrations [3]. One possible solution is to develop an inexpensive, real-

time, portable, reusable, and robust monitoring systems or sensors for the in-situ

detection and classification of harmful OPs in water, which is the purpose of this work.

One approach is the development of chemical sensors. In the next section, a brief review

of chemical sensors including their characteristic, configuration, and platforms is

presented.

1.2 Overview of Chemical Sensors

A chemical sensor is a device that converts a chemical stimulus produced by the

presence of a chemical analyte or chemical reaction into an electrical signal. This output

signal is used for identification and quantification of the chemical analytes in gaseous and

liquid states. A typical chemical sensor system consists of a recognition element (often a

coating that is specific to certain chemicals or reactions), a transduction element, and a

readout technology for continuous monitoring of chemical concentrations. The sensing

process is illustrated in Fig. 1.1. First, the analyte interacts with the coating, changing its

mechanical, electrical, and/or optical properties. This in turn changes one or more

characteristics of the sensor platform. Finally, a readout technology (electronics and

measuring circuitry) is used to measure and convert the chemical perturbation into an

electrical signal.

Various sensor technology platforms can be used to probe the changes induced by

the interaction of analyte molecules with the recognition element. These include resistive

devices, capacitive devices, optical devices, micro-cantilever devices, and acoustic wave

devices. As a result, chemical sensors are often classified based on the sensor platform.

Regardless of the sensor platform, the performance of chemical sensors is characterized

by the following main parameters:

- Sensitivity (S): Change in the measurement signal per concentration unit of the

    analyte [34;35], i.e. the slope of the calibration graph . It is the product of the

    sensitivity of the recognition element (coating) to the analyte and the sensitivity of

    the transducer to changes in its operating characteristic. The former depends on

    the physicochemical interaction of the analyte and coating and the sorption

    capacity of the coating and the latter by the design and performance characteristic

    of the sensor platform [34].

- Time constant (τ_s): Time it takes for the sensor response to reach 63% of its final

    value when exposed to a step change in concentration.

- Sensor response time (t_{90}): Time it takes the sensor signal to reach 90% of its final

    value when exposed to a step change in concentration [35]. This value depends on

    the rates of sorption and the nature of analyte-coating interactions. It is noted that

the sensor response time and time constant are related and is given by the expression $t_{90} = 2.3(\tau_s)$. This assumes exponential behavior of the response mechanism.

- Detection limit or limit of detection (LOD): Smallest concentration of an analyte a chemical sensor can reliably detect. "Reliably" is often taken to mean that the signal measured is no smaller than three times the root-mean-square noise level [36].

- Dynamic range: Concentration range between the detection limit and the upper limiting concentration [35].

- Selectivity: Degree to which the sensor can distinguish target analytes from non-target analytes [37]. This depends on the ability of the coating to recognize the size, shape, or dipolar properties of the analytes [38].

- Linearity: Relative deviation of an experimentally determined calibration from an ideal straight line. Usually values for linearity are specified for a definite concentration range [35].

- Stability: Ability of a sensor to maintain its performance for a certain period of time. As a measure of stability, drift values are used, e.g. the signal variation for zero concentration [35].
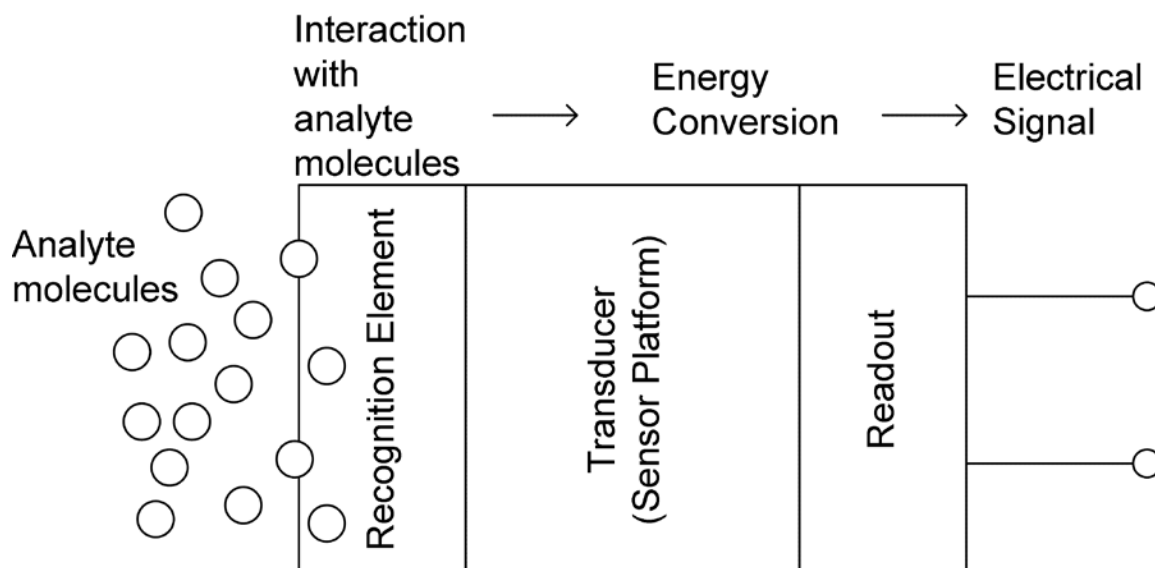
Figure 1.1: Transduction process of a typical sensor system.

For a given sensor platform, the coating is arguably the most important element in the sensor system because it significantly affects the overall sensor performance (i.e., sensitivity, selectivity and response time of the chemical sensor to a class of analytes). As mentioned earlier, there are various sensor technology platforms that can be used to implement chemical sensors. These include resistive devices, capacitive devices, optical devices, micro-cantilevers, electrochemical devices, and acoustic wave devices. In the next section, a brief overview of acoustic wave sensor physics, materials, and sensor types is presented. Emphasis is placed on the guided shear-horizontal surface acoustic wave device since that is the sensor platform used in this dissertation.

1.3   Acoustic Wave Devices as Chemical Sensors

Acoustic wave (AW) devices are devices on which a mechanical or acoustic wave (and hence the name) can be generated. These devices are typically fabricated on piezoelectric crystals and employ the piezoelectric effect to generate the acoustic waves [39;40]. Here, an oscillating voltage is applied at an input electrode to create an electric field and a mechanical wave that propagates through the crystal (in the bulk and on the surface) and is then converted back to an electrical field at an output electrode for measurement. For sensing applications, the characteristics (i.e. velocity and/or amplitude) of the wave of the propagating wave are monitored by measuring the frequency and/or phase and insertion loss of the device. Any perturbation of the wave changes its velocity and/or amplitude, which can be correlated to the source of the perturbation (i.e., the stimulus).

AW devices have been commercially available for over 60 years and have found wide applications in communications [39;41]. In recent times, AW devices have also been used for sensor applications [36;39]. From the class of sensor platforms previously mentioned, AW devices hold the greatest potential for implementing field deployable sensors because of their performance and economic characteristics (i.e., sensitivity, speed of response, dynamic range, ruggedness, miniature dimensions, low cost, and manufacturability and compatibility with IC fabrication technologies) [34;39]. Furthermore, some AW devices can be wirelessly interrogated [42-44],thus indicating the possibility of remotely collecting the sensor data. An AW device is used in the present work as the sensing platform.

As mentioned earlier, AW devices are fabricated on piezoelectric materials. The most common piezoelectric substrate materials used as acoustic wave sensor platforms are lithium niobate ($LiNbO_3$), lithium tantalate ($LiTaO_3$), and quartz (SiO_2). Each crystal has advantages and disadvantages, including temperature dependence, propagation velocity, attenuation, and cost. Table 1.1 shows some of the common design parameters for these crystals. In general, a given crystal with a particular cut is chosen depending on the intended application. For example, in an application where various gases are being detected and temperature variation has to be minimized, the ST X quartz supporting a surface acoustic wave would be a suitable candidate as a sensor platform because it has temperature coefficient of zero near 25 °C.

Table 1-1: Commonly used shear horizontal surface acoustic wave (SH-SAW) piezoelectric materials

Material	Orientation	Velocity: Metal surface (m/s)	Temperature Coefficient (ppm/°C)	Cost
42.75° YX-Quartz (ST-90° X Quartz)	42.75° rotated, Y-cut, X-propagating	4960	~ 0 near 25 °C	Lowest
LST-Quartz	15° rotated, Y-cut, X-propagating	4990	~ 0 near 25 °C	Lowest
36° YX-LiTaO$_3$	36° rotated, Y-cut, X-propagating	4112	~ -32	Medium
64°/41° YX-LiNbO$_3$	64°/41° rotated, Y-cut, X-propagating	4478/4379	~ -81/-80	High

AW devices are differentiated by their velocities and displacement directions. There are three main modes of particle displacement: (1) longitudinal, when particle displacement is in the same direction as the direction of propagation of the wave; (2) shear-horizontal, when particle displacement is parallel to the device surface and normal to the direction of propagation; and (3) shear-vertical, when particle displacement is normal to the device surface and perpendicular to the direction of propagation. Furthermore, the wave may propagate through or on the surface of the substrate. In the latter case, the wave is known as a surface wave and devices with this type of propagation are called surface-acoustic wave (SAW) devices. They include the Rayleigh SAW (longitudinal and shear-vertical particle displacement) and the shear-horizontal surface acoustic wave (SH-SAW) device (shear-horizontal particle displacement). When the wave propagates through the substrate, the wave is called a bulk wave and devices with this type of propagation are called bulk acoustic wave (BAW) devices. Examples of such devices include the thickness-shear mode (TSM) resonator (shear-horizontal), the acoustic plate mode (APM) device (shear-horizontal, shear vertical or longitudinal), and film bulk acoustic resonator (FBAR) (shear mode or longitudinal).

Only a few of these devices can operate efficiently in liquid because they have no shear-vertical component of displacement to radiate longitudinal waves into the liquid, and hence they dissipate a negligible amount of acoustic energy into the liquid. These devices include TSM, SH-SAW, FBAR, and SH-APM (see Table 1-2). In general, the sensitivity of an AW device is proportional to the amount of energy that is in the

propagation path that is being perturbed [39] and the operating frequency [45]. As a result, surface wave devices are more sensitive than bulk wave devices. As shown in Table 1.2, the SH-SAW device holds the most potential for the development of very sensitive (bio)chemical sensor for direct liquid-phase sensing because of the surface nature of the wave and its high operational frequency. In this work, the SH-SAW device fabricated on quartz and lithium tantalate substrates (see Table 1-1) are investigated for the development of a chemical sensor for *in-situ* detection and monitoring of organophosphate pesticides. A brief review of SH-SAW sensors is given in the next section.

Table 1-2: Comparison of acoustic sensors [10;36;39;41;46;46;47;47-49]

Sensor Device	Sensitivity	Factors Determining Sensitivity	Operation in Viscous Liquid	Operating Frequency (Fundamental)	**D**elay-line or **R**esonator Configuration
TSM	Low (0.014)	Operating frequency, Acoustic energy	Yes	Low (5-20 MHz)	Resonator
SH-APM	Low-Med	Operating frequency, Acoustic energy	Yes	Med-High (25-200 MHz)	Delay-line
SAW	High	Operating frequency, Acoustic energy	No	High (0.03-3 GHz)	Both
SH-SAW	High	Operating frequency, Acoustic energy	Yes	High (0.03-3 GHz)	Both
FBAR	High	Operating frequency, Acoustic energy	Yes	High (0.1-10 GHz)	Resonator

1.4   Shear Horizontal Surface Acoustic Wave (SH-SAW) Sensor Platforms

The shear Horizontal Surface Acoustic Wave (SH-SAW) is a surface wave and is structurally similar to a Rayleigh SAW. It is obtained by rotating the cut of the piezoelectric substrate appropriately so that the wave propagation mode changes from shear vertical SAW to SH-SAW [36;39]. Unlike the Raleigh SAW, SH-SAWs often

propagate slightly deeper within the substrate (in some cases, referred to as surface skimming bulk waves)[50-52]. Hence the uncoated SH-SAW device is less sensitive to surface perturbations than a Rayleigh SAW device. The device sensitivity to surface perturbation can be increased by depositing a thin guiding layer on the device surface. The effect of the overlayer is to trap the acoustic energy near the sensing surface [50-52], thus increasing the sensitivity to surface perturbations. The resulting acoustic wave is analogous to a Love wave on an isotropic substrate with an overlayer [51]. The amount of acoustic energy that is trapped increases with the thickness up to an optimum value. Therefore, device sensitivity increases as the wave displacement amplitude increases at the surface i.e., as the film thickness is increased [53;53;54]. In the present work, the guiding layer is a polymer material that also acts as the chemically sensitive layer. It is noted that waveguiding occurs when the shear wave velocity of the overlayer is less than the shear wave velocity of the piezoelectric substrate.

The SH-SAW devices used in this work are fabricated in a dual delay-line configuration with the input and output interdigital transducers (IDTs) fabricated on the crystal surface, or sensing surface. Figure 1.2 shows the geometry for the excitation of the SH-SAW by the IDTs. The transducers have a length of L and consist of N split finger pairs having a periodicity d. The transducer width is in the y-direction and the crystal axis is rotated with respect to this axis. On this geometry, a shear horizontal SAW is generated when an alternating voltage is applied between two adjacent electrodes. This wave propagates from the input IDTs to the output IDTs with a velocity, v, determined by the crystal material and crystal cut. The center frequency is given by $f_o = v / \lambda$, where λ is the SH-SAW wavelength determined by the transducer periodicity d (center-to-center

distance between two adjacent electrodes of one comb of the IDT [36]). The length of the

delay-line and acoustic path length are denoted by l_s and l_T, respectively. The theory and

sensing principles are discussed in more detail in Chapter 2.
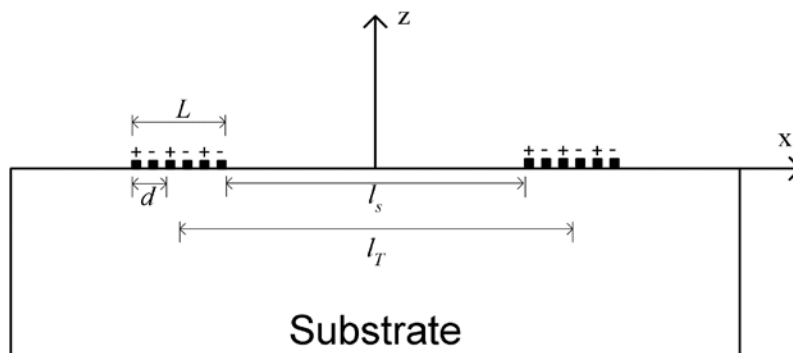
Figure 1.2: Transducer orientation for excitation of SH-SAW. It is noted that the cut is Y-rotated with respect to the crystal axis.

1.5   Applications of Acoustic Wave Chemical Sensors

Acoustic wave-based chemical sensors have numerous applications. Specifically,

SAW devices are ideal candidates for applications requiring miniaturized and portable

trace chemical detection capabilities because they are extremely sensitive gravimetric

detectors and can be implemented using semiconductor microfabrication techniques. As a

result, compact, light, robust, and power-efficient modules can be mass produced, leading

to reduced cost. Due to its high mass sensitivity, the SAW device can be coated with a

film to detect chemical species of interest. Using SAW devices as the transducer, sensor

systems have been developed that can detect trace (ppm to ppb) levels of airborne

analytes such as hydrogen (H), sulfur dioxide (SO_2), hydrogen sulfide (H_2S), and

dimethyl methylphosphonate (DMMP) [55-59]. These devices can be employed for various applications including:

- environmental monitoring/remediation (including pesticides)

- counterterrorism (including airport security)

- nonproliferation (including chemical and biological weapons detection)

- *in-situ* industrial process monitoring and control

- personal health and safety

- vehicle pollution monitoring

- study of thin-film properties

One of the chemicals receiving much interest recently are pesticides [10;26;60-62].

1.6 Microsensor Arrays

For most of the applications described in Section 1.5, the response of the chemical sensor is not specific for particular analytes and consequently methods are needed to improve selectivity. One approach to solve this problem, proposed by Zaromb and Stetter in 1984, is to use an array of chemical sensors for a particular application [63]. In this strategy, identical sensor platforms having different partially selective coatings are used to study multicomponent samples (mixtures). Here, the response of the entire sensor array to known chemical analytes (supervised learning) or to an unknown complex mixtures (unsupervised configuration) forms a pattern, like a fingerprint. Provided these coatings are chosen to offer as many orthogonal[1] or nearly orthogonal measurements as possible,

---

[1] Orthogonal measurements are independent, complementary measurements which increase the ability of a sensor to correctly identify a particular analyte. Orthogonal measurements are critical for providing

the patterns can be analyzed using various chemometric (pattern recognition) techniques [65-68] including principal component and cluster analysis, for analyte identification, quantification, and classification.

The first step in designing and developing a chemical sensor array is to appropriately select the coating materials. There are several approaches for selecting materials for a sensor array, and they can be categorized into three main groups: (1) diversity in structures and properties, (2) unsupervised learning methods that explore experimental or simulated sensor array data, and (3) methods that evaluate the success of various arrays in performing classification or quantification tasks [69]. Most often, several approaches are used in any given study where subsets of multiple coatings are selected for an array. The initial selection approach used in this work is based on the work of Grate et al. [70] and Abraham et al. [71-73]. Here, they use linear solvation energy relationships (LSERs) to estimate polymer/vapor partition coefficient. This approach requires the LSER coefficient for a given polymer and solvation parameters for given vapor species. It is noted that the solvation parameters for OPs in water is not available in the literature [72]. However, based on their work, it is known that polymers exhibiting strong hydrogen bond acidity e.g., fluoropolyol (FPOL) and hexafluoro-2-propanol-substituted polysiloxanes (SXFA), are desired in an array for detecting basic vapors such as organophosphorus compounds [69;71;73-76]. Most of these coatings are not available commercially at affordable prices and more importantly, have not been characterized for liquid environments. Therefore, the final selection of any coating for the

---

accurate identification of a sample. An orthogonal measurement is the quantification of a property unrelated to other measurements performed. The ability to measure numerous properties of a sample increases the probability of accurate identification since many different samples have some properties in common but none have all properties in common [64].

development of an integrated SAW array for the detection and quantification of OPs in water will require testing and characterization of the coating.

Furthermore, for the purpose of continuous monitoring of organophosphorus compounds in ground and surface waters, it is necessary to select or design polymers that are stable in water and rapidly sorb organophosphorus compounds reversibly, without hysteresis. It has been established that rapid sensor responses are promoted by polymers with glass transition temperatures below the temperature of operation for the sensor [57;74;77]. Polysiloxanes are porous and exhibit low glass transition temperatures (T_g). However, commercially available polysiloxanes lack the strong hydrogen-bond acidic functional groups that are desirable for the detection of organophosphates with high sensitivity.

1.7   Sensor Signal Processing

After designing the sensor array appropriately, the response of the chemical sensor has to be processed for analyte identification and quantification. In general, the steady-state (equilibrium) sensor response for chemical sensors is used as the key parameter to identify and quantify chemical analytes. Typically, this steady-state feature is either the difference measurement, the relative difference, the fractional change, and the log relative difference [78]. The major drawback with using the steady-state feature for identification and quantification is that one has to wait for the sensor response to reach equilibrium. This approach is especially problematic for liquid-phase sensing where the sensor response times are relatively long, and in some cases, are on the order of hours [60;79]. Clearly, waiting for the steady-state feature can make it difficult to implement real-time

sensing of harmful levels of contaminants present in surface and ground waters. To overcome this problem, a derivative technique based on the initial response has been used to decrease the time required for analyte classification and quantification [60;80]. The initial derivative correlates well with analyte concentration. However, this parameter can be greatly influenced by, for example, flow effects, i.e. how quickly the sensor is exposed to the sample [78]. Moreover, the derivative of a signal is inherently noisy and therefore this approach has a high probability of error in classifying and quantifying chemical analytes. As a result, finding a new approach to decrease the time required for analyte classification and quantification is needed.

1.8   Problem Statement and Objective of Research

The presence of pesticides in the environment continues to be of great concern to public health and the environment. As mentioned earlier, from the six major classes of pesticides, the agricultural industry has increasingly relied upon organophosphate pesticides (OPs) to control pests because of their perceived rapid degradation in the environment [10]. However, recent research shows that OPs persist in the environment for relatively long periods [10]; as a result, their residues have been found in ground waters, soil, and agricultural products. In order to ensure the quality and safety of water supply, early detection of contaminants including pesticides is necessary.

Current methods for monitoring contaminants, such as OPs, include gas/liquid chromatography and mass spectroscopy [60]. Although these methods are very accurate, they often require samples to be taken to laboratories for analysis, are extremely time

consuming, and expensive. Moreover, vital information can be lost during sample collection, transportation, and storage. Therefore, there is a need to develop *in-situ* monitoring systems for rapid analysis and characterization of samples. To make these possible, various bio(chemical) sensor technologies including acoustic wave devices are being investigated to implement real-time sensing [54;60].

The key science and technology issues for these chemical monitoring systems include: sensitivity, selectivity, sensor response time, and reproducibility. It is desired that the sensors exhibit high sensitivity so that the detection of trace amounts of the chemical analyte is possible and that they possess a high degree of partial selectivity so that the sensors can distinguish interfering substances from target species and be reusable. In addition, the sensors should have short response times for rapid analyte identification and quantification, and high reproducibility to minimize rates of false alarms. Poor selectivity and reproducibility as well as the presence of interferents, sensor aging, and drift due to environmental influences can all result in a low probability of detection and a high false alarm rate. Each one of these issues limits the current applicability of chemical sensors [78].

The objective of this work is to develop a chemical sensor that will allow for rapid on-line monitoring of organophosphorus compounds in contaminated ground and waste water. The approach being used by Josse's team at Marquette University to address this challenge is the development of smart sensor systems. This approach requires the development and modeling of novel and sensitive sensor platforms, the development of sensitive and selective coatings for various chemical analytes, and the development of new signal processing and pattern recognition techniques specifically focused on

chemical sensors to improve the detection time, probability of detection, and to reduce false alarm rates [78].

The work in this dissertation focuses on integrating all aspects of the above approach with particular emphasis on the synthesis and characterization of a hybrid organic/inorganic chemically sensitive layer for rapid detection and analysis of organophosphate pesticides in aqueous solutions using SH-SAW devices. SH-SAW devices on 36° YX-LiTaO$_3$ with center frequency of 103 MHz and 42.75° YX-Quartz (ST-90° X Quartz) with center frequency of 155 MHz are used to determine the optimum operating conditions for achieving rapid sensor responses with high sensitivity. This work involves characterizing the coating (i.e., preparation techniques, water stability, aging, density, and glass transition temperature), analyzing the effect of coating thickness on sensor response time or rate of analyte absorption, and studying the effect of solution pH on analyte properties in aqueous solution. The individual sensors are characterized by evaluating sensor properties of interest including reproducibility, sensitivity, selectivity, and other relevant sensor parameters, which leads to an understanding of the sensor response and allows one to design an optimum chemical sensor. An accurate physics-based model of the sensor response is presented. This model takes into account added mass and viscoelastic changes, utilizes state space techniques, and enables nonlinear estimation theory (in the form of the Extended Kalman Filter (EKF)) to be used to extract transient information online to improve analyte recognition (i.e., selectivity) and reduce the time required for analyte identification and quantification.

1.9   Dissertation Organization

This dissertation is comprised of six chapters. Chapter 1 reviews the history of pesticide usage and discusses the problems (health and environmental hazards) associated with their widespread use. Significant emphasis is placed on the contamination of ground and surface waters by pesticides. Chapter 1 also introduces chemical sensors, with a focus on acoustic wave-based chemical microsensor arrays and sensor signal processing, as tool to meet the need for online monitoring of organophosphate pesticides in water. The main goals of this dissertation are introduced, namely, to synthesize and investigate a hybrid organic/inorganic chemically sensitive layer for rapid detection and analysis of organophosphate pesticides in aqueous solutions using SH-SAW devices and to use online sensor signal processing based on nonlinear estimation theory during the detection process to further reduce the time required for analyte identification and quantification. In Chapter 2, the theory of the guided SH-SAW liquid sensor is reviewed. Perturbation theory in conjunction with the acoustic impedance technique is reviewed and used to analyze the three-layer geometry in liquid phase sensing before and after the perturbation. The device design and sensing principles are also presented. Chapter 3 presents the chemistry associated with analyte-coating interaction and describes the two types of absorption processes: absorption rate limited by penetration (rate limited by the surface resistance) and absorption rate limited by diffusion. Furthermore, the design of sensor coatings for organophosphate pesticides is discussed. Chapter 4 contains a brief description of the experimental methods including coating synthesis and characterization, analyte characterization, and device characterization. In addition, the experimental setup is illustrated and the measurement procedures are described. Results and discussion of

this dissertation are presented in Chapter 5. The device and analyte characterization are presented followed with typical sensor responses for different analytes and different devices. Individual sensors are compared by evaluating sensor properties of interest including reproducibility, sensitivity, selectivity, and sensor response time. A detailed analysis of the sorption kinetics of organophosphate pesticides into a hybrid organic/inorganic coating in aqueous solution is presented. Here, the effect of coating thickness on the absorption process is evaluated. A test for statistical significance is performed. Considering relevant contributions to the sensor response, namely mass loading and viscoelastic properties of coating, state-space formulation is used to model the sensor response. The nonlinear estimation-based sensor signal processing technique is introduced. How the technique can be used to obtain online estimates of the steady-state response and transient parameters and thus reduce the time required for analyte identification and quantification is demonstrated. Finally, Chapter 6 provides a synopsis of the results from this work followed by proposals for possible extensions of this work.

2 GUIDED SH-SAW DEVICE AS A LIQUID-PHASE SENSOR PLATFORM: A REVIEW

2.1 Introduction

The guided SH-SAW sensor consists of a piezoelectric crystal ($LiTaO_3$) supporting a shear horizontal surface acoustic wave (SH-SAW), a polymer coating acting as both the waveguiding material and chemically sensitive layer, and a liquid layer for transporting of the analytes. In order to model and interpret the response of the sensor to an analyte, it is necessary to understand the characteristics of the perturbed wave. This requires one to examine each layer of the multilayer sensor configuration separately before considering the system as a whole.

In this chapter, the theoretical analysis of the sensor platform is reviewed, with the aim of providing a basis for evaluating the various contributions to the sensor response. These contributions include mass loading and viscoelastic loading. Furthermore, the sensing mechanism and changes in device characteristics are related to physical changes is described in detail.

2.2   Formulation of the Sensor Problem

For the bio(chemical) SH-SAW liquid-phase sensor, a coating/polymer (isotropic viscoelastic dielectric material) is deposited on the piezoelectric substrate. In biosensor applications, the coating acts as a waveguide and is used to bind a thin bioreceptor layer [45;81;82]. In chemical sensors, the coating acts as a waveguide and/or chemically sensitive layer. It is the piezoelectric substrate, the coating, and the liquid layer that form the sensor. Any perturbation (mechanical and/or electrical) at the coating surface and/or within the coating changes the characteristics of the propagating acoustic wave, resulting in sensing. The SH-SAW liquid sensor can be modeled as a multilayered structure [83]. The structure used in this investigation is shown in Figure 2.1. In this figure, the three-layer structure consists of the piezoelectric substrate, a polymer layer of finite thickness, h, having a lower shear wave velocity than the substrate, and a liquid layer for transport of target species. The polymer layer acts as both the waveguide and the chemically sensitive layer. The guided SH-SAW is assumed to propagate in the x_1 direction, x_3 is normal to the sensing surface, and x_2 is in the direction of the acoustic wave particle displacement (or the aperture of the IDTs).

The next step is to review the solutions for the acoustic field and electric field, in each layer using the acoustic wave equations, Maxwell's equations (under the quasistatic approximation [84;85]), and the appropriate boundary conditions at each interface. The following assumptions are made in finding the solutions [86]:

1. The liquid layer is assumed to be a Newtonian fluid because the solutions under test are very dilute aqueous solutions i.e., in the range of low mg/L (ppm) to μg/L (ppb).

2. The liquid layer and substrate are assumed semi-infinite media (thickness $\rightarrow \infty$).

3. The polymer has a finite thickness, h.

4. Metallization of the propagation path is assumed to eliminate acousto-electric interaction in the sensing region. As such, perturbation of the wave will be due only to mechanical loading.
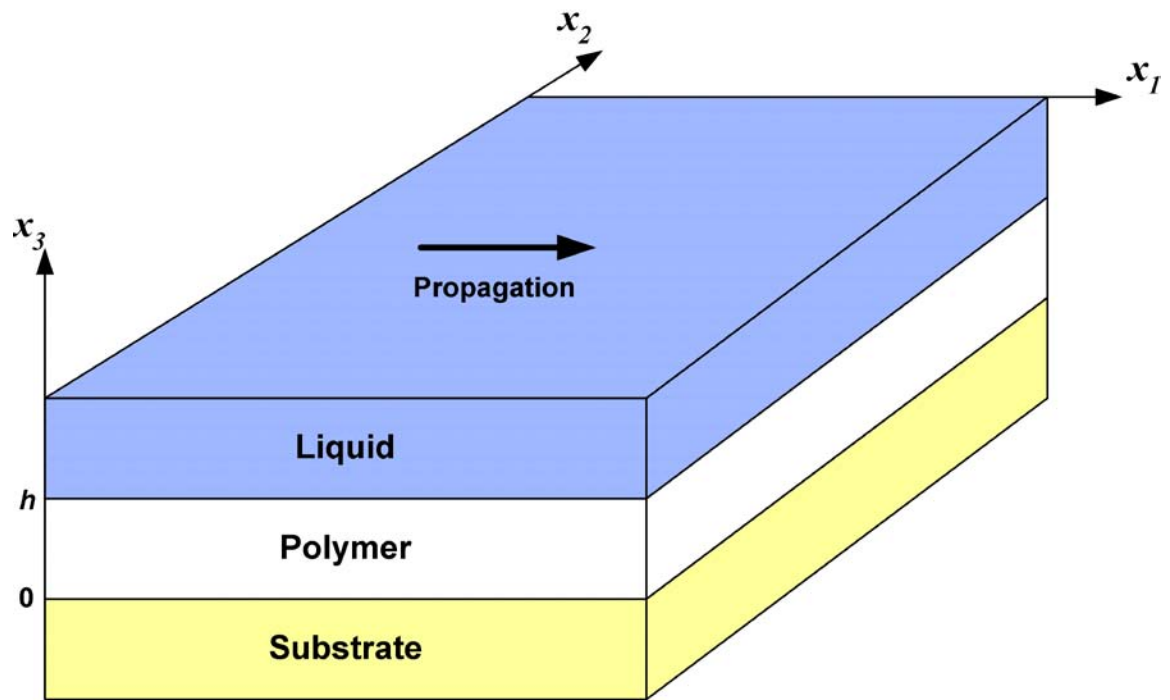
Figure 2.1: Multilayer structure and coordinate system.

2.3 Fundamentals of Acoustic Waves

In general, for any piezoelectric material, the equations describing the coupled acoustic waves and electric fields under the quasistatic approximation are given by [83;87]

$$\rho \ddot{u}_i = T_{ij,j} \qquad i,j = 1, 2, 3 \tag{2.1a}$$

$$D_{m,m} = 0 \qquad m = 1, 2, 3 \tag{2.1b}$$

where u_i = the acoustic displacement in the x_i direction,

T_{ij} = the acoustic stress tensor,

D_m = the electric displacement in the x_m direction,

ρ = the density of the crystal, and

i, j, k = the spatial directions.

In all the equations, a subscript proceeded by a comma denotes a partial derivative with respect to the spatial coordinates and a dot above a variable indicates the derivative with respect to time.

The piezoelectric constitutive relation i.e., the stress tensor and electric displacement are defined by [83;86]

$$T_{ij} = C_{ijkl}S_{kl} - e_{nij}E_n \tag{2.2a}$$

$$D_m = e_{mkl}S_{kl} + \varepsilon_{mn}E_n \qquad i, j, k, m, n = 1, 2, 3 \tag{2.2b}$$

where C_{ijkl} = the elastic stiffness tensor for a constant electric field,

e_{nij} = the piezoelectric constant tensor,

ε_{mn} = the dielectric permittivity tensor for constant mechanical strain,

S_{kl} = the strain tensor (dimensionless), and

E_n = the electric field in the x_n direction.

It is noted that the elastic constants are symmetric i.e., $C_{ijkl} = C_{jikl} = C_{ijlk} = C_{jilk}$. The strain tensor, which describes the local stretching of the solid, and the electric field are related to the mechanical displacement and the electric potential (ϕ), respectively, as [83]

$$S_{kl} = \frac{1}{2}\left(u_{k,l} + u_{l,k}\right) \tag{2.3a}$$

$$E_n = -\phi_{,n}. \tag{2.3b}$$

Substituting Eqs. (2.3) into (2.2) and the resulting Eqs. into (2.1) yields the set of differential equations that govern acoustic wave propagation in a piezoelectric medium. These equations are known as the Christoffel wave equations and are given by [83]

$$C_{ijkl}u_{k,li} + e_{nij}\phi_{,ki} = \rho \ddot{u}_j \tag{2.4a}$$

$$e_{mkl}u_{k,il} - \varepsilon_{mn}\phi_{,ik} = 0. \tag{2.4b}$$

The above notation can be simplified using the Voigt indices (I and J) defined as [83;86]

$$I = \begin{cases} i & \text{if } i = j \\ 9-(i+j) & \text{if } i \neq j \end{cases} \quad \text{and} \quad J = \begin{cases} k & \text{if } k = l \\ 9-(k+l) & \text{if } k \neq l \end{cases}.$$

where $i, j, k, l = 1, 2, 3$ and $I, J = 1, 2, \ldots, 6$.

Therefore, Eqs. (2.4) can be rewritten as

$$T_I = C_{IJ} S_J - e_{nI} E_n \tag{2.5a}$$

$$D_m = e_{mJ} S_J - \varepsilon_{mn} E_n . \tag{2.5b}$$

In the above derivation, it is assumed that the crystallographic coordinate system coincides with the AW coordinate system i.e., geometric axes. If the two do not coincide, Euler transformation can be used to rotate the elastic, piezoelectric, and permittivity tensors from the crystalline axes to the geometric axes constants [84].

In analyzing acoustic wave propagation in piezoelectric sensors, two methods (numerical analysis and perturbation theory) are commonly used. The next two sections will discuss these techniques.

2.4 Numerical Analysis

This method yields numerical solutions to the Christoffel wave equations. The wave solutions in a piezoelectric crystal are assumed to be a linear combination of the partials waves given by [83;84]

$$u_i^c = \alpha_i e^{jk_3 x_3} e^{jk_1(1+j\gamma)x_1} e^{-j\omega t}, \qquad i = 1, 2, 3 \tag{2.6a}$$

$$\phi^c = \alpha_4 e^{jk_3 x_3} e^{jk_1(1+j\gamma)x_1} e^{-j\omega t} \tag{2.6b}$$

where u_i = the acoustic particle displacement in the ith direction,

     ϕ = the electric potential,

     k_1, k_3 = the components of the wave number k in the x_1 and x_3 directions,

         respectively,

ω = the angular frequency ($\omega = v_p k_1$, v_p is the phase velocity),

α_i = the amplitudes (i = 1, 2, 3, 4), and

γ = the exponential decay/attenuation constant.

Note that the superscript 'c' represents the piezoelectric crystal and there is no variation in the x_2 direction because the acoustic aperture of the IDT is assumed to be infinite in this direction.

Substituting the partial waves (2.6) into the Christoffel wave equations gives the following matrix equation [83]

$$\begin{bmatrix} A_{11} & A_{12} & A_{13} & A_{14} \\ A_{21} & A_{22} & A_{23} & A_{24} \\ A_{31} & A_{32} & A_{33} & A_{34} \\ A_{41} & A_{42} & A_{43} & A_{44} \end{bmatrix} \begin{bmatrix} \alpha_1 \\ \alpha_2 \\ \alpha_3 \\ \alpha_4 \end{bmatrix} = [A][\alpha] = 0. \tag{2.7}$$

[A] is a symmetric matrix whose elements are a function of the density of the crystal, the phase velocity, the elastic constants, piezoelectric constant, and dielectric constant. The elements of the 3 x 3 sub-matrix in the upper left corner are associated with the elastic constants and intercouple the mechanical displacement; A_{44} is a purely elastic constant; and the remaining elements are associated with the piezoelectric properties of the solid and couple the electric potential to the mechanical displacements, i.e., α_4, α_1, α_2, and α_3 [84]. Given that a wave exists in the piezoelectric crystal, only the nontrivial solution will satisfy Eq 2.7. In order to have nontrivial solutions, the determinant of [A] must go to zero, i.e.,

$$\det[A] = 0 \tag{2.8}$$

Equation (2.8) yields an 8th order algebraic equation in terms of the normalized transverse wave number ($b = k_3/k_1$) [83] in the form

$$\sum_{n=0}^{8} B_n b^n = 0,$$ (2.9)

where B_n is a complex function of v_p, γ, and the material constants. Equation (2.9) has eight roots and each one corresponds to a partial wave which satisfies the equation of motion in the piezoelectric crystal. These roots are either purely real or complex conjugate pairs. For surface wave solutions, where the piezoelectric crystal is assumed to be semi-infinite, only the fours roots lying within the lower half of the complex plane that lead to partial waves that decay with depth are valid [84]. The explicit behaviour of these roots as a function of v_p and γ is presented in detail in [83].

The general [A] matrix in Eq. (2.7) can take several forms and this has been discussed in [83]. For an SH-SAW device, the matrix [A] has the form

$$[A] = \begin{bmatrix} A_{11} & 0 & A_{13} & 0 \\ 0 & A_{22} & 0 & A_{24} \\ A_{31} & 0 & A_{33} & 0 \\ 0 & A_{42} & 0 & A_{44} \end{bmatrix}.$$

If

$$[A_1] = \begin{bmatrix} A_{11} & A_{13} \\ A_{31} & A_{33} \end{bmatrix} \quad \text{and} \quad [A_2] = \begin{bmatrix} A_{22} & A_{24} \\ A_{42} & A_{44} \end{bmatrix},$$

then det [A] is given by

$$\det[A] = \det[A_1] \times \det[A_2] = 0.$$

In this case, there are two possible wave solutions. The first one is given by

det $[A_1] = 0$. This solution corresponds to an electrically decoupled AW with particle

displacement in the x_1 and x_2 directions. The second solution is given by det $[A_2] = 0$.

This is an electrically coupled AW with the particle displacement in the shear horizontal

(x_2) direction. Hence, the final solution involves only the particle displacement (u_2) and

the electric potential (ϕ) [83]. It is noted that for a multilayer sensing system, each layer

has its own [A] matrix with appropriate material constants with the piezoelectric constant

being set to zero for non-piezoelectric materials e.g., polymer and liquid layers.

Furthermore, each layer must satisfy Eq. (2.9) with appropriate boundary conditions at

the interfaces. The boundary conditions include continuity of acoustic displacement

across the boundary, the continuity of mechanical stresses, and the continuity of the

electric field.

The phase velocity is determined by searching numerically until a value is found

that yields a system solution [88]. This method of determining the acoustic modes in a

system is effective and very accurate. However, the major disadvantage of this technique

is that it fails to clearly relate the effects of changing physical parameters in the system.

Moreover, it requires that material parameters as well as subsequent changes to the

parameters be known. Consequently, for sensing applications, it is very challenging to

use the numerical technique to model the presence or absence of a given perturbation in

the system. To overcome this problem, analytical approximation techniques are used. The

two most common techniques used in applied mathematics are perturbation theory and

the variation method [87]. In the next section, the basic principles of perturbation theory

are reviewed and applied to model small changes of physical parameters for the guided

SH-SAW sensor.

2.5 Perturbation Theory

In the context of acoustic wave sensor problems, perturbation theory is generally

used to calculate the effects of small parameter changes on known numerical solutions to

the wave equations. In this method, the unperturbed system is solved first and then the

solution is adapted for the case of the perturbed system [86]. The underlying assumption

in the use of perturbation theory is that the changes are small. This assumption allows one

to use an exact expression as a starting point for the derivation of the perturbed model.

The exact perturbation expression is given by [87]

$$\Delta\beta_n = \beta'_n - \beta_n = \frac{-j\left\{-v_n^* \cdot T'_n - v'_n \cdot T_n^* + \Phi_n^*\left(j\omega D'_n\right) + \Phi'_n\left(j\omega D_n\right)^*\right\} \cdot \hat{x}_3\Big|_0^h}{\int_0^h \left\{-v_n^* \cdot T'_n - v'_n \cdot T_n^* + \Phi_n^*\left(j\omega D'_n\right) + \Phi'_n\left(j\omega D_n\right)^*\right\} \cdot \hat{x}_2 dx_3} \qquad (2.10)$$

In the above equation, $\Delta\beta$ represents the change in the propagation constant, v_n is the

particle velocity in the n direction, T_n is the surface stress, Φ is the electrical potential, D

is the electrical displacement, ω is the angular velocity, h is the crystal thickness, and β is

the propagation constant [86]. Here, the signs $'$ and $*$ denote perturbed quantities and

complex conjugate, respectively. However, the above equation cannot be used because

the perturbed quantities are not available. This problem is overcome by searching for an

approximate solution for the perturbed fields. Since the perturbation in (2.10) is assumed

to be small, the perturbed fields in the denominator may be replaced by the unperturbed

fields as [87]

$$4P_n = 2\,\mathrm{Re}\int_0^h \left[-\, v_n^* \cdot T_n + \Phi\left(j\omega D_n\right)^*\right]\cdot \hat{x}_2 dx_3 \tag{2.11}$$

where P_n is the average unperturbed power flow per unit width along x_1. Unfortunately,

the same simple approximation cannot be made in the numerator, because this would

simply give $\Delta\beta_n = 0$ [86]. As a result, the general boundary perturbation formula is [87],

$$\Delta\beta_n = \frac{-\,j\left\{-\,v_n^* \cdot T_n' - v_n' \cdot T_n^* + \Phi_n^*\left(j\omega D_n'\right) + \Phi_n'\left(j\omega D_n\right)^*\right\}\cdot \hat{x}_3\Big|_0^h}{4P_n} \tag{2.12}$$

In the present work, only the upper surface ($x_3 = 0$) is perturbed because the SH-

SAW platform is considered as semi-infinite in the $-x_3$ direction due to the shallow

penetration depth of the surface acoustic mode into the bulk of the crystal. Furthermore,

with the sensing surface electrically shorted, only mechanical perturbations are

considered and Eq. (2.12) reduces to

$$\Delta\beta_n = \frac{\left(-\,j\left\{-\,v_n^* \cdot T_n' - v_n' \cdot T_n^*\right\}\cdot \hat{x}_3\right)_{x_3=0}}{4P_n}. \tag{2.13}$$

In order to use Eq. (2.13), it is necessary to relate the surface stress (T) to the

surface acoustic impedance (Z). This relation is given by [86]

$$-T \cdot \hat{x}_3\Big|_{x_3=0} = Z \cdot v\Big|_{x_3=0} \qquad \text{(Unperturbed case)} \tag{2.14a}$$

and
$$-T' \cdot \hat{x}_3\Big|_{x_3=0} = Z' \cdot v'\Big|_{x_3=0} \qquad \text{(Perturbed case).} \tag{2.14b}$$

Taking the complex conjugate of both sides of Eq. (2.14a) gives

$$-T^* \cdot \hat{x}_3\Big|_{x_3=0} = Z^* \cdot v^*\Big|_{x_3=0}. \tag{2.15}$$

In the above equations, $\hat{x}_3$ is the unit vector in the direction x_3. If the amplitude of the

particle velocity (v) field at the surface is assumed to be unchanged by surface

perturbations, i.e.,

$$v'\big|_{x_3=0} = v\big|_{x_3=0}, \tag{2.16}$$

then substituting Eqs. (2.14) to (2.16) into Eq. (2.13), the normalized perturbation

equation is given by

$$\frac{\Delta\beta}{k} = -\frac{jV\left(v^* \cdot Z' \cdot v + v \cdot Z^* \cdot v^*\right)}{4\omega P}. \tag{2.17}$$

For the SH-SAW, the particle motion is horizontal and perpendicular to the

direction of propagation and hence the particle displacement amplitude is given by [89]

$$u(x_1, x_2, x_3, t) = u(x_2, t)e^{j\omega t - \beta x_1}, \tag{2.18}$$

where β is a complex propagation factor representing both attenuation, α, and wave

number, k, as

$$\beta = k - j\alpha = \frac{\omega}{V} - j\alpha. \tag{2.19}$$

If frequency is held constant, then variation in the wave propagation constant is given by

$$\frac{\Delta\beta}{k} = -\frac{\Delta V}{V} - j\frac{\Delta\alpha}{k}. \tag{2.20}$$

From Eq. (2.20), it is clear that the fractional phase velocity, $\Delta V/V$, and the normalized

attenuation, $\Delta\alpha/k$, are orthogonal components of change in the complex propagation

factor, β, caused by a surface perturbation. Using (2.17) and (2.20), the fractional change in the wave velocity and normalized attenuation is given by

$$\frac{\Delta V}{V} = \mathrm{Re}\left[\frac{\Delta\beta}{k}\right] = \mathrm{Re}\left[\frac{jV\left(v^* \cdot Z' \cdot v + v \cdot Z^* \cdot v^*\right)}{4\omega P}\right] \qquad (2.21a)$$

and
$$\frac{\Delta\alpha}{k} = \mathrm{Im}\left[\frac{\Delta\beta}{k}\right] = \mathrm{Im}\left[\frac{jV\left(v^* \cdot Z' \cdot v + v \cdot Z^* \cdot v^*\right)}{4\omega P}\right], \qquad (2.21b)$$

respectively.

2.6   Analysis of the Three Layer Sensor System

In Eq. (2.21a), it is seen that the changes in the phase velocity and attenuation of the propagating SH-SAW wave are dictated by the changes in surface acoustic impedance. In order to relate the changes in the surface acoustic impedance to the changes in the phase velocity and attenuation, it is necessary to analyze the geometry before and after perturbation. There are three possible cases and this has been discussed in [86]. In this work, the configuration before and after perturbation is the coated device in contact with the liquid (see Figure 2.2) without and with the analyte, respectively. It is assumed that because the analyte solutions are dilute, the mechanical properties of the liquid are unchanged and only the viscoelastic properties of the film (G', G'') are changed upon analyte absorption.
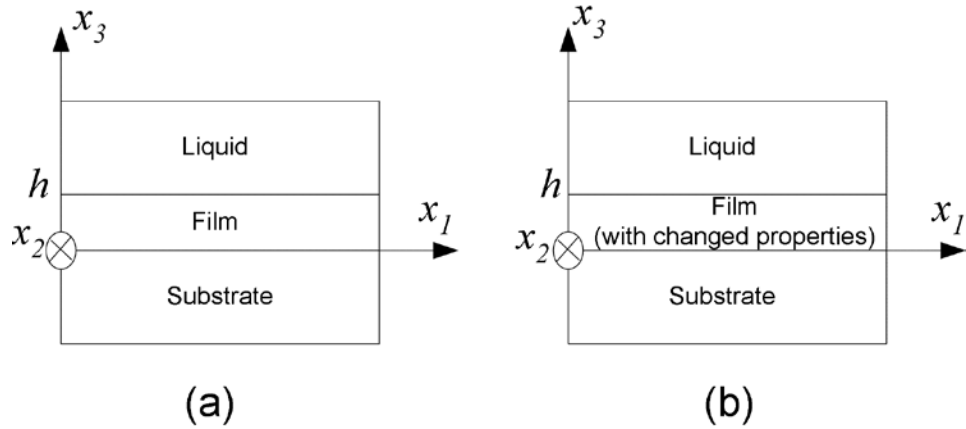
Figure 2.2:Three-layer geometry configuration used in the simulation of viscoelastic effect: (a) before (b) after perturbation [86].

Acoustic impedance before perturbation

The surface wave is assumed to be a plane wave, thus differentiation with respect to x_2 is zero. Using the equation of motion, the continuity equation is obtained as [86]

$$\frac{\partial T_{i3}^f}{\partial x_1} + \frac{\partial T_{i3}^f}{\partial x_3} = \rho_f \dot{v}_i \qquad i = 1, 2, 3 \qquad (2.22)$$

where T_{ij} is the stress tensor and it represents the force per unit area in the i-direction in the plane normal to the j-direction; ρ_f is the mass density of the film. The superscript "f" denotes the film. The propagation of the surface wave causes periodic displacement fields to be imposed on the lower film surface [90]. This surface displacement induces a strain. For an acoustically thin film, the displacement gradients are in-plane whereas for an acoustically thick film, both in-plane and cross-film (caused by the inertial lag of the upper film portion of the film with respect to the "driven" lower film surface) displacement gradients, with cross-film gradients dominating [90]. The in-plane displacement gradients in the film are given by [86]

$$T_{i1}^f = E_f^i \frac{\partial u_i^f}{\partial x_1} \tag{2.23}$$

and the cross-film gradients are given by

$$T_{i3}^f = M_f^i \frac{\partial u_i^f}{\partial x_3}. \tag{2.24}$$

E_f^i and M_f^i are given by [86]

$$E_f^1 = \frac{\partial u_{x_1}^f}{\partial x_1} = \frac{T_{11}}{S_{11}} = \frac{4G(3K+G)}{3K+4G} \quad \text{(Compression strain mode),} \tag{2.25a}$$

$$E_f^2 = \frac{\partial u_2^f}{\partial x_1} = \frac{T_{21}}{2S_{21}} = G \quad \text{(Transverse shear strain mode),} \tag{2.25b}$$

$$E_f^3 = \frac{\partial u_{x_3}^f}{\partial x_1} = \frac{T_{31}}{2S_{31}} \approx 0 \,\text{(Bending mode),} \tag{2.25c}$$

$$M_f^1 = M_f^2 = G \tag{2.25d}$$

and
$$M_f^3 = K. \tag{2.25e}$$

M_f^i is the generalized modulus of the film layer associated with the ith displacement

component and E_f^i is the Young's modulus for the film layer generated i^{th} displacement

component. G and K are the shear modulus and bulk modulus of the film, respectively.

Substituting equations (2.23), (2.24) and the harmonic solution $\vec{u}_i = \hat{u}_i(x_3)e^{j(\omega t - \beta x_1)}$ into

(2.22) yields a homogenous ordinary differential equation for the displacement profile $u_i(x_3)$ in the film:

$$\frac{d^2 u_i^f}{dx_3^2} + \beta_i^2 u_i^f = 0 \tag{2.26}$$

with
$$\beta_i = \omega \sqrt{\left(\frac{\rho_f - E_f^i / V^2}{M_f^i} \right)}. \tag{2.27}$$

β_i is the complex propagation factor, associated with the displacement u_i ($i = 1, 2, 3$), that describes wave propagating across the film. The solution to (2.26) is given by

$$u_i^f(x_3) = A_i e^{j\beta_i x_3} + B_i e^{-j\beta_i x_3}, \quad 0 \leq x_3 \leq h \tag{2.28}$$

where h is the film thickness and A_i and B_i are constants determined using boundary conditions.

In general, motion in a viscous liquid is described by the Navier-Stokes equations. However, in the present study, the amount of liquid at an instant of time in the flow cell is small and the flow rate is low. Therefore, the liquid is considered to be an isotropic non-piezoelectric material. The wave equation and stress are thus sought as an analogy to a solid [86]. The liquid layer is considered as semi-infinite layer, and the wave equation in the liquid layer can be expressed as [86]

$$u_i^l(x_3) = C_i e^{-\beta_c(x_3 - h)}, \qquad h \leq x_3 \leq \infty \tag{2.29}$$

where

$$\beta_c = \frac{1+j}{\delta_l}, \qquad \delta_l = \sqrt{\frac{2\eta_l}{\omega\rho}}.$$

The stress is given by

$$T_{i3}^l = M_l^i \frac{\partial u_i^l}{\partial x_3} \tag{2.30}$$

where M_l^i is the generalized modulus of the liquid layer associated with the ith displacement component, E_l^i is the Young's modulus for the film layer generated i^{th} displacement component, δ_l is the decay length in the liquid, η_l is the viscosity of the liquid, ρ_l is the mass density of the liquid, β_c is the complex shear wave propagating constant across the liquid, and C_i is a constant determined using the boundary conditions. In the liquid, $M_l^1 = M_l^2 = G_l$ and $M_l^3 = K_l$.

The boundary conditions are the continuity of the particle displacement and stress at the polymer/substrate interface $x_3 = 0$ and the polymer/liquid interface $x_3 = h$, i.e.,

$$u_i^f(0) = u_{i0} \tag{2.31a}$$

$$u_i^f(h) = u_i^l(h) \tag{2.31b}$$

$$T_{i3}^f(h) = T_{i3}^l(h) \tag{2.31c}$$

where u_{i0} is the particle displacement of the substrate at the polymer/substrate interface.

Substituting the wave displacement in Eqs. (2.28) and (2.29) and the stress relations (2.24) and (2.30) into the boundary conditions (2.31), three equations with three unknowns (A_i, B_i, and C_i) are obtained as

$$A_i + B_i = u_{i0},$$

(2.32a)

$$A_i e^{j\beta_i h} + B_i e^{-j\beta_i h} = C_i,$$

(2.32b)

$$M_f^i (j\beta_i)(A_i e^{j\beta_i h} - B_i e^{-j\beta_i h}) = M_l^i(-\beta_c C_i).$$

(2.32c)

Solving Eq. (2.32) simultaneously for the unknowns (A_i, B_i, and C_i) in (2.32) in terms of the material properties of the substrate, polymer, and liquid layer, gives [86]

$$A_i = \frac{(W_1 - W_2)e^{-j\beta_i h}}{(W_1 + W_2)e^{j\beta_i h} + (W_1 - W_2)e^{-j\beta_i h}} \cdot u_{i0},$$

(2.33a)

$$B_i = \frac{(W_1 + W_2)e^{j\beta_i h}}{(W_1 + W_2)e^{j\beta_i h} + (W_1 - W_2)e^{-j\beta_i h}} \cdot u_{i0},$$

(2.33b)

$$C_i = \frac{2W_1}{(W_1 + W_2)e^{j\beta_i h} + (W_1 - W_2)e^{-j\beta_i h}} \cdot u_{i0},$$

(2.33c)

where $W_1 = j\beta_i M_f^i$ and $W_2 = \beta_c M_l^i$.

The surface mechanical impedances Z_i experienced by the surface displacement components u_i in translating and deforming the polymer layer is given by [86;90]

$$Z_i = -\frac{T_{i3}}{v_i}\bigg|_{x_3=0}$$

(2.34)

where T_i, and v_i, evaluated at $x_3 = 0$, denote interfacial stress and particle velocity in the i-direction, respectively. For an isotropic film, the displacement components can be considered independently in calculating Z_i. In evaluating this impedance, interfacial shear stress is found from Eq. (2.24) using Eq. (2.28) for u_i:

$$T_{i3}(0) = M_f^i \left.\frac{\partial u_i}{\partial x_3}\right|_{x_3=0} = j\beta_i M_f^i (A_i - B_i) \qquad (2.35)$$

and the interfacial particle velocity is found from Eq. (2.28) as:

$$v_i(0) = \dot{u}_i(0) = j\omega u_i(0) = j\omega(A_i + B_i). \qquad (2.36)$$

Substituting Eqs. (2.35) and (2.36) into Eq. (2.34) and using Eq. (2.33) gives the surface

mechanical impedance associated with each displacement u_i as:

$$Z_i = -\frac{\beta_i M_f^i}{\omega}\left(\frac{A_i - B_i}{A_i + B_i}\right) = \frac{\beta_i M_f^i}{\omega} F_i \qquad (2.37)$$

where

$$F_i = \frac{\left(j\beta_i M_f^i + j\beta_c M_l^i\right)e^{j\beta_i h} - \left(j\beta_i M_f^i - j\beta_c M_l^i\right)e^{-j\beta_i h}}{\left(j\beta_i M_f^i + j\beta_c M_l^i\right)e^{j\beta_i h} + \left(j\beta_i M_{f_1}^i - j\beta_c M_l^i\right)e^{-j\beta_i h}}. \qquad (i = 1, 2, 3) \quad (2.38)$$

<u>Acoustic impedance after perturbation</u>

The geometry after perturbation is the same as the geometry before perturbation,

i.e., coated substrate in contact with the liquid. Here, the properties of the liquid are

assumed unchanged before and after perturbation while the properties of the polymer

layer are changed by analyte absorption. Therefore, the surface acoustic impedance will

have the same form as in Eq. (2.38) with the film properties changed to prime terms. The

surface acoustic impedance is given by

$$Z_i' = -\frac{\beta_i' M_f'^i}{\omega} F_i' \qquad (2.39)$$

where

$$F_i' = \frac{\left(j\beta_i'M_f''^i + j\beta_c M_l^i\right)e^{j\beta_i h} - \left(j\beta_i'M_f''^i - j\beta_c M_l^i\right)e^{-j\beta_i h}}{\left(j\beta_i'M_f''^i + j\beta_c M_l^i\right)e^{j\beta_i h} + \left(j\beta_i'M_{f1}''^i - j\beta_c M_l^i\right)e^{-j\beta_i h}}. \qquad (i = 1, 2, 3) \qquad (2.40)$$

Substituting Eqs. (2.37) and (2.39) into Eq. (2.17), the change in the complex propagating

factor is found as:

$$\frac{\Delta\beta}{k} = -\frac{jV}{4\omega P}\sum_{i=1}^{3}\left[\left(\frac{\beta_i'M_f''^i}{\omega}F_i'\right) + \left(\frac{\beta_i M_f^i}{\omega}F_i\right)^*\right]\cdot v_i^2 \qquad (2.41)$$

Under metallization, the 36° rotated Y-cut LiTaO$_3$ crystals are assumed to support a pure

SH-SAW [51;86]. As a result, the fractional change in velocity and attenuation are given

as

$$\frac{\Delta V}{V} = \mathrm{Re}\left\{\frac{jV}{4\omega P}\left[\left(\frac{\beta_2'M_f'^2}{\omega}F_2'\right) + \left(\frac{\beta_2 M_f^2}{\omega}F_2\right)^*\right]\cdot v_2^2\right\} \qquad (2.42a)$$

$$\frac{\Delta\alpha}{k} = \mathrm{Im}\left\{\frac{jV}{4\omega P}\left[\left(\frac{\beta_2'M_f'^2}{\omega}F_2'\right) + \left(\frac{\beta_2 M_f^2}{\omega}F_2\right)^*\right]\cdot v_2^2\right\} \qquad (2.42b)$$

From Eqs. (2.42), it is clear that the sensor performance is a function of polymer material

properties (mass density, viscoelasticity, film thickness) and the liquid properties. To

determine the significance of each parameter, one can analyze F_2. For sensor

applications, this means that if we know the initial values for the parameters that change

in F_2, one can accurately predict the sensor response for an unknown concentration of an

analyte, provided a calibration curve has been established. Futhermore, this will allow one to quantify the dominant contribution to the sensor response.

2.7   Transduction Mechanism

Figure 2.3 shows the basic configuration of a guided SH-SAW sensor platform. It consists of an SH-SAW device (in this case a delay line) with an overlayer having a lower shear wave velocity and a liquid layer [51]. A thin metal layer is used between the input and output IDTs to create an electrical short and eliminate acoustoelectric interaction with the load. Therefore, only sensing caused by mechanical loading is considered in this work. The effect of the polymer layer is to trap the acoustic energy near the sensing surface, reducing propagation velocity and increasing the sensitivity to surface perturbation [51]. Moreover, the polymer layer acts as the chemically sensitive layer. The liquid layer acts as a transport medium for the target species, also known as analytes. As the acoustic wave propagates along the substrate, any surface perturbations will change its complex propagation factor, β, i.e. phase velocity, V, and attenuation, α,. By monitoring these changes, a sensor can be implemented, where ΔV and $\Delta \alpha$ can be related to the amount and type of analytes. Hence, the key to SH-SAW chemical sensors is to understand which factors affect the phase velocity and attenuation. In this section, the sensing mechanism is reviewed.
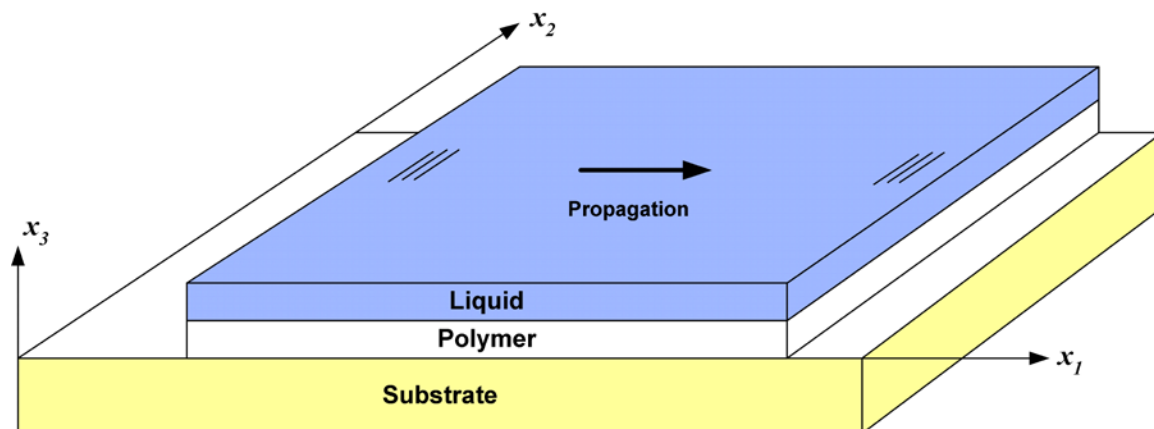
Figure 2.3: Schematic of guided SH-SAW sensor. For simplicity, only one delay line is shown.

In general, the change in phase velocity and attenuation due to perturbation is a function of the added mass, Δm; the stiffness change, Δc; the change in dielectric constant, $\Delta \varepsilon$; the change in conductivity, $\Delta \sigma$; the change in temperature, ΔT; and the change in pressure, ΔP. This is generally expressed as a sum of the partial derivatives of the phase velocity and/or attenuation with respect to the phase velocity and attenuation [40;86;89]. However, due to the design of the guided SH-SAW device, all electrical load interactions are eliminated. Moreover, the design of the SH-SAW device employs a dual delay line configuration with one line as a sensing line and the other as a reference [51]. Therefore, common environmental interactions (such as temperature and pressure) eliciting responses from both lines can be eliminated by subtraction (known as differential measurement). In Figure 2.4, both lines are exposed to the analyte solution at the same time. The reference line responds to environmental effects but not the presence of analyte in the solution. At 60 minutes, there is a drastic decrease in temperature and a corresponding upward shift in IDT center frequency because of the negative temperature coefficient of delay of the LiTaO$_3$ substrate. As a result, the response of the sensing line is perturbed. However, the effect of the temperature change is eliminated by substraction,

as indicated by the difference signal. It is noted that for chemical sensor applications, an ideal reference coating will have the same physical properties as the sensing layer with the exception that it is inert to the analyte of interest. In addition, a temperature control system (described in chapter 4) is used for temperature control to eliminate ΔT variations. Ideally, the dual delay line should also eliminate temperature variations through the device.

Guided SH-SAW velocity and attenuation responses arise from the mechanical interaction that occurs between the SH-SAW and the polymer layer along the sensing path. A film that is rigidly bonded to the surface of the piezoelectric substrate undergoes both translation and deformation under the influence of the propagating wave [90]. Translation causes a decrease in the SH-SAW velocity that is proportional to the areal mass density (ρh) of the film. This effect is known as mass loading. In addition, the deformation produces energy storage in the film, which results in a change in SH-SAW propagation velocity, and power dissipation in the film, which causes wave attenuation [90]. These effects are known as viscoelastic changes.
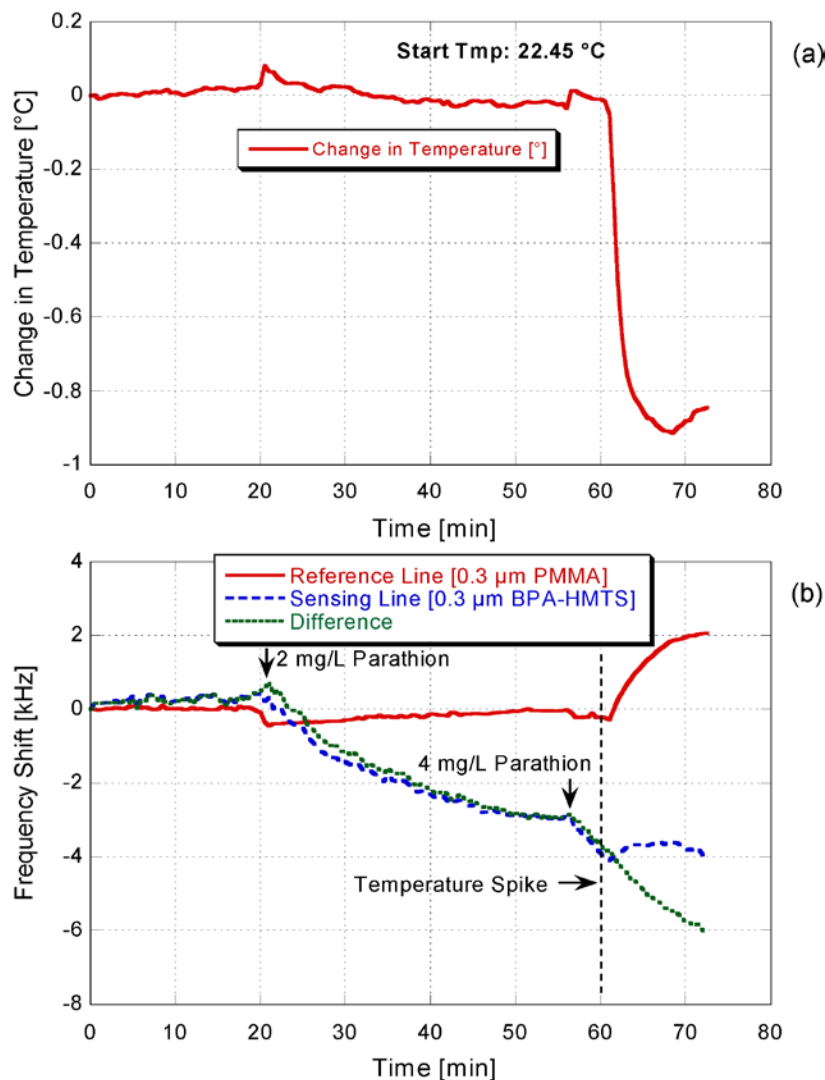
Figure 2.4: Temperature compensation for a guided SH-SAW device using dual delay line configuration: (a) change in ambient temperature (b) frequency response of the two delay lines to analyte injection (2 and 4 mg/L parathion) and drastic change in ambient temperature. The difference signal (sensing line minus reference line) is shown.

The viscoelastic properties of a polymer are described by its modulus: bulk modulus, K, and shear modulus, G. Under linear, sinusoidal deformation, the mechanical properties of a viscoelastic material are complex quantities[91]: $K = K' + jK''$ and $G = G' + jG''$. The real parts of K and G represent the component of stress in phase with strain, giving rise to energy storage in the film (consequently K' and G' are referred to as storage moduli); the imaginary parts represent the component of stress 90° out of phase with

strain, giving rise to power dissipation in the film (thus, K'' and G'' are called loss moduli) [90]. It is noted that polymer film/AW interactions are dominated by the shear component of displacement in the present device [36]. Thus, it is the shear modulus which is effectively probed by the devices.

Therefore, assuming that acoustoelectric interaction, temperature effects, and pressure effects have been eliminated, the sensor response for a polymer-coated SH-SAW device can be described by

$$\frac{\Delta V}{V} = \frac{1}{V}\left[\frac{\partial V}{\partial m}\Delta m + \frac{\partial V}{\partial G'}\Delta G'\right] \tag{2.43a}$$

$$\frac{\Delta \alpha}{k} = \frac{1}{k}\left[\frac{\partial \alpha}{\partial G''}\Delta G''\right]. \tag{2.43b}$$

Experimentally, frequency shifts are measured instead of changes in phase velocity, and insertion loss instead of normalized attenuation. Thus it is important to know how these parameters are related. Given the delay line shown in Figure 2.5, where l_T is the IDT center-to-center separation (acoustic path length), and l_s is the sensing path length, the relationship between the fractional velocity shift caused by changes in the film and the frequency shift measured with a SAW oscillator circuit is [86;92]
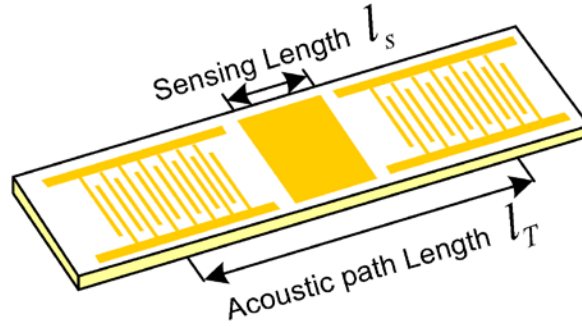
Figure 2.5: Delay line configuration of a guided SH-SAW device. For simplicity, only one delay line is shown.

$$\frac{\Delta f}{f} = \frac{l_s}{l_T}\frac{\Delta V}{V}.$$

(2.44)

It should be noted that in deriving Eq. (2.44), it is assumed that there is no dispersion of the propagating wave [86], i.e. phase velocity, v, equals the group velocity, v_g. In the present work, the sensitive coating is on the entire device, $l_s = l_T$ and $\Delta f/f = \Delta V/V$. In addition to monitoring the frequency of the guided SH-SAW sensor, the insertion loss is also monitored. The change in insertion loss, ΔL_I, can be easily converted to normalized attenuation using the relation

$$\frac{\Delta \alpha}{k} = \frac{\Delta L_I}{54.6 N_\lambda},$$

(2.45)

where ΔL_I is the change in insertion loss expressed in dB and N_λ is the length, in acoustic wavelengths, of the region perturbed by the film [36;92].

3 POLYMER COATINGS FOR LIQUID-PHASE SENSING

3.1 Introduction

The coating properties (both mechanical and chemical) ultimately determine the response of the sensor to an analyte. Therefore, in order to model and predict the response of a guided SH-SAW sensor, it is necessary to understand the sorption process associated with an analyte/coating pair as well as the mechanical (viscoelastic) properties of the coating, often a polymeric material.

In this chapter, the mechanical properties of coating (polymeric) materials, analyte absorption, and the effect of analyte absorption on the mechanical properties of coating will be discussed in detail. Furthermore, the chemistry of organophosphate pesticides and the rationale of the design of sensitive layers for their detection in liquid-phase are presented.

3.2 Viscoelastic Properties of Polymers

A polymer can be defined as a compound consisting of a large number of repeating units, called monomers [36]. The monomers are held together by covalent bonds. In general, polymeric materials that are applied to AW devices are considered to be viscoelastic. Their mechanical/viscoelastic properties are between those of a purely elastic solid (stress is directly proportional to strain for small deformation but independent of the rate of strain) and a pure viscous liquid (stress directly proportional to

the rate of strain but independent of strain) [40;91]. As mentioned earlier, the viscoelastic

properties of a polymer experiencing shear deformation is characterized by the complex

shear modulus, G. The properties of the polymer depend on the inter- and intra-molecular

forces holding the polymer together, as well as the overall size of the polymer chain (i.e.,

average molecular weight) [36;86]. The intra-molecular forces are the covalent bonds

that join the repeat units into chains and any covalent bonds that may join adjacent chains

together (cross-linkages) [36]. In addition, the polymer chains are held together by a

variety of inter-molecular forces, including hydrogen bonding, dipole-dipole interaction,

and London dispersion forces resulting from synchronization of electron motion in the

interacting atoms [36]. In general, the relative strengths and types of these forces dictate

the physical and chemical properties of the polymer.

In this work, polymer-coated SH-SAW devices are used to develop a chemical

sensor for real-time monitoring of OPs in aqueous solution. It is assumed that the sensor

responses are due to analyte absorption. In order to accurately interpret the sensor

responses, it is necessary to model the viscoelastic behavior of the coating. For an

uncross-linked polymer, the absorption of analyte into the coating induces stress which

the coating alleviates by undergoing conformational changes. During these changes, the

stress slowly relaxes until a stable configuration of low energy is obtained. This

viscoelastic behavior can be adequately described a simple Maxwell model, as shown in

Figure 3.1. In this model, the spring/elastic element (shear stiffness μ) represents the

restoring forces arising from the tendency of deformed polymer chains to return to a more

probable configuration, thus maximizing entropy and the dashpot/viscous element (shear

viscosity η) represents the frictional resistance of the polymer chains moving past each other [93].
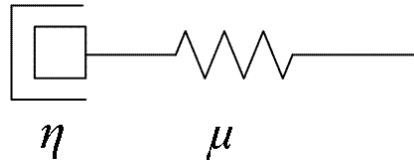
Figure 3.1: Maxwell model

The viscoelastic function for the Maxwell model as a function of frequency is given by [91;94]

$$G'(\omega) = \frac{\mu(\omega\tau_r)^2}{1+(\omega\tau_r)^2}, \tag{3.1a}$$

$$G''(\omega) = \frac{\mu(\omega\tau_r)}{1+(\omega\tau_r)^2}, \tag{3.1b}$$

$$\tan\delta = \frac{G''(\omega)}{G'(\omega)} = \frac{1}{\omega\tau_r}, \tag{3.1c}$$

$$\tau_r = \frac{\eta}{\mu}, \tag{3.1d}$$

where $G'(\omega)$, $G''(\omega)$, tan δ, and τ_r represent the storage modulus, loss modulus, loss tangent, and relaxation time (time required for stress relaxation), respectively.

3.3 Analyte Absorption

The response characteristics of a sensor are a function of the nature of the interaction between the analyte and the chemically sensitive layer and the sorption process (mass transport process). Sorption is a general term used to describe the detection process; it is a combination of three processes. Namely, (1) analyte molecules adhering to

the polymer surface (adsorption), (2) passing through the surface into the polymer (penetration), and (3) dispersing/dissolving throughout the bulk of the polymer (diffusion) [78;95]. Penetration and diffusion are collectively referred to as absorption [78]. In general, the sorption process is either adsorption and/or absorption based. It is assumed that the sensor response will be based on the absorption of analyte molecules into the coating and the corresponding effect on the viscoelasticity of the coating. Therefore, the absorption process will be discussed in detail and modelled in this section.

The absorption process consists of analyte molecules first penetrating the surface followed by diffusion through the bulk of the coating. Thus, either phenomenon can be the rate limiting step for the absorption process. In order to determine whether the absorption process is rate limited by penetration or rate limited by diffusion, it is necessary to model each step of the absorption process.

For the case where the absorption process is rate limited by penetration, penetration occurs much slower than diffusion. This would be true if the diffusion coefficient is quite large or if the polymer coating is thin [78]. To model this case, it is assumed that concentration is uniform throughout the coating at all times. The flux of the analyte through the surface of the polymer can be expressed by [78;95]

$$F = \xi\left(\gamma_p C_{amb} - C_s(t)\right),$$ (3.2)

where F is the mass flux of the analyte [g/cm^{2}s]; ξ is the mass transfer coefficient into the polymer [cm/s]; $\gamma_p C_{amb}$ is the concentration of analyte in the coating at equilibrium; and $C_s(t)$ is the prevailing surface concentration, which is usually zero at the start of an absorption process. The partition coefficient (γ_p) is a thermodynamic parameter that

describes the distribution of analyte molecules between the coating and the ambient

medium (gas or liquid) and is given by

$$\gamma_p = \frac{C_\infty}{C_{amb}} = \frac{\left(m_\infty \middle/ V_s\right)}{C_{amb}}, \tag{3.3a}$$

where

$$m_\infty = hC_\infty = h\gamma_p C_{amb}, \tag{3.3b}$$

is the mass (per unit area) of analyte absorbed into a coating of thickness, h, and volume,

V_s; C_∞ is the concentration of analyte in the coating at equilibrium, and C_{amb} is the

concentration of analyte in the liquid. The preferred unit of C_{amb} is mass per unit volume.

Using Eqs. (3.2) and (3.3), it is possible to describe the absorption process that is rate

limited by penetration by a first order differential equation [78]

$$\frac{dm}{dt} = \frac{\xi}{h}\left(h\gamma_p C_{amb} - m(t)\right), \tag{3.4a}$$

with the solution

$$m(t) = m_\infty\left(1 - \exp\left\{-\frac{t}{\tau_s}\right\}\right). \tag{3.4b}$$

Here, τ_s is the effective time constant of absorption.

Alternatively, it is possible that the absorption process is limited by diffusion. In

this case, surface penetration is much faster than diffusion. Thus, for modelling purposes,

the surface analyte concentration is assumed to reach equilibrium instantaneously and

remain constant afterwards. The absorption process can be described by a one-

dimensional Fickian diffusion equation [96]. For a polymer layer of thickness, h,

deposited on an impermeable substrate and initially free of analyte (see Figure 3.2), the

amount of analytes absorbed in the polymer, $m(t)$, at time t, upon exposure to ambient

analyte concentration can be expressed as [96;97]

$$\frac{m(t)}{m_\infty} = 1 - \frac{8}{\pi^2} \sum_{n=0}^{\infty} \frac{1}{(2n+1)^2} \exp\left\{ -\frac{D(2n+1)^2 \pi^2 t}{h^2} \right\}, \quad (3.5a)$$

where

$$m_\infty = h\gamma_p C_{amb}, \quad (3.5b)$$

is the equilibrium mass (per unit area) uptake and D is the diffusion coefficient [cm^2s^{-1}].
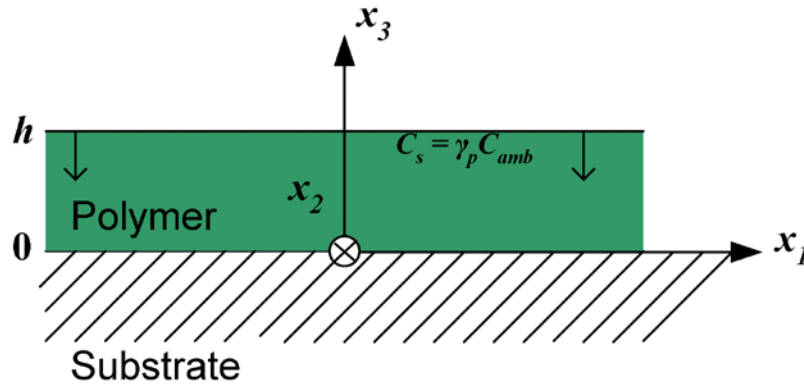
Figure 3.2: Schematic representation of a thin polymer coating attached to an impermeable SH-SAW device substrate. The concentration on the upper surface is constant and there is no flux through the bottom of the coating.

If only the first term, $(n = 0)$, of the series is considered, Eq. (3.5a) reduces to

$$m(t) \approx m_\infty \left(1 - \frac{8}{\pi^2} \exp\left\{ -\frac{D\pi^2 t}{h^2} \right\} \right). \quad (3.6)$$

 The above equation is a good approximation because the second term ($n = 1$) is nine

times smaller than the first term and has a decay rate that is nine times larger

[78].Comparing Eqs. (3.4b) and (3.6), it is seen that the two absorption models have a

solution of the same form. However, when the effective time constants are compared, it is

observed that if absorption is controlled by diffusion, the effective time constant is

proportional to the square of the coating thickness, whereas for absorption that is

controlled by penetration, the time constant is a linear function of the coating

thickness[78]. Table 3-1 gives a summary of the two absorption models.

Table 3-1: Comparison of absorption processes [78].

Absorption Process (Small Concentrations)	Mass (per unit area) Sorbed at Equilibrium	Effective Time Constant
Absorption, rate limited by penetration	$m_\infty = h_2 \gamma_p C_{amb}$	$\tau_s = h/\xi$
Absorption, rate limited by diffusion	$m_\infty = h_2 \gamma_p C_{amb}$	$\tau_s = h^2/D\pi^2$

It is noted that in deriving Eq. (3.4b) and (3.5a), it is assumed that the thickness of

the coating is constant as absorption proceeds. In practice, the coating may swell and

increase in thickness as analyte is absorbed. Furthermore, the mass transfer coefficient

and diffusion coefficients may vary with concentration [96;97].

3.4 Effect of Analyte Absorption

Absorption of analyte molecules by the polymer-coated SH-SAW device from the liquid environment results in mechanical loading. This mechanical loading is a combination of added mass (Δm) and change in the complex shear modulus ($\Delta G(\omega)$) of the coating [36;53]. This, in turn, will modify the acoustic wave velocity and attenuation. The degree of these effects depends on the amount of analyte absorbed and the nature of the analyte/coating interaction, respectively.

The mass loading contribution to the change in the phase velocity is expressed as the change in the product of the film density and film thickness, $\Delta(\rho h)$, after exposure to analyte solution. The film thickness and density varies with the concentration of the absorbed analytes and this has been modeled in the literature for gas phase sensing[90;98;99]. The general properties of the absorption process for analyte in aqueous phase should be similar to those described for gas phase sensing. However, for detection to occur in aqueous solutions, the analyte molecules must displace molecules present in the reference solution from the region near the coating surface. As will be discussed later in Chapter 4, the reference solution is a phosphate buffer solution consisting of water, methanol, and phosphates (potassium monobasic [KH_2PO_4] and potassium dibasic [K_2HPO_4]). Assuming that the effects of the reference and analyte molecules are additive, after exposure to aqueous analyte solution, the film thickness and film density at equilibrium is given, respectively, by

$$h(C_{amb}) = h_0\left(1 + C_a V_a + C_m V_m + C_{mref} V_{mref} + C_{dref} V_{dref} + C_w V_w\right) \tag{3.7a}$$

$$\rho(C_{amb}) = \frac{\rho_0 + C_a M_a + C_m M_m + C_{mref} M_{mref} + C_{dref} M_{dref} + C_w M_w}{\left(1 + C_a V_a + C_m V_m + C_{mref} V_{mref} + C_{dref} V_{dref} + C_w V_w\right)} \tag{3.7b}$$

where

$$C_a = \frac{\gamma_p C_{amb}}{M_a}, \tag{3.7c}$$

$$C_m = \frac{\gamma_m C_{MeOH}}{M_m}, \tag{3.7d}$$

$$C_{mref} = \frac{\gamma_{mref} C_{KH_2PO_4}}{M_{mref}}, \tag{3.7e}$$

and

$$C_{dref} = \frac{\gamma_{dref} C_{K_2HPO_4}}{M_{dref}}. \tag{3.7f}$$

Here, ρ_0 and h_0 are the unperturbed film density and thickness; γ_p, γ_m, γ_{mref}, and γ_{dref} are the polymer-liquid partition coefficients for the analyte, methanol, potassium monobasic, and potassium dibasic, respectively; C_{amb}, C_{MeOH}, $C_{KH_2PO_4}$, and $C_{K_2HPO_4}$ are the concentrations (g/mL) of the analyte, methanol, potassium monobasic, and potassium dibasic, respectively, in the aqueous solution; C_a, C_m, C_{mref}, and C_{dref} are the concentrations (mol/mL) of absorbed analyte, methanol, potassium monobasic, and potassium dibasic at equilibrium, respectively; C_w is the concentration (mol/mL) of water in the polymer and is calculated based on the percent water uptake when the polymer is continuously immersed in water; V_a, V_m, V_{mref}, and V_{dref} are the molar volumes (mL/mol) of the analyte, methanol, potassium monobasic, and potassium dibasic at equilibrium, respectively; M_a, M_m, M_{mref}, and M_{dref} are the molar masses (g/mol) of the analyte, methanol, potassium monobasic, and potassium dibasic at equilibrium, respectively. It

should be pointed out that the concentration of methanol and phosphates in the reference solution and the analyte sample(s) is the same.

Typically, analyte absorption also causes the polymer to swell (increase in volume of the polymer) and soften or plasticize. Both effects are a direct consequence of analyte/polymer interaction and change the viscoelasticity of the polymer, resulting in a change in the shear modulus of the coating. Modulus changes associated with swelling and plasticization produce both phase velocity and attenuation changes.

As analyte absorbs into the polymer, it interrupts the intermolecular forces at work between the individual polymer chains, and the polymer swells [36]. For polymers in which these forces are strong, highly cross-linked or crystalline polymers (e.g., glassy polymers), the swelling will be minimal [36]. For lightly cross-linked or linear polymers (e.g. rubbery polymers), the swelling can be significant [36]. As the polymer swells, its density and modulus (which is strongly dependent on density and free volume) decrease [100]. Concurrent with the swelling phenomenon, the presence of absorbed analyte molecules in the polymer causes the polymer chains to undertake various conformations until a thermodynamically stable condition is achieved [101]. Furthermore, the analyte molecules lubricate the polymer chains (which are primarily responsible for the modulus of the polymer) so that they move more freely. This effect is known as polymer dilution, softening, or plasticization [93;100;101] and it increases the shear viscosity, η, of the polymer without an equivalent increase in the shear stiffness, μ. This changes the polymer shear relaxation time (time required for the polymer to recover to equilibrium after it is disturbed), $\tau_r = \eta/\mu$, and loss tangent, *tan δ = G''(ω)/G'(ω)*. It is noted that it is also possible that analyte/polymer interaction can result in the polymer shrinking and

becoming stiffer or exhibiting stronger elastic properties [40;102]. The degree of

plasticization depends on the amount of absorbed analyte [36;86], with higher analyte

uptake plasticizing the polymer to a greater extent and inducing larger conformational

changes in the polymer. Note that the amount of analyte absorbed depends on the

partition coefficient for an analyte/coating pair, the ambient concentration, and the film

thickness.

Substituting Eqs. (3.1) and (3.7) into Eq. (2.42), the changes in the wave (SH-

SAW) propagation velocity and attenuation caused by changes in Maxwellian

viscoelastic film properties can be determined. For low-loss surface material, and

assuming $h << \lambda$, (where λ is the wavelength), an approximate analytical expression for

the velocity and attenuation is given by [36;93]

$$\frac{\Delta V}{V} = -c_1 \omega (\rho h) - c_2 \omega \Delta \left(h G'(\omega) \right), \tag{3.8a}$$

$$\frac{\Delta \alpha}{k} = c_2 \omega \Delta \left(h G''(\omega) \right), \tag{3.8b}$$

where c_1 and c_2 are substrate-dependent parameters and Δ denotes changes in the

associated quantities.

3.5   Chemistry of Organophosphate Pesticides

Organophosphates pesticides (OPs) are esters of phosphorus and have the general

structure:
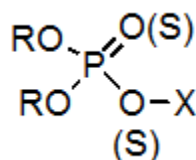
Figure 3.3: General chemical structure of organophosphate pesticides [103].

where R represents an alkyl group [methyl (CH_3) or ethyl (C_2H_5)] and X an organic

radical, which is often aromatic [10;103]. OPs are soluble in water but more soluble in

organic solvents such as methanol because of their organic nature. As a result of their

solubility in water, they often enter surface and ground waters. [10].

As mentioned earlier, the major reason the agricultural industry has increasingly

relied upon OPs is that it is assumed that they break down rapidly in the environment

after application. The major chemical break down mechanisms is oxidation, photolysis,

and hydrolysis. In water, the most important process for OPs degradation is hydrolysis.

Hydrolysis of OPs results in the introduction of a water molecule or a hydroxyl group (-

OH) into the chemical structure, commonly with the loss of the OX or (SX) radical

[10;103], as shown in Figure 3.4.
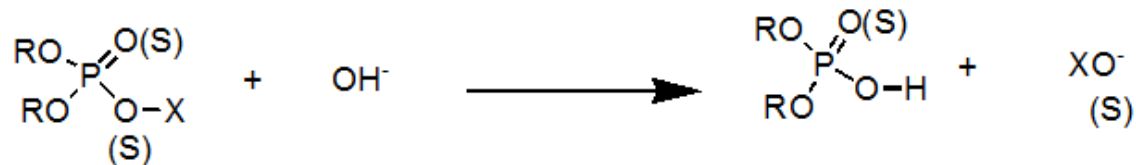
Figure 3.4: Hydrolysis reaction for organophosphate pesticides[103].

Hydrolysis of OPs is typically a first order reaction. The rate equation for this reaction, assuming that the hydroxyl ion concentration, [OH⁻], is held constant, is given by [10;103]

$$-\frac{dC(t)}{dt} = k_2 \left(C_0 - C(t)\right)\left[OH^-\right],$$ (3.9)

where C_0 is the initial concentration of the OP, $C(t)$ is the concentration of the OP at time t, and k_2 is the rate constant. Under these conditions, a half-life for the environmental persistence of OPs can be estimated. The half-life $(t_{1/2})$ for OPs or the time required for removal of 50% of the initial concentration of OPs, can be obtained by integrating Eq. (3.9) with respect to time to give [10]

$$t_{1/2} = \frac{\ln 2}{k_2}.$$ (3.10)

From Eq. (3.9), it is seen that as [OH⁻] increases and hence pH increases, the rate of hydrolysis increases and the half-life decreases, as illustrated in Figure 3.5a. It is noted that temperature also affects the rate of hydrolysis, with lower temperatures decreasing the reaction rate (see Figure 3.5b). Additionally, under comparable conditions, the rate of hydrolysis is also influenced by the substituents (alkyl group and O(S)) of the phosphorus compound with substituents that make the phosphorus atom more electropositive

increasing the hydrolysis rate [103]. Therefore, OPs with methyl group (CH_3) or oxygen (O) hydrolyze at a faster rate than their ethyl and sulphur (S) analogues, respectively. In the field, the pH and temperature for surface and ground waters vary between 5-9 [10;103] and 10-20 °C [10;104] respectively. As a result, OPs can persist in the environment for periods longer than what is predicted for laboratory conditions (pH 7, 25 °C). Consequently, OPs are more hazardous than commonly reported and assumed.

As result of the persistence of OPs in surface and ground waters, both being sources of drinking water, a need exists for developing in-situ real time monitoring systems for OPs. Parathion is one of the most commonly used OPs and is also one of the more persistent compounds in this class of pesticides. Furthermore, when it does degrade, its by-product (p-nitrophenol) is still very toxic [105]. It is for this reason that parathion is chosen as the primary analyte in this work, whereas the analogues, methyl parathion and paraoxon, are also selected to study the effect of the alkyl functional group and oxygen-analogue on rate of analyte absorption by polymers.
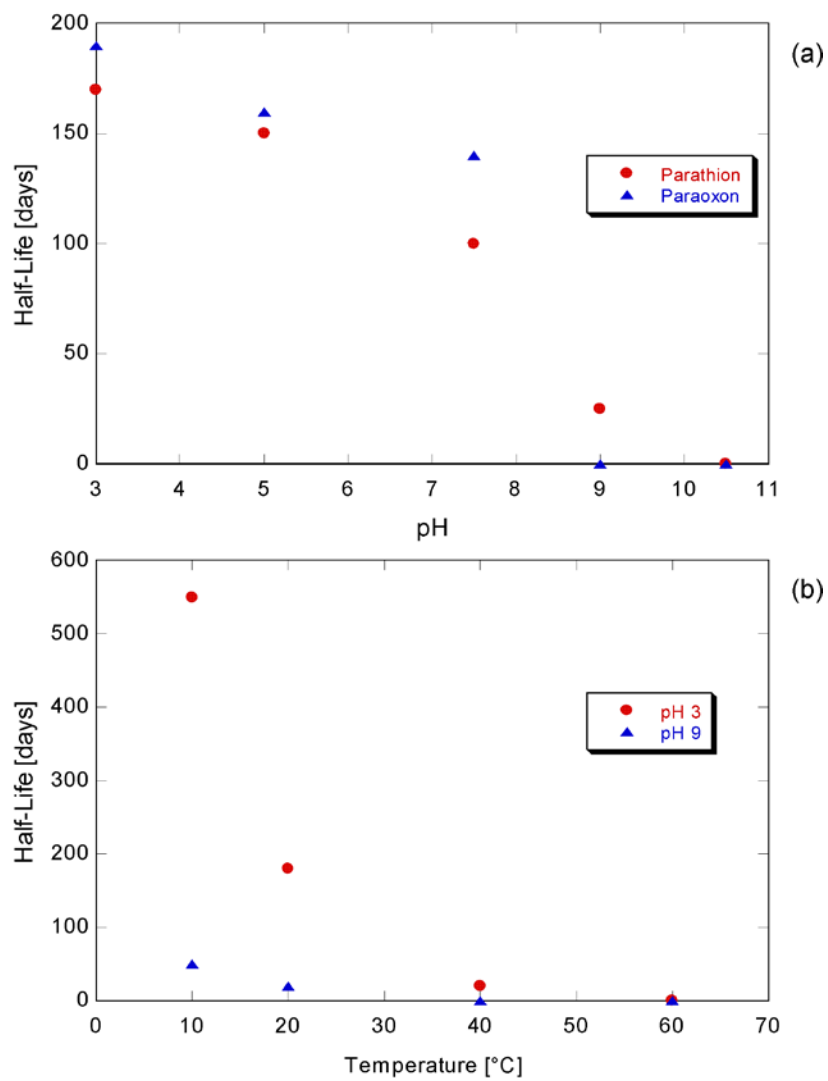
Figure 3.5: (a) Hydrolysis half-life of parathion and paraoxon as a function of pH. (b) Hydrolysis half-life of parathion as a function of temperature [10].

3.6   Design of Sensor Coatings for Organophosphates

A number of materials have been used as the chemically sensitive layer for the implementation of chemical microsensors. The materials range from conventional chromatographic stationary phases and polymers to unusual materials such as soot extracts [74]. Regardless of the material, the key design challenge is the functionality of the coating and the extent to which it enhance the sensor performance in terms of sensitivity, selectivity, response time, reversibility, and reproducibility. Consequently, several factors have to be considered when selecting the coatings for sensing applications. For near-real time liquid-phase detection, the primary consideration is that the coating is stable in water [106] and does not peel off or wash out under the experimental conditions in the liquid environment. Second, the glass transition temperature, T_g, of the polymer is considered. It is desirable that the T_g of the polymer coating be below room temperature and/or the operating temperature so that the sorption process is fast[74;76;107]. For gas-phase sensing, it has been shown that vapor absorption and desorption is rapid when this condition is met, whereas the response times of sensors with glassy polymers are typically much slower than those of rubbery-based polymers [74]. For experiments conducted with thin films on SAW devices, glassy polystyrene exhibited longer response times in contrast to the rapid responses for polysiloxanes films, which are low glass transition temperature materials [74]. After considering the physical properties of the coating (which dictates aspects of the sensor performance such as stability, reproducibility, and response time), the chemical properties must also be considered because they influence the sensitivity and selectivity of the sensor. Therefore, the functional groups of the coating are considered so as to

increase the strength of analyte/film interaction. These fundamental interactions include

dispersion interactions, dipole-induced dipole interactions, dipole-dipole interactions, and

hydrogen-bonding interaction (acidic analyte/basic coating or basic analyte/acidic

coating) [36]. Vapor sorption (gas-phase sensing) as a function of these interactions has

been systematically examined using linear solvation energy relationships (LSERs)

[69;74;108]. Although LSERs has been performed for gas-phase sensing, the results can

be used in aqueous environments as starting points to design polymer structures to

promote particular interactions for improved sensitivity and selectivity.

The analytes (OPs) studied in this work are organophosphorus compounds and

exhibit strong hydrogen-bond basicity. Therefore, hydrogen-bond acidic polymers are

ideal chemically sensitive layers for OP detection. A consideration of the chemical

structures that lead to hydrogen-bond acidity leads to a choice of fluorinated alcohols and

phenols as the functionality that should be incorporated into a polymer [108;109].

Furthermore, studies done by Abraham et al. [71] to compare hydrogen-bond acidities of

several propyl- or allyl-substituted bisphenol structures using inverse gas

chromatography and LSERs showed that fluorinated bisphenol-A structures were more

hydrogen-bond acidic than non-fluorinated analogs [71;108].These considerations

provide the design criteria for the synthesis of the hybrid organic/inorganic sensing layer,

bisphenol A-hexamethyltrisiloxane (dubbed BPA-HMTS), used in this work. The use of

the HMTS monomer introduces the desired low T_g and improves the adhesion of the thin

film to the gold surface of the SH-SAW device while the Bisphenol A monomer provides

targeted interactions for absorption of OPs. The coating was synthesized using the

hydrosilylation reaction.

In its most basic form, the hydrosilylation reaction involves the formation of a silicon-carbon (Si-C) bond by adding a hydrosily group ($\equiv$Si-H) across an alkene (-C=C-) in the presence of a noble metal catalyst, usually platinum (Pt) [108]. The hydrosilylation reactions and its use for the synthesis of BPA-HMTS are shown in Figures 3.6 and 3.7. The hydrosily group is present in HMTS whereas the alkene group is present in BPA. The disappearance of the hydrosily group at the end of the reaction is an indication that the reaction is complete. This reaction allows for diverse polymers with various functional groups to be synthesized with the resulting polymers exhibiting low glass transition temperatures. In addition, the hydrosilylation reaction has the desirable feature that it does not bias the selectivity of the resulting material since it produces only Si-C bonds and does not introduce any polar functionalities into the final material [74]. It is worth noting that by varying the ratios of the organic/inorganic materials, this synthetic technique can be used to prepare a variety of sensing layers with tunable chemical and physical properties. For example, by increasing the length of the siloxane chain, polymers exhibiting very low glass transition temperatures can be obtained [107].
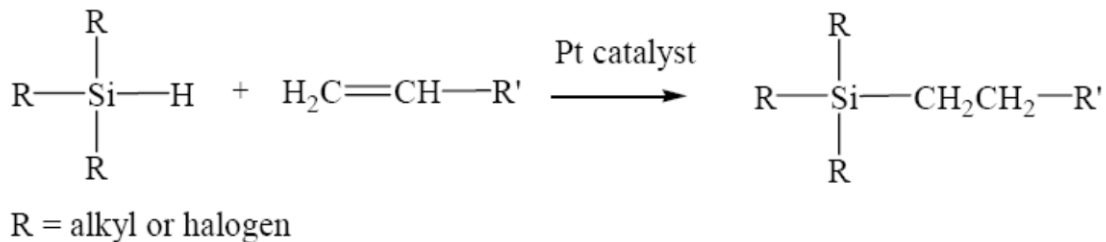
Figure 3.6: Hydrosilylation reaction showing the addition of Si-H bond across a -C=C-.
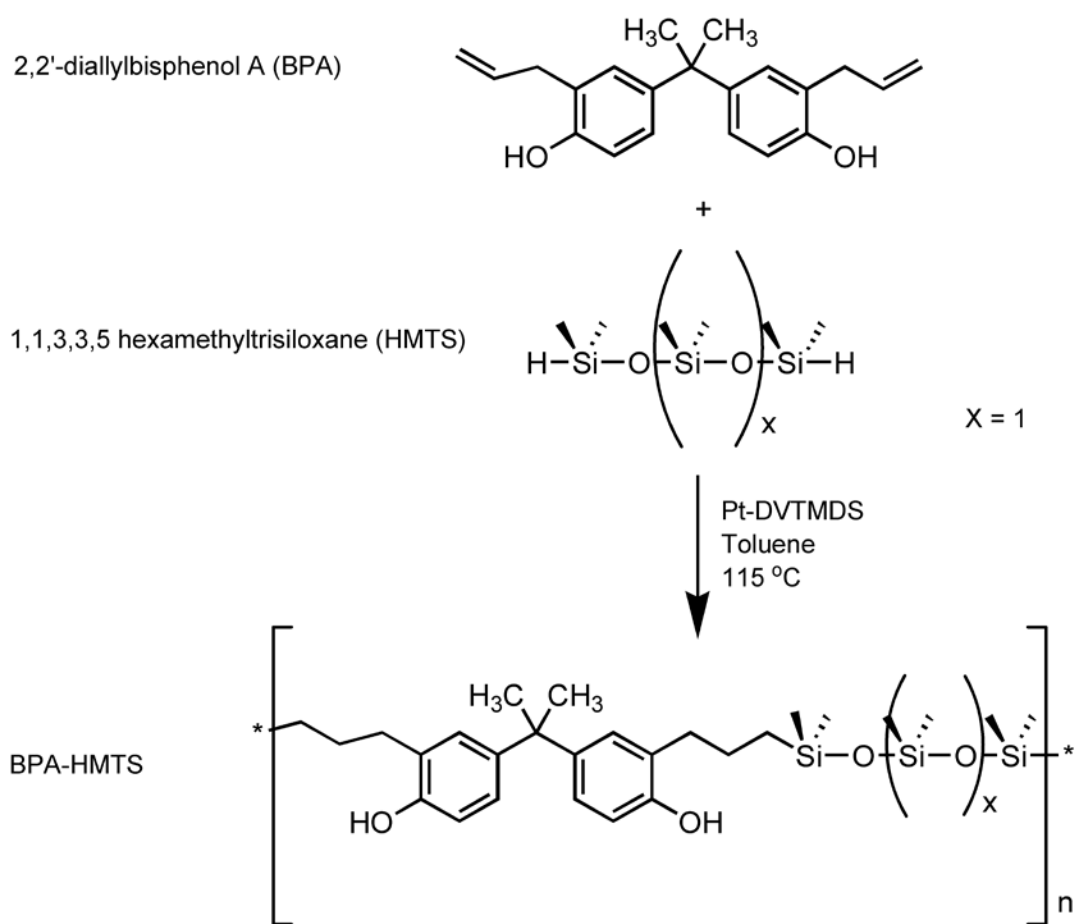
Figure 3.7: Polymerization reaction for the synthesis of BPA-HMTS.

4 EXPERIMENTAL METHODS

4.1 Introduction

In Chapters 2 and 3, the transduction mechanism, analyte sorption process, and sensor coating design for organophosphate pesticides were discussed. In this chapter, the methods used to achieve the research objective of designing and developing a highly sensitive chemical sensor for rapid in-situ detection and analysis of organophosphate pesticides in aqueous solutions using SH-SAW devices will be presented. This includes the list of the materials, equipment, analyte and coating characterization methods and results, sensor device preparation, and measurement procedures. The methods used to minimize noise variables (e.g. temperature fluctuations and pH variation) are also discussed. Some of the experimental procedures described in previous work [53;54;79;89;110].

4.2 Materials

Chloroform (99.8%), acetone (99%), anhydrous toluene (99.8%), 2-propanol, monobasic dihydrogen phosphate, 1,1,3,3,5 hexamethyltrisiloxane (HMTS), Platinum(0)-1,3-divinyl-1,1,3,3-tetramethyldisiloxane (Pt-DVTMDS) complex solution in xylene (Pt ~2 %), 2,2'-diallylbisphenol A (BPA), dibasic monohydrogen phosphate, epichlorohydrin, poly(epichlorohydrin), parathion-methyl, parathion, and paraoxon were purchased from Sigma-Aldrich (Milwaukee, WI) and used as supplied. Medium

molecular weight (M_w = 35,000) poly(methyl methacrylate) was purchased from Scientific Polymer Products, Inc. and used as supplied.

4.3 Equipment and Instruments

4.3.1 Spin Coater

A Specialty Coating System (SCS) Model P6024 spin coater is used in this experiment for film deposition on the SH-SAW device. This process deposits a relatively uniform film on the surface of the device [89]. The final film thickness and other properties depend on the nature of the polymer solution (i.e., viscosity, drying rate, percent solids, surface tension, etc.) and the spin parameters (i.e., final spin speed, acceleration, and ramp time) chosen for the spinning process [89]. A vacuum chuck holds the devices in place as they are spun at speeds between 2000 and 6000 rpm. In this work, final speeds and spin cycles of (3000/4500/5000) rpm and (30 sec/50 sec) were used, respectively. The final speed and spin cycle are shown in Figure 4.1.
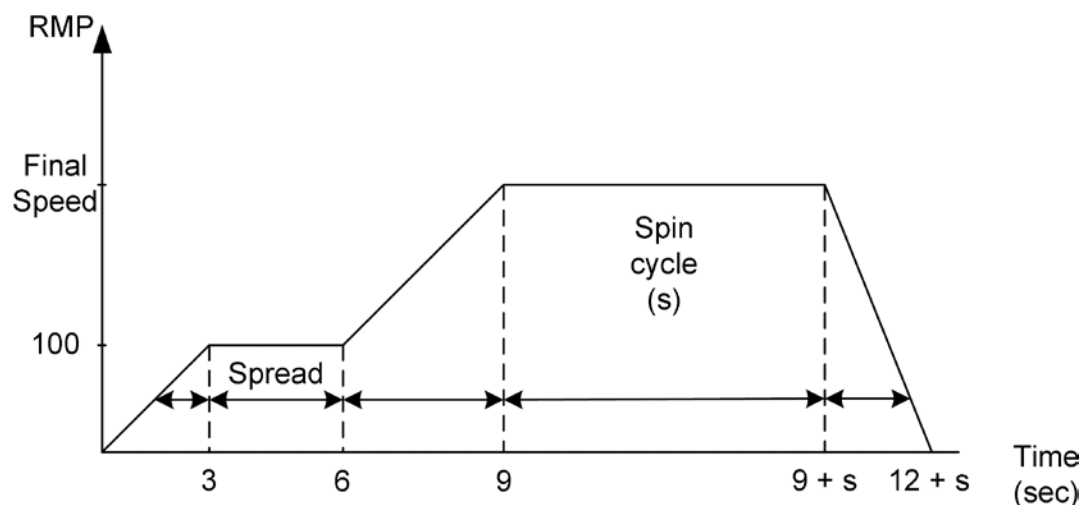
Figure 4.1: Spin coating cycle.

4.3.2 Profilometer (Surface Profiler)

A KLA-Tencor Alpha-Step IQ (a computerized, high-sensitivity surface profiler) is used in this work to measure the thickness of the film deposited on the device. This information is needed to analyze the sensor response. The chemically sensitive layers used in this investigation are rubbery in nature and hence a surface profiler with a pointed stylus cannot be used for direct thickness measurement. This problem is solved by depositing a layer of chromium on the entire substrate, as shown in Figure 4.2, before taking a profile. Figure 4.3 is a sample profile of the step height analysis measurement done with the profilometer. In this profile, the trace before 1500 μm and after 8000 μm represents the chromium layer. The polymer layer is represented by the wavy profile and its thickness is given by the difference between the delta regions, indicated by the cursors. Table 4-1 and Figure 4.4 provide a summary of the film thickness measurement results obtained with the corresponding spin coating conditions (polymer, polymer concentration, final spin speed, ramp time, and hold time) for this study. This is an

improvement in accuracy over previous film thickness estimation performed using the

TSM in conjunction with the Sauerbrey equation [53;79;89].
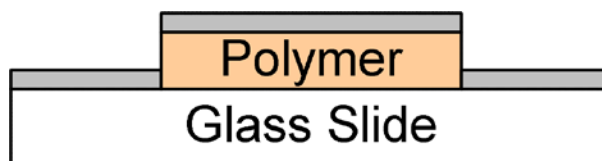
Figure 4.2: Schematic of film thickness measurement configuration. Note that Chromium is the grey layer.

Results from Step Height Analysis	
Pos (L)	715.61 μm
Pos (R)	4889.6 μm
Height (L)	-5850.5 Å
Height (R)	1809.7 Å
Width	4174 μm
Height	7660.2 Å
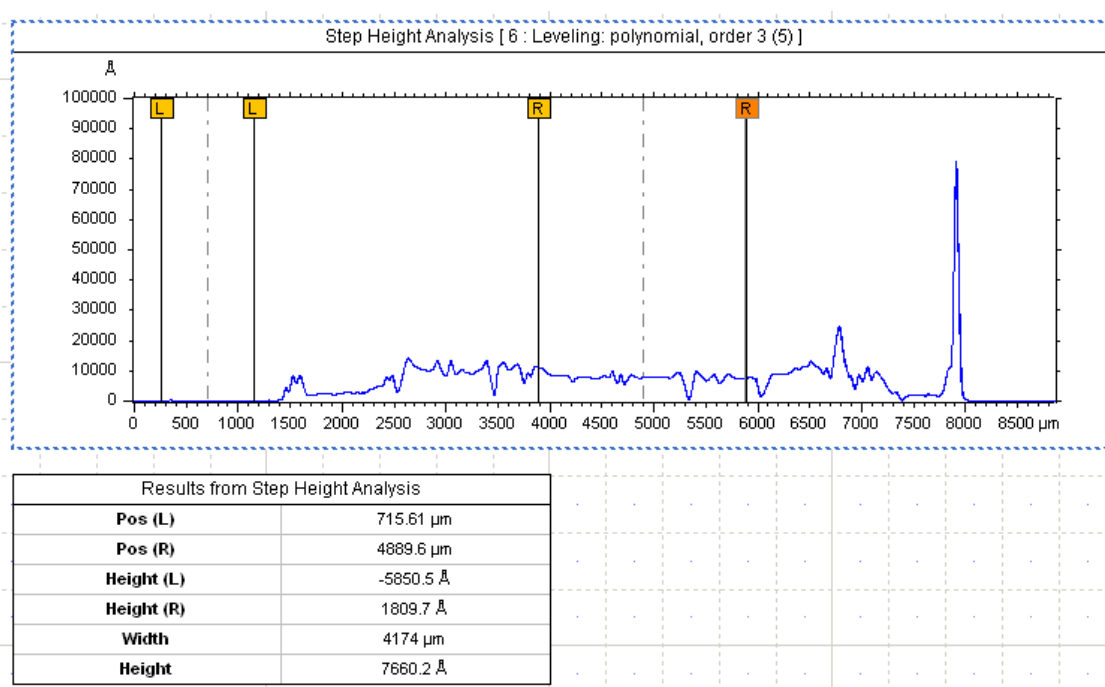
Figure 4.3: Step height measurement of 5.6%wt BPA-HMTS spin coated at 3000rpm, 33s (30s hold + 3s ramp) using delta averaging (opened cursors). A Gaussian filter (filter size 80 μm) and a 3rd order polynomial fit is used to measure the waviness and level the profile, respectively, before step height measurement .
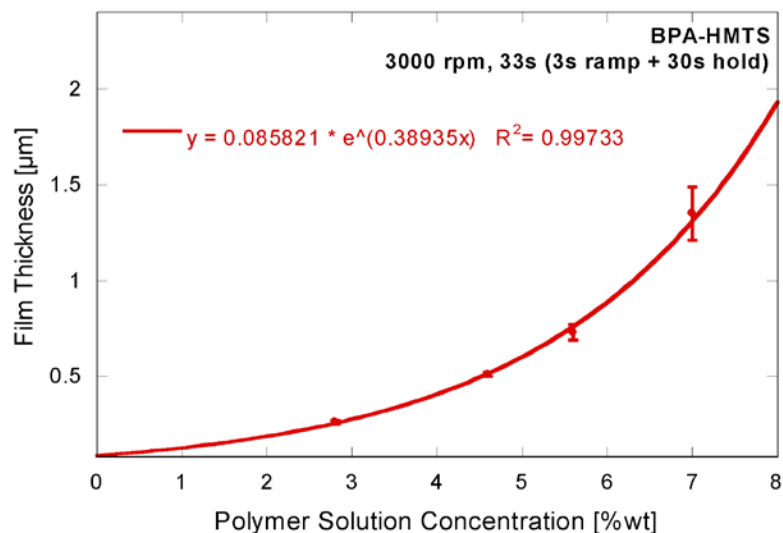
Figure 4.4: Film thickness calibration curve for BPA-HMTS.

Table 4-1: Film thickness characterization

Spin Coating Condition	Average Film Thickness (µm)	Standard Deviation
2.8%wt BPA-HMTS 3000rpm,33s	0.26	0.01
4.6%wt BPA-HMTS 3000rpm,33s	0.51	0.01
5.6%wt BPA-HMTS 3000rpm,33s	0.73	0.04
6.6%wt BPA-HMTS 3000rpm,33s	1.06	Estimated from fit
7.0%wt BPA-HMTS 3000rpm,33s	1.23	0.01
1.05%wt PECH 5000rpm,33s	0.25	0.01
2.10%wt PECH 5000rpm,33s	0.48	0.03
14.95%wt PMMA 4500rpm, 53s	0.39	0.03

4.3.3 Vector Network Analyzer

An Agilent 8753ES vector network analyzer (VNA) is used for device

characterization and the sensing measurement. The 8753ES has an integrated synthesized

radio frequency (RF) source, S-parameter test set, and a tuned receiver. A full-two port

calibration is performed for high measurement accuracy. This instrument is used to

measure the insertion loss (log magnitude), frequency, phase associated with S_{21} transmission response.

4.3.4 Switch Control Unit

In this investigation, an Agilent 3499A switch control unit is used to switch from one delay line to another periodically. This allows for differential sensor measurements to be performed.

4.3.5 FTIR Spectrometer

In order to identify the functional groups in the coating, infrared absorption spectra were obtained using a Perkin Elmer Spectrum 100 Fourier Transform Infrared (FTIR) spectrometer equipped with a single reflection ZnSe attenuated total reflectance (ATR) accessory from Pike Technology. Infrared spectra were recorded at a resolution of 2 cm^{-1}, averaged over 4 scans, in the range 675-4000 cm^{-1}.

4.3.6 NMR Spectrometer

In order to obtain information on the number and types of chemical entities in the coating, a Varian 400 HMz spectrometer is used to perform ^{1}HNMR and ^{13}CNMR spectroscopy in chloroform-d (CDCl$_3$).

4.3.7 UV Spectrophotometer

A Perkin Elmer LAMBDA 35 spectrometer was used to perform UV- VIS absorption spectroscopy on the analytes. This aided in the characterization of the analytes the pH range of 4.7 to 9.

4.3.8 Differential Scanning Calorimeter

Differential Scanning Calorimetry (DSC) was performed under nitrogen on a DSC 822e Mettler Toledo Inc (Columbus Ohio) instrument. The glass transition temperature, T_g, for the polymers is reported as the inflection point in the DSC trace. The sample was heated at a rate of 5 °C/min in the temperature range -80 °C to 120 °C. During this measurement, the difference in the amount of heat required to increase the temperature of the sample and the reference is measured as a function of temperature. During heating, the sample undergoes a phase transition and more or less heat is needed to flow to it than to the reference to maintain both at the same temperature. In determining the T_g for BPA-HMTS, more heat is required to convert BPA-HMTS from the solid form to the liquid form. DSC data for BPA-HMTS is shown in Appendix A.

4.4 Coating Synthesis

BPA-HMTS was synthesized by modifying a procedure reported by Grate et al [107]. Below are step-by-step directions for preparing BPA-HMTS. A general description of the synthesis process is given in [54].

1. Turn on Corning (420D) hotplate and set plate temperature to 250 °C to heat oil bath (100-110 °C).

2. Add 10 mL of toluene into 40 mL vial and reset scale to zero.

3. Add (0.882 g, 0.00286 mol) of BPA (M_w = 308.41 g/mol).

4. Stir mixture on stir plate for about 5 min at 400 rpm until a homogeneous mixture is obtained.

5. Add 10 mL of toluene and reset scale to zero.

6. Add (0.566g, 0.00271 mol) of HMTS (M_w = 208.48 g/mol) to give a mole ratio for reacting functional groups, r = [SiH]/[CH$_2$=CH], of 0.95.

7. Stir for about a 1 min and monitor the presence of the Si-H (2125 cm^{-1}) group by FTIR (see Figure 4.5a).

8. Set scale to zero and add two drops (~ 0.02 g) of Pt-DVTMDS.

9. Stir the solution at 400 rpm in the oil bath (110-115 °C) for 20 minutes.

10. Monitor the disappearance of the Si-H (2125 cm^{-1}) group by FTIR (see Figure 4.5b).

11. Add 0.17 g (for a total of 0.736 g, 0.00353 mol, r = 1.23) of HMTS to the reaction mixture and stir for 20 minutes.

12. Monitor the presence of excess Si-H by FTIR spectra (see Figure 4.5c)

13. Add five drops (~ 0.058 g) of the catalyst to terminate the polymer with vinyl groups.

14. Repeat steps 1-13 for another vial.

15. Transfer samples into three-neck round-bottom flask.

16. Polymerize using a reflux set-up in an oil bath at 100-110 °C for 2 hours while stirring.

17. Monitor the disappearance of the Si-H (2125 cm^{-1}) group by FTIR.

18. Add activated carbon to mixture and stir in oil bath for 30 minutes to remove the catalyst.

19. Filter solution to remove activated carbon. Finest particle size filter paper is recommended. Filter at least three times.

20. Remove solvent by rotary evaporation. Care must be taken to not perform rotary evaporation for too long, otherwise some of the sample may be lost.

21. Transfer to a watch glass and heat under vacuum at 60 °C for 36 hours to remove residual solvent.

22. Monitor the disappearance of the Si-H (2125 cm^{-1}) group by FTIR (see Figure 4.5d). Note that the amplitude associated with O-H stretching mode is larger because the solvent has been removed.

4.5 Coating Characterization

Spectroscopic characterization was obtained on a Perkin Elmer Spectrum 100 FTIR spectrometer and Varian 400 NMR spectrometer. Differential Scanning Calorimetry (DSC) was perfomed under nitrogen on a DSC 822e Mettler Toledo Inc (Columbus Ohio) instrument. Glass transition temperature, T_g, is reported as the

inflection point in the DSC trace. Decomposition temperature, T_d, is reported as the temperature at 10 % mass loss in Thermogravimetric data. The film density, ρ_f, was estimated using a 1 mL volumetric flask. Briefly, a 2.8 %wt BPA-HMTS or 4.4 %wt BPA-HMTS in chloroform was prepared. The empty flask with the stopper was then weighed (W_1) and partially filled (50%) with BPA-HMTS solution. The flask was placed in an oven and heated at 50 °C for 24 hrs to remove the solvent. Afterwards, the flask with the lid and just the polymer was weighed (W_2). The flask was then filled with deionized (DI) water to a total volume of 1mL and weighed (W_3). The density of the film (ρ_f), in g/cm^3, was then estimated using the relation

$$\rho_f = \frac{Mass}{Volume} = \frac{W_2 - W_1}{1 - V_1} \ , \tag{4.1}$$

where the volume of water, V_1, is given by W_3-W_2 because the density of water is 1 g/cm^3. The results obtained for BPA-HMTS characterization are shown in Figure 4.5 and described as:

FTIR (cm^{-1}): 3411 (O-H stretch), 2953, 2917, 2861 (C-H stretch), 1603 (C=C ring stretch), 1500 (Benzene ring vibration), 1411 (C-OH stretching mode), 1344 (O-H in-plane bending), 1255 (14B, Wilson's notation), 1040 (Si-O-Si stretch), 789 (CH3 rocking). ^{1}HNMR (σ 400 MHz, CDCl$_3$) 7.25 (d), 7.08-7, 15 (m), 6.69 (m), 5.31 (br), 5.03 (br), 4.6 (s), 3.7 (d), 2.5-2.6 (m), 1.32-1.6 (m), 0.5-0.59 (m), -0.02 – 0.1 (m). ^{13}CNMR (CDCl$_3$) σ 153.8, 133.0, 122.1, 127.9, 128.9, 128.1, 125.6, 124.5. T_g (DSC) **4.95 °C**, T_d (TGA) 255 °C, ρf 1.15 g/cm.

These numbers are characteristics of the various groups present in the polymer.
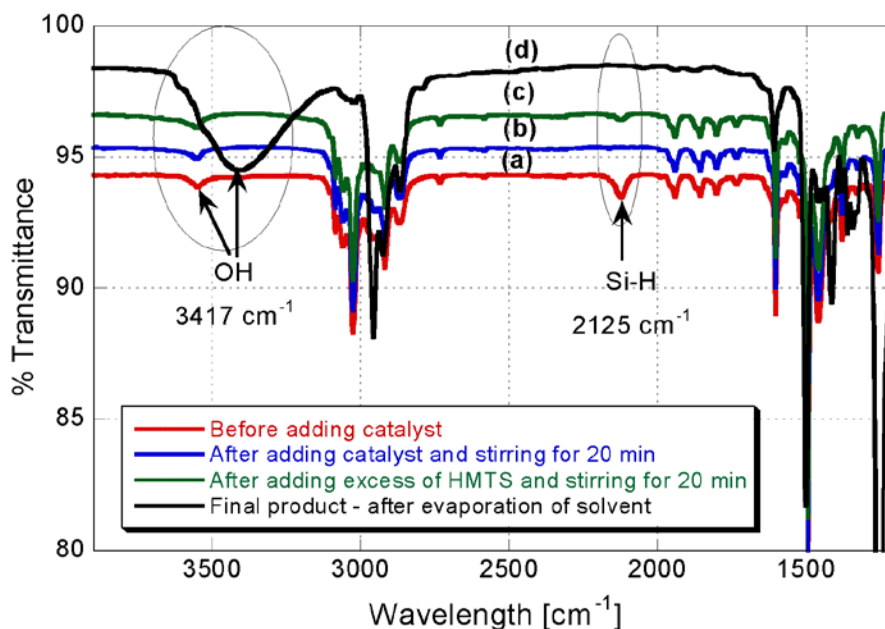
Figure 4.5: FTIR spectra characterization for the funtionalization of 1,1,3,3,5,5-hexamethyltrisiloxane (HMTS) with 2,2'-diallybisphenol A (BPA) using the hydrosilylation reaction (a) before adding catalyst (b) after adding catalyst and stirring for 20 min (c) after adding excess HMTS and stirring for 20 min (d) final product after evaporation of the solvent.

The structure of the final product, BPA-HMTS, is shown below (Figure 4.6). As discussed earlier, the organic portion (BPA) provides the functional group for analyte coating interaction while the inorganic portion (HMTS) provides the porous backbone for rapid analyte absorption.
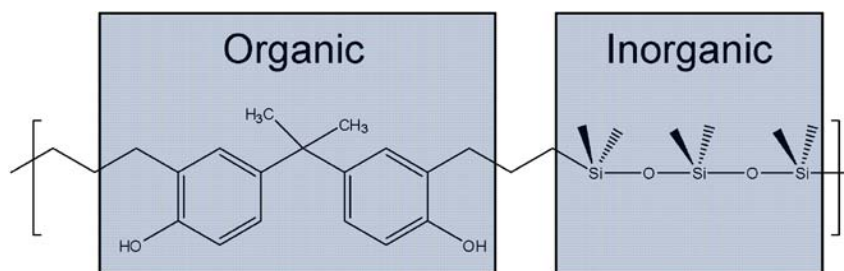
Figure 4.6: Chemical structure of BPA-HMTS.

4.6   Analyte Characterization

Three OPs (parathion-methyl, parathion, and paraoxon) are studied in this work. These analytes were chosen to study the effect of the alkyl functional group and oxygen-analogue on rate of analyte absorption by polymers. Additionally, this will help to determine if pattern recognition techniques can distinguish between analytes having only one molecule difference in their chemical structures. The physical properties of the OPs studied in this work are shown in Table 4.2. Note that the slight difference in physical properties is due to the alkyl group, sulfur atom, and oxygen atom (see Figure 4.7).
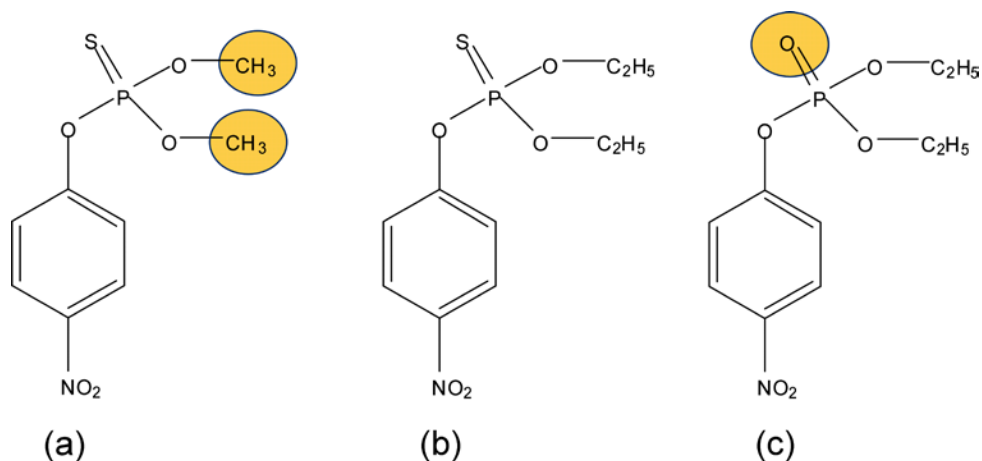
Figure 4.7: Chemical structures of organophosphates (a) parathion-methyl (b) parathion (c) paraoxon. The difference in chemical structure, with respect to parathion, is shaded.

Table 4-2: Physical properties of analytes

Analyte	Molar Mass (g/mol)	Area ($Å^2$)	Volume ($Å^3$)	Solubility (ppm or mg/L)
Parathion-Methyl	263.21	267.18[a]	227.73[a]	38.0[b] at 20 °C
Parathion	291.26	298.26[a]	261.30[a]	12.9[b] at 20 °C
Paraoxon	275.20	290.05[a]	251.72[a]	Not available

a. Calculation done using semi-empirical computational method at the PM3 level
b. [111]

As mentioned earlier, in the aqueous solutions, OPs degrade by means of chemical hydrolysis [10;103;112]. In general, this reaction is a first order process [10;103]. They also exhibit a second-order breakdown process in which the hydrolysis reaction depends on the pH of the solution [10]. To study the effect of solution pH on the temporal behaviour of the reacting species (deprotonated and protonated) for the decomposition of the analytes in aqueous solutions, the concentration of analyte in solution was fixed at 6 ppm (mg/L). The UV absorbance of the analytes at various pH conditions was then measured. It is noted that protonated and deprotonated species

possess different absorbance characteristics of UV light at various wavelengths [113].

From Figure 4.8, it is seen that the absorption spectra in both (a), (b), and (c) do not

change in the studied pH range, indicating that the analyte characteristics are not affected

by pH in this range i.e., the species distribution does not change. Similar results were

found for diazinon, another OP, in [113]. Here, the hydrolytic rate constant was found to

be approximately zero for the pH range 4-10. Based on these results, a phosphate buffer

solution of pH 6.20 ± 0.3 is used in this work because it offers a suitable compromise in

the range from pH 5.5 to 8.5 typically found in surface, ground, and river waters

[10;103;114].
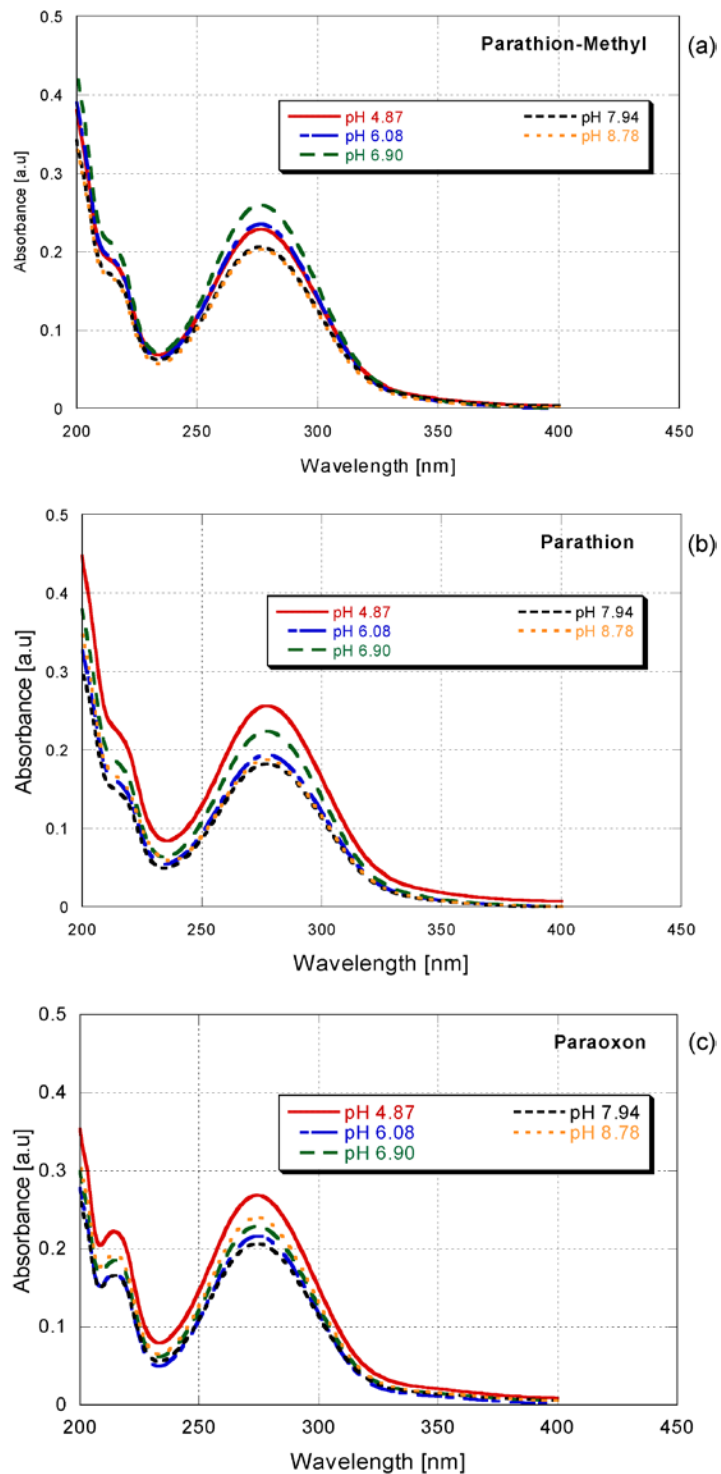
Figure 4.8: UV-vis absorption spectra for (a) parathion-methyl, (b) parathion, and (c) paraoxon in the pH range typically found in groundwater (i.e., 4.9 - 8.8). The absorption spectra in both (a), (b), and (c) do not change in the studied pH range, indicating that the analyte characteristics are not affected by pH in this range.

4.7   Experimental Setup

The measurement setup consists of the VNA measurement system, the sensing system, and a liquid sample delivery system. This is available in the Microsensor Research Laboratory at Marquette University for liquid-phase biochemical sensor work.

4.7.1   Measurement System

The measurement system is made up of the vector network analyzer (VNA), the switch control unit, an HP 34401A multimeter, and a PC based HP VEE control software for data acquisition. These instruments are connected together via a general purpose interface bus (GPIB), as illustrated in Figure 4.9. The HP VEE program is used to collect data (loss, frequency, phase, and temperature) every 30s. This information is transmitted between the measurement system and the PC via a general purpose interface bus (GPIB) and is saved in standard ASCII text format (.dat) for analysis using Excel and MATLAB$^{\circledR}$ R2008a.

4.7.2   Sensing System

The sensing system includes the guided SH-SAW device, the mounting elements and a specially designed flow-through cell to facilitate exposure of the coated device to the liquid of interest. The flow-through cell has a volume of 0.134 mL.

4.7.3 Temperature Control System

Temperature control of the sensor was achieved by placing the device holder in contact with a Peltier thermo-electric cooler (TEC) module. The Peltier TEC module was mounted on a heat sink and placed in a temperature controlled chamber. A MAX1978 EV kit, a DC power supply, and a10 kΩ NTC thermistor (YSI 44006) was used to implement a temperature control system for the Peltier TEC module.

The MAX1978 EV kit is a fully assembled PC board that implements a switch-mode temperature control for the Peltier TEC module. The MAX1978 EV kit can operate in either a closed loop or open loop configuration. In the present measurement, the open loop configuration was used because the switching action in the closed loop configuration affected the device response adversely. In the open loop configuration, a constant DC voltage between 1.46 V to 1.48 V is applied to the current-control input on the board to set the temperature. The thermistor is glued to the top surface of the Peltier element to monitor its temperature. An HP 34401A multimeter is used to read an output voltage from the PC board that is related to the thermistor reading. The flow cell is placed on top of the Peltier element enclosed in the temperature chamber, as shown in Figure 4.10. Thermal grease was applied at the interface of the Peltier element and flow cell to achieve good thermal conduction.

4.7.4 Liquid Delivery System

The liquid sample delivery system is comprised of a peristaltic pump (Cole Parmer Model 7553-30), a waste container, aqueous solution, polytetrafluoroethylene (PTFE) tubes, and fittings.
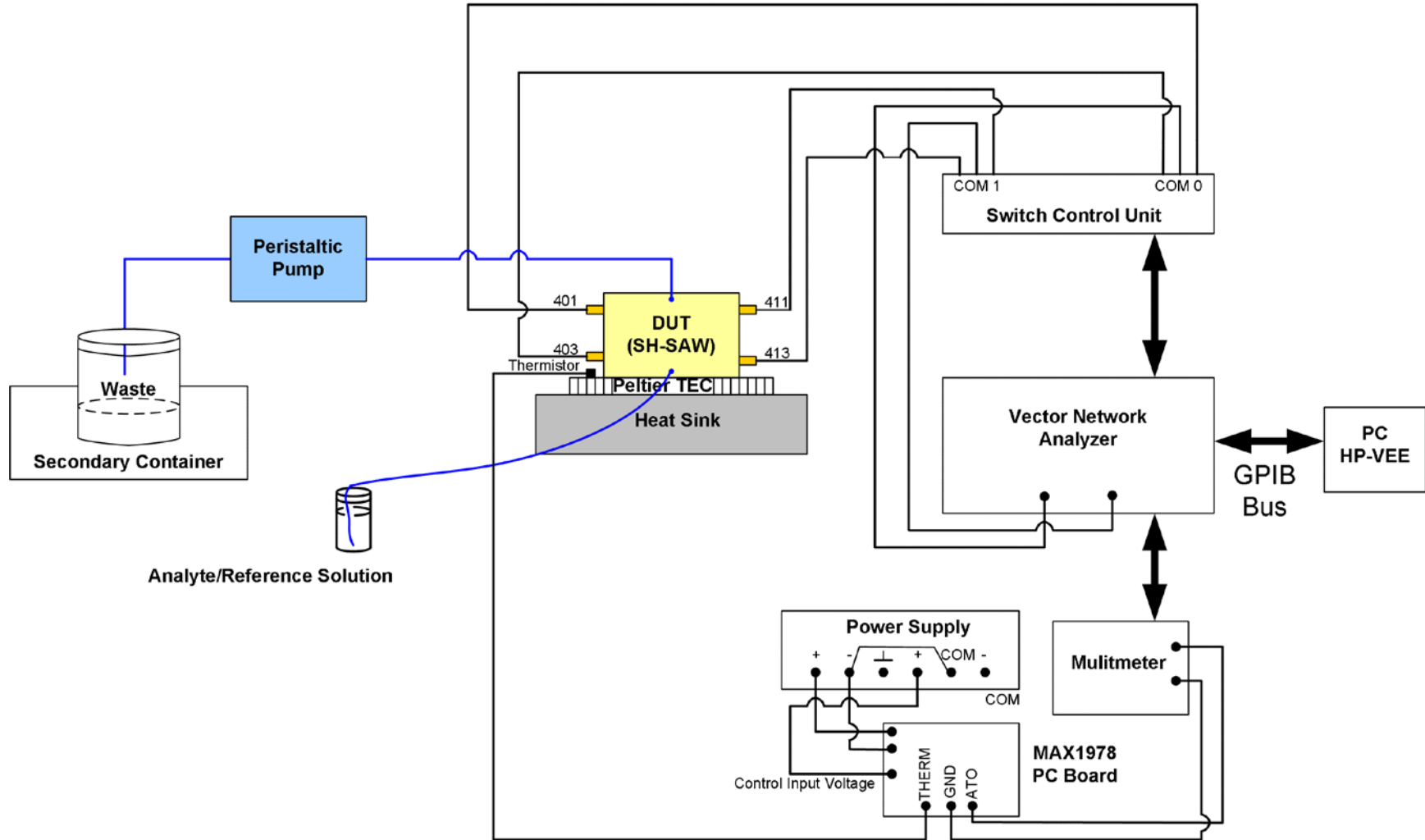
Figure 4.9: Schematic of the experimental setup used for sensor measurements. The system collects data via the GPIB bus.
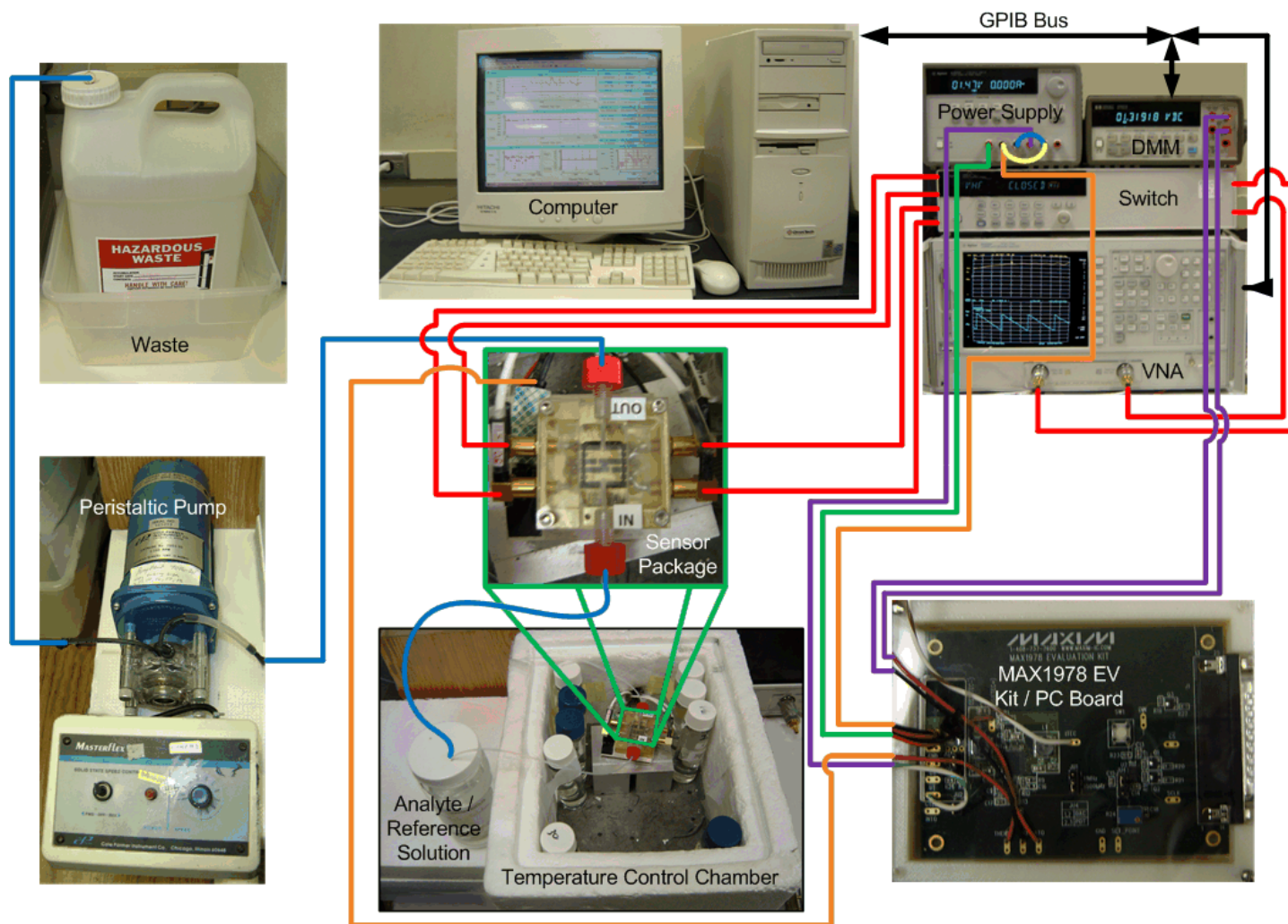
Figure 4.10: Experimental setup used for sensor measurements.

4.8 Measurement Procedures

4.8.1 Device Preparation and Characterization

Guided SH-SAW devices on $LiTaO_3$ are used as the primary sensor platform for the implementation of high-sensitivity chemical detectors for OPs in liquid environments. This substrate has both a high piezoelectric coupling constant and a high dielectric constant of $\varepsilon = 47$. The high piezoelectric coupling coefficient allows for the implementation of low-loss acoustic devices, and the high dielectric constant helps confine a sufficient portion of the electric fields generated by the IDTs to the substrate, even in direct contact with aqueous solutions ($\varepsilon = 75$) [51].

The device is fabricated on a 36º – rotated Y-cut X-propagation Lithium Tantalate (36º YX-$LiTaO_3$) piezoelectric substrate [79;115]. The device has twenty-eight 10/80 nm thick Cr/Au split finger pairs interdigital transducers (IDTs) having a periodicity of 40 µm. This periodicity corresponds to an operating frequency of approximately 103 MHz for the uncoated devices [45]. A dual delay line configuration with a delay time of ~ 2.15 µs is used. This configuration allows for one line to be used as a reference line and the other as the sensing line in order to reduce the effect of noise variables such as temperature variation and pressure interaction. In designing the devices, a metallized delay path (a thin Cr/Au (10/80 nm)) is used between the input and output IDTs to eliminate the acoustoelectric interactions between the IDTs [45;51]. This interaction, if not eliminated, will make it impossible to obtain reproducible results because of minor variations in ionic concentration of solutions in experiments [86]. Gold is chosen for the

IDT in chemical detection applications because it is inert and resistant to corrosion [36;89]. However, gold does not adhere well to acoustic wave substrates, so an under-layer of chromium or titanium is usually used to promote the adhesion and durability of the gold IDTs [36;89].

In addition, guided SH-SAW devices on quartz are investigated for the implementation of high-sensitivity chemical detectors for OPs in liquid environments. However, this substrate has a relatively low piezoelectric coupling coefficient as well a low dielectric constant of $\varepsilon = 4.5$. The low piezoelectric coupling coefficient allows for the implementation of high-frequency acoustic wave devices with linear phase. However, the low dielectric constant prevents a sufficient portion of the electric fields generated by the IDTs to be confined to the substrate in direct contact with aqueous solutions. As a result, the acoustic wave is completely attenuated in liquid. To overcome this problem, fused quartz layers (6 to 10 μm) are typically used to shield the IDTs. In this work, a novel solution combining Kapton® tape and a plastic sheet of thickness 25 μm and 12.7 μm, respectively, is used to shield the IDTs. The plastic sheet is used to reduce the amount of attenuation caused by the silicone adhesive on the tape. As a result, only the propagation path was coated for the quartz device.

The quartz device was fabricated on a quartz crystal with 92 electrode finger pairs. The devices are fabricated with 120-nm-thick Cr/Au (20/100 nm) split finger IDTs having a period of 32 μm. This periodicity corresponds to an operating frequency of approximately 155 MHz for the uncoated devices [45]. As for the LiTaO$_3$ device, a metallized dual delay line configuration is used so that one line can act as the reference line and the other as the sensing line.

Device Preparation

The devices first have to be prepared and treated to obtain optimal performance. This process involves several steps to reduce acoustic wave reflections from the ends of the substrate and bulk wave components which can affect the sensitivity and reproducibility of the device negatively. The steps used in preparing the devices include:

1. Measuring the spectrum of the unprepared device and saving it into memory.

2. Using sand paper with grit #40 to bevel the short ends of the substrate [89].

3. Periodically monitoring the device on VNA to check if passband ripple has been reduced.

4. When the peak to peak amplitude of the ripple has decreased, focusing sanding between the IDTs and contact pads.

5. Filing the device from the top, between the IDTs and contact pads.

6. Before performing an experiment, applying insulation tape to the bottom of the device to absorb reflected bulk wave energy.

4.8.2 Polymer Solution Preparation

Polymer solutions of BPA-HMTS, and PMMA, and PECH were prepared using the same solution preparation procedure, with slight modifications for PECH. The various concentrations of polymer solutions used in this study are shown in Table 4-1.

Final film thickness is a function of the viscosity (hence concentration) of the polymer solution and spin coating conditions (time and speed) and hence a thickness characterization experiment is performed to determine the appropriate spin coating speed

and polymer solution concentration (i.e., viscosity) for a desired film thickness, as shown in Figure 4.4.

Polymer solutions are prepared by using the weight/weight definition for percent solutions given by

$$wt\% = \frac{mass\ of\ polymer\,(g)}{total\ mass\ of\ solution\,(g)} \times 100\,. \qquad (4.2)$$

The general directions for preparing polymer solution are given below.

1. Calculate the mass of solvent and polymer needed to prepare a specific *%wt* polymer solution.

2. Clean solution container (vial) and dry.

3. Place the dried vial on an electronic balance and tare. Add polymer until desired mass is reached.

4. Using a pipette, add chloroform (for BPA-HMTS) and 2-ethoxyethylacetate (for PMMA) to the container until the total mass of the polymer and the added solvent reaches the determined value for the desired *wt%* solution.

5. Seal the vial and place on a magnetic stirrer at 1000 rpm for 10 minutes (BPA-HMTS) and at least 24 hours for PECH and PMMA. It is noted that for PECH, the plate temperature is set to 120 ℃ for 2 hours and then turned off. Stirring is then continued for another 22 hours.

4.8.3 Film Deposition

Before depositing the film, the devices are first cleaned for 3 min in ultrasonic baths of chloroform, acetone, and 2-propanol, respectively. The devices are then rinsed

with Milli-Q de-ionized (DI) water (resistivity 18.2 MΩ-cm) and dried with nitrogen [54]. This is done to ensure that the surface of the device is "wet" (this improves the adhesion of the polymer to the substrate). The electrical contacts and sensing line are masked, using Kapton tape, to prevent them from being coated by the polymer. After a final cleaning with nitrogen gas, the device is placed on the vacuum chuck. Using a disposable glass pipette, PMMA solution is dispensed onto the sensing area and the spin-coater is started (see Table 4-3 for spin coating conditions). For good reproducible coating, the device should be centered on the chuck, sufficient polymer solution dispensed in the middle, and the bowl covered [116]. After spin coating, the mask is removed and the device is baked at 180 °C for 90 minutes. Forty five minutes is allowed for the oven temperature to rise from room temperature to 180 °C. After baking, the device is allowed to cool down to room temperature. The electrical contacts and reference line are masked, using Kapton tape, and the sensing layer (BPA-HMTS or PECH) is deposited on the sensing layer.   The coated device was allowed to dry at room temperature 21.7 – 22.5 °C in a desiccator for at least 15 hours. The film thickness was calibrated using identical coating conditions to deposit films on glass slides having the same dimensions as the devices. As mentioned earlier, due to the rubbery nature of the sensing layers (BPA-HMTS and PECH), a layer of chromium was deposited over the entire surface so that the profilometer could be used for step-height measurement [54]. It is noted that baked PMMA acts as the reference line during sensor measurement.

4.8.4 Reference and Analyte Solution Preparation

The apparatus used to prepare the potassium phosphate buffer solution (PBS), reference solution, and analyte solution consists of vials, beakers, measuring cylinders, burettes, volumetric flasks, and pipettes. Since water is not the primary solvent, weight fraction definition for concentration (ppm) is used in this work. The equations used in preparing sample solutions are

$$ppm = \frac{M_{solute}}{M_{solution}} \times 10^6 , \qquad (4.3)$$

$$Concentration\ of\ solute = \frac{M_{solute}}{M_{solute} + M_{solvent} + M_{water}} \times 10^6 , \qquad (4.4)$$

$$Concentration\ of\ solvent = \frac{M_{solvent}}{M_{solute} + M_{solvent} + M_{water}} \times 10^6 , \qquad (4.5)$$

$$Density = \frac{Mass}{Volume} \qquad (4.6)$$

where M_{solute}, $M_{solvent}$, and M_{water} are the mass of solute, solvent (or methanol), and water in grams, respectively. The above equations were used to develop a spreadsheet, from which the input variables (M_{solute}, $M_{solvent}$, and M_{water}) could easily be manipulated to determine the required mass of analyte needed to obtain a desired concentration (ppm) of analyte solution. Below are the steps used to prepare the reference and analyte solutions

1. **Prepare potassium phosphate buffer solution (PBS)**

    a. 0.01M monobasic dihydrogen phosphate (KH_2PO_4)

       i. Measure 1.361g of KH_2PO_4 and transfer into 1000 mL flask

       ii. Add degassed water to 1000 mL mark.

    b. 0.01M dibasic monohydrogen phosphate (K_2HPO_4)

        i. Measure 1.742g of K_2HPO_4 and transfer into 1000 mL flask.

        ii. Add degassed water until 1000 mL mark.

    c. Combined solution

        i. Measure 13.2 mL of K_2HPO_4 solution.

        ii. Add 86.8 mL of KH_2PO_4 solution.

        iii. Dilute the combined 0.01M stock solution to 1 liter with degassed water. This gives a solution of pH 6.20 ± 0.1.

2. Prepare Reference Solution

    a. Measure 960 mL of PBS into flask.

    b. Add 1.11 mL of methanol.

    c. Stir at 1000 rpm for 1 hour.

3. Prepare concentrated analyte stock solution

    a. Measure 3 mL of methanol

    b. Add 25.8 µL, 25.7 µL, and 24.1 µL for parathion, paraoxon, and parathion stock solutions, respectively.

    c. Stir at 1000 rpm for 15 minutes and store sample in refrigerator.

4. Prepare analyte stock solution

    a. Measure 120 mL of PBS using burette into 120 mL jar.

    b. Add 140 µL of either parathion/paraoxon/parathion-methyl stock solution.

    c. Cap, seal, and stir at 600 rpm for 2 hours.

5. Dilute analyte stock solution using reference solution (see Table 4-3 to 4-5) to get appropriate concentrations.

Note: Methanol is used to increase the solubility of the analytes in water and diluting the analyte solution with the reference solution ensures that the pH of the solutions is constant from sample to sample.

Table 4-3: Dilution chart used to prepare aqueous samples of parathion

Volume of Reference Solution (mL)	Volume of Analyte Solution (mL)	Concentration of Parathion (ppm)	Concentration of Methanol (ppm)	Concentration of Phosphates (ppm)
121	5	0.50	913.70	146.53
116	10	1.00	913.71	146.53
111	15	1.50	913.72	146.53
106	20	2.00	913.74	146.53
101	25	2.50	913.75	146.53

Table 4-4: Dilution chart used to prepare aqueous samples of parathion-methyl

Volume of Reference Solution (mL)	Volume of Analyte Solution (mL)	Concentration of Parathion-methyl (ppm)	Concentration of Methanol (ppm)	Concentration of Phosphates (ppm)
121	5	0.50	913.72	146.53
116	10	1.00	913.75	146.53
111	15	1.50	913.78	146.53
106	20	2.01	913.82	146.53
101	25	2.51	913.85	146.53
96	30	3.01	913.89	146.53

Table 4-5: Dilution chart used to prepare aqueous samples of paraoxon

Volume of Reference Solution (mL)	Volume of Analyte Solution (mL)	Concentration of Paraoxon (ppm)	Concentration of Methanol (ppm)	Concentration of Phosphates (ppm)
116	10	1.00	913.71	146.53
111	15	1.50	913.73	146.53
106	20	2.00	913.74	146.53
101	25	2.50	913.76	146.53
96	30	3.00	913.77	146.53

4.8.5 Data Acquisition

A typical experimental run is started by exposing the coated device to the reference

solution (PBS with methanol) at a flow rate of 0.70 mL/min. This flow rate minimized

the hydrodynamic coupling between the flowing liquid and the crystal surface, but was

fast enough to purge the entire cell in less than one minute. This ensured that the sensor

sees a "step" in analyte concentration that is much faster than the dynamics of the analyte

sorption into the polymer coating [117]. An operating point of 101.4 MHz/101.45 MHz is

then selected and the HPVEE program started to collect data (insertion loss, frequency,

phase, and temperature). The data is saved for later signal processing. The reference

solution is pumped until the frequency response is stable. The coated device is then

exposed to various analyte concentrations. Between analyte exposures, the sensor

response was returned to its initial value by flushing the flow-cell with the reference

solution. The differential measurement thus reflects the sensor response due to

perturbations caused by only analyte absorption [54].

5 RESULTS AND SENSOR SIGNAL ANALYSIS

5.1 Introduction

The key science and technology issues for chemical monitoring systems include: sensitivity, selectivity, sensor response time, reversibility, and reproducibility. It is desired that the sensors exhibit: (1) high sensitivity so that the detection of trace amounts of the chemical analyte is possible; (2) high degree of partial selectivity so that the sensors can distinguish interfering substances from target species; (3) short response times for rapid analyte identification and quantification; (4) reversibility so that the sensors can be reused; and (5) high reproducibility to minimize false alarm rates.

These issues are examined in relation to the development of a portable chemical sensor that will allow for rapid on-line monitoring of organophosphorus compounds in contaminated ground and waste water. First, a brief review of previous work and the major conclusion will be presented. This will provide the motivation for the polymer synthesis and characterization studies performed in this work. The hybrid organic/inorganic coating, BPA-HMTS, is used to detect three organophosphate pesticides: parathion-methyl, parathion, and paraoxon. These analytes were chosen because of their similarity in chemical structure to investigate the selectivity of the new coating. In order to study the effect of coating thickness on sensor performance, the thickness of BPA-HMTS was varied from 0.25 μm to 1.23 μm. Several experiments were performed for different analyte/coating pairs. Each experiment was repeated at least three times for reproducibility/repeatability. For each analyte/coating pair, each measurement

was performed continuously over 72 hours using freshly prepared samples in order to examine the stability/reproducibility of the coating. The performance of the new coating, BPA-HMTS, was compared with PECH. All sensor measurements were compensated for baseline drift before analysis using either the reference sensor when possible or linear interpolation. An on-line technique for compensation of chemical sensor baseline drift has been previously developed by Josse's team [78;117] and it will be used in a field deployable smart sensor system. In section 5.8, the Extended Kalman Filter (EKF) is used to extract response parameters (i.e., the steady-state response and the absorption time constant) before the sensor response reaches equilibrium. As a result, a chemical sensor is able to perform analyte quantification and/or identification in a significantly shorter period of time. In the case of a sensor array, it is possible to extract the parameters before the steady-state values are reached and then use them as features in a classical pattern recognition technique [78]. In order to use the EKF, the sensor response has to be modelled. The model for the sensor response is presented and then used to perform on-line sensor signal analysis. It is shown that the additional information contained in the transient parameters may be unique to a class of analyte/coating pairs and thus can be used to improve array selectivity. The information presented here is useful when designing and developing smart sensor system for the detection of contaminants.

5.2   Preliminary Work: Review

As discussed in Chapter 1, there is a need to develop *in-situ* monitoring systems for rapid analysis and characterization of OPs in aqueous solutions. Initial work towards achieving this goal began with the use of SH-SAW devices coated with poly(epichlorohydrin) (PECH), polyurethane (PU), and poly(methylhydrosiloxane) (PMHS) for the detection of phosmet and parathion. In this section, the results from those studies and how they influenced the synthesis of BPA-HMTS will be discussed briefly. A detailed discussion can be found in [53;79;89;110].

Figure 5.1 shows typical responses (frequency shift) for a guided SH-SAW sensor coated with 0.7 µm-thick PECH exposed to various concentrations of phosmet (5-25 ppm) and parathion (2-8 ppm) in aqueous solutions. It is seen that the coating is very sensitive towards the analytes. However, the response time of the sensor (time taken for the sensor response to reach 90% of its total response, t_{90}) is relatively long, on the order of hours, hindering rapid analyte identification and quantification. A similar trend was observed for PU.

The response time depends on the absorption process. In turn, this process is influenced by temperature and coating thickness. As a result, the effect of temperature and film thickness on the absorption kinetics and hence the sensor response time for OPs were studied in an attempt to reduce the response time. Figure 5.2 and Figure 5.3 show that it is possible to decrease the sensor response time by increasing temperature and/or decreasing film thickness but at the expense of sensitivity. Furthermore, the results from this investigation suggested that the absorption process for OPs may be penetration limited. Therefore, it was hypothesized that coatings which have high surface-area to

volume ratios (i.e., high porosity and lower glass transitions than PECH and PU) would promote rapid OP absorption around room temperature. Consequently, PMHS was studied next. PMHS exhibited a drastic improvement in sensor response time with corresponding drastic reduction in sensitivity (see Figure 5.4). An alternative approach involving state-space modelling and nonlinear estimation-based signal processing was also investigated to decrease the time required for identification and quantification without decreasing sensitivity. This approach was able to reduce the time required for analyte identification and quantification by 40% [53;79]. While this was an excellent reduction in response time, it was still necessary to develop functionalized coatings to physically reduce the sensor response times while simultaneously offering a high degree of sensitivity for OP detection so that the full potential of the estimation technique could be realized. The findings from these studies led to the synthesis of a hybrid organic/inorganic chemically sensitive layer [bisphenol A-hexamethyltrisiloxane (BPA-HMTS)] for the rapid *in-situ* detection and analysis of OPs in the liquid-phase. In the following sections, the results obtained for BPA-HMTS will be analysed and discussed.
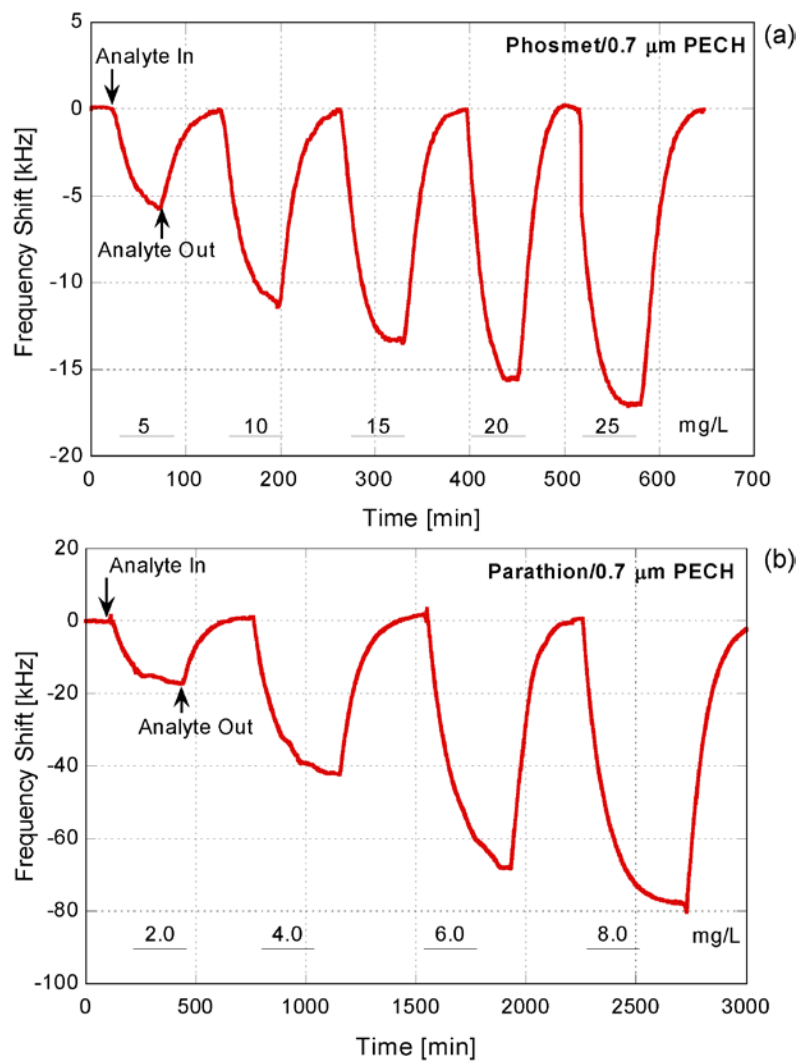
Figure 5.1: Measured frequency shift in the detection of (a) 5–25 ppm of phosmet (b) 2–8 ppm of parathion using a guided SH-SAW device coated with ~ 0.7 μm PECH layer.
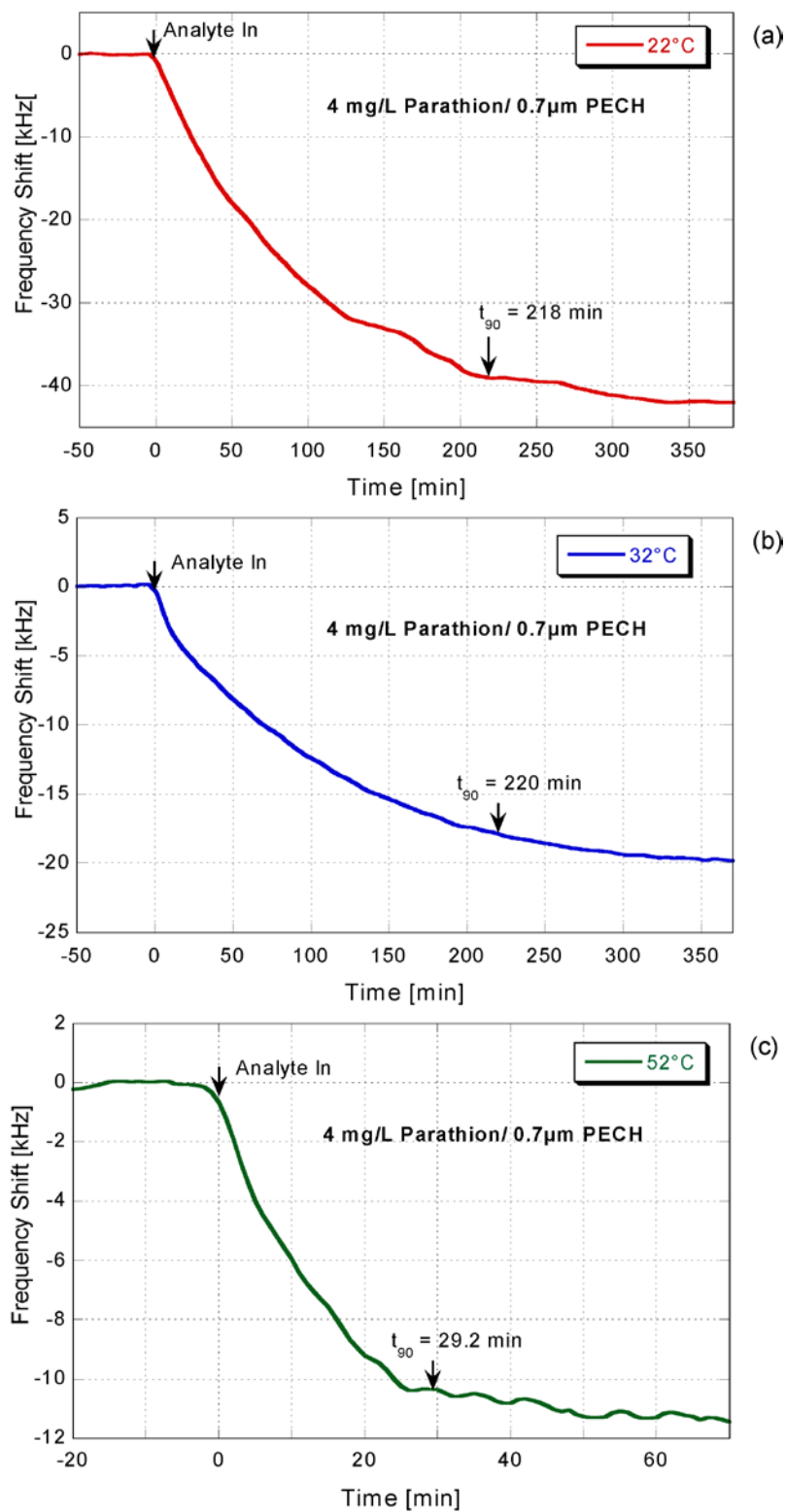
Figure 5.2: Effect of temperature (a) 22°C (b) 32°C (c) 52°C on the sensor response time for the detection of parathion (4 ppm) using ~0.7µm PECH-coated SH-SAW device. The response time is improved by 86% when the operating temperature is increased to 52°C.
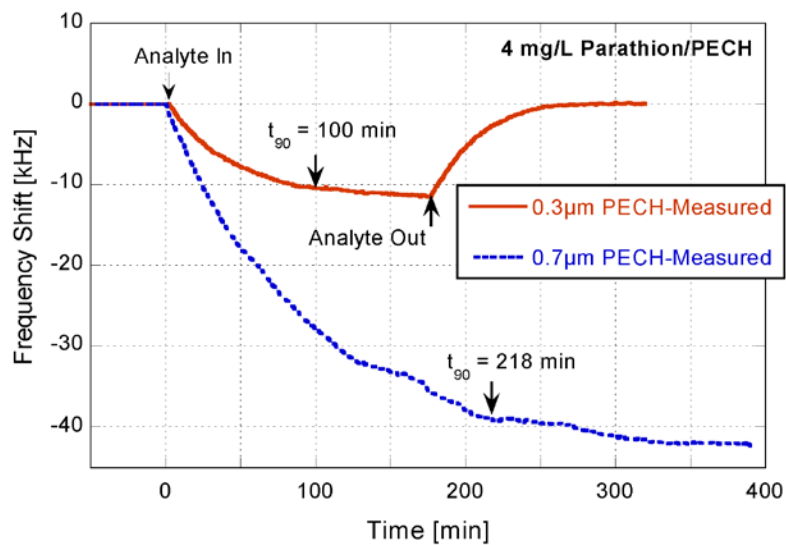
Figure 5.3: Effect of film thickness on the response time for the guided SH-SAW exposed to 4 ppm of parathion using ~0.3μm and ~0.7μm PECH layer, respectively. The experiment is performed at 22°C. The response times were determined by fitting an exponential to the measured.
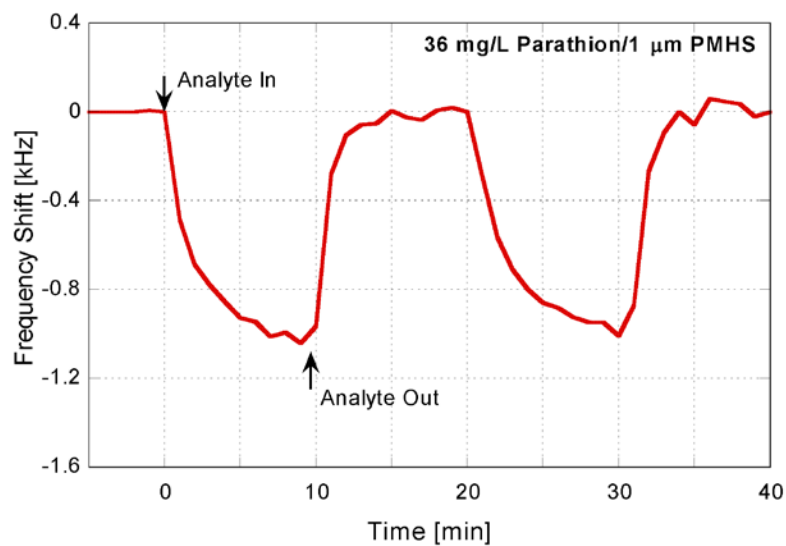
Figure 5.4: Frequency shift for the detection of parathion using poly(methylhydrosiloxane) (PMHS)-coated SH-SAW device with an estimated thickness of 1 μm. Measurement was performed at 22°C.

5.3 Device Characterization

Because the sensitivity of chemical sensors depends on both the transducer and chemically sensitive layer used, it is important to compare different acoustic wave devices for the detection of the same target analyte. For this reason, the performance of two acoustic wave-based chemical sensors are compared as a function of operating frequency and piezoelectric substrate. The two devices used here are a lithium tantalate (LiTaO$_3$) device operating at 103 MHz (LT103) and a quartz device operating at 155 MHz (Q155).

Two configurations were used for the deposition of BPA-HMTS because the piezoelectric substrates have different permittivity. For the LT103, both the propagation path and IDTs were coated with BPA-HMTS. For the Q155, only the propagation path was coated.

Before each experiment, the transmission spectrum of the uncoated device, coated device in air, and coated device in reference solution was monitored using the VNA. The deposition of a lossy polymer layer changed the insertion loss and transmitted frequency. Figure 5.5 shows the transmission and corresponding phase spectra of the LT103 device before and after it is coated with 0.5 μm BPA-HMTS and exposed to the reference solution. It is seen that the coating traps the acoustic energy (as indicated by the upward phase shift for the coated device in air) to the surface and minimizes the ripples present in the passband as a result of triple-transit interference (TTI). TTI is minimized further when the coated device is immersed in liquid because it experiences three-times the damping experienced by the main wave [86]. This results in a more linear phase in

the passband. Also, immersion in liquid results in a downward shift of the phase as a result of mass loading and change in the viscoelastic properties of the coating due to water and other molecules present in the reference solution. Figure 5.6 shows the transmission and corresponding phase spectra of the Q155 device before and after it is coated with 0.3 μm BPA-HMTS and exposed to the reference solution. The uncoated device has a lower passband distortion and better phase linearity than LT103. This is because the excitation of unwanted bulk waves is minimal and outside the device's passband for this quartz orientation. The characteristics of the coated device in air and reference solution are similar to that of the $LiTaO_3$ with the exception that the system is more damped; the average loss at the operating frequency of 101.4 MHz and 155.4 MHz is -30 dB and -35 dB for LT103 and Q155, respectively. It is noted that the thickness of the BPA-HMTS layer on Q155 was limited to less than 0.5 μm because this thickness resulted in a damped system of more than -40 dB, which is the maximum acceptable loss for the device because the noise floor for the device is -50 dB.
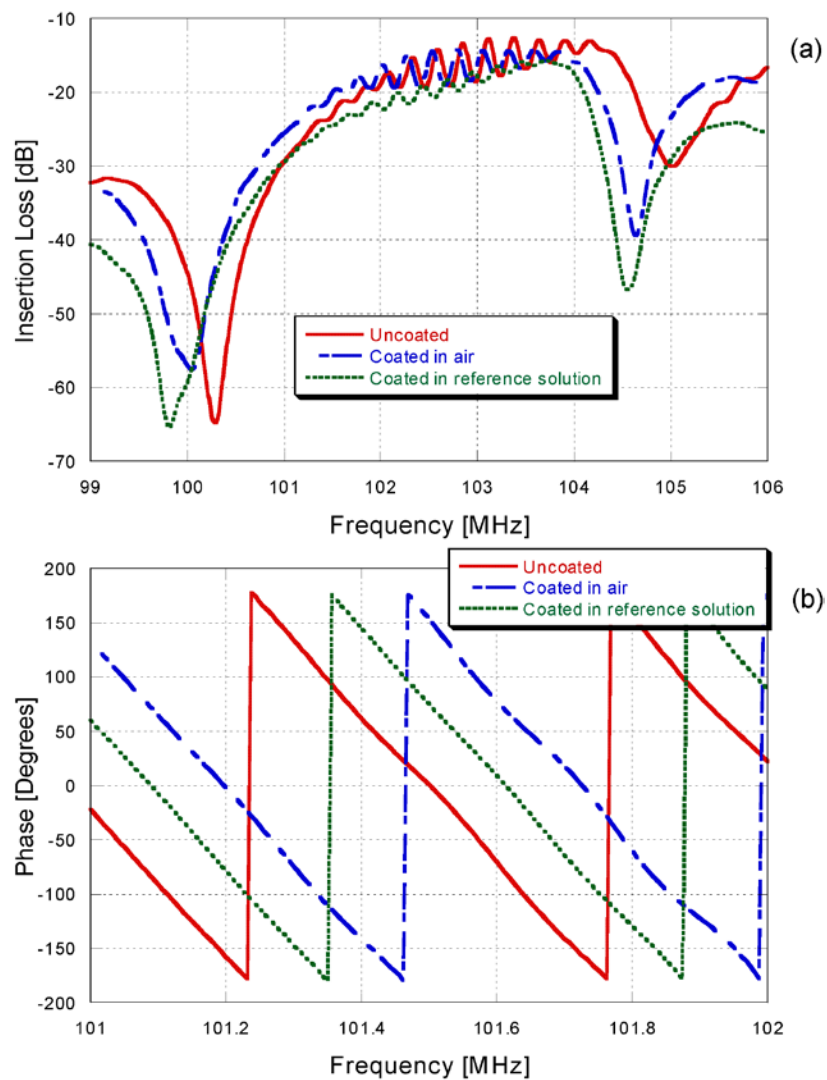
Figure 5.5: Measured spectrum of the LT103 device where the (a) insertion loss and (b) phase of the uncoated, coated device in air, and coated device in reference solution is plotted as a function of frequency. The device is coated with 0.5 µm-thick BPA-HMTS.
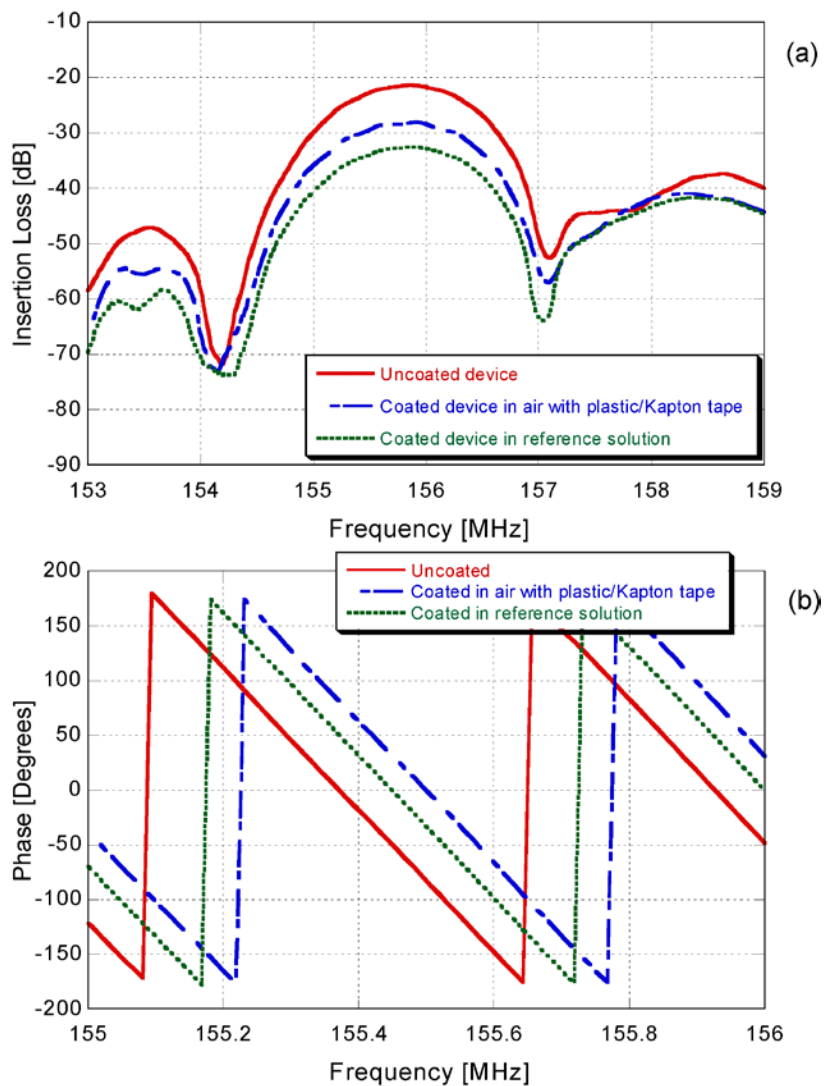
Figure 5.6: Measured spectrum of the Q155 device where the (a) insertion loss and (b) phase of the uncoated, coated device in air, and coated device in reference solution is plotted as a function of frequency. The device is coated with 0.3 µm-thick BPA-HMTS.

5.4 Sensor Response and Discussion

Several experiments were conducted for three analyte/coating pairs for the same coating thickness. Figure 5.7 shows sensor responses (frequency shift) for a guided SH-SAW sensor coated with 0.5 µm-thick BPA-HMTS exposed to various concentrations of parathion-methyl (0.5–2.5 mg/L), parathion (0.5–2.5 mg/L) and paraoxon (1-3 mg/L) in aqueous solutions. The reversible nature of the sensor response indicates that the analyte/coating interaction is physical rather than chemical. Therefore, the present sensor could be reused. Within the measured range, the frequency shift (Δf) is linear with analyte concentration and any slight deviations from linearity may be due to fluctuations in the concentration of the prepared solutions. Figure 5.8 shows the change in loss for repeated exposure to 2 mg/L of parathion-methyl, parathion, and paraoxon, respectively. It is seen that the device loss increases as a result of the coating becoming more rubbery upon analyte absorption, with parathion producing the greatest change in loss, an indication of larger plasticization effect. In Figure 5.9, the same device was used in three different experiments to demonstrate reproducibility/stability of the measurement. Note that the signal variation for zero concentration is relatively small and the value for the steady-state frequency shift are in good agreement.
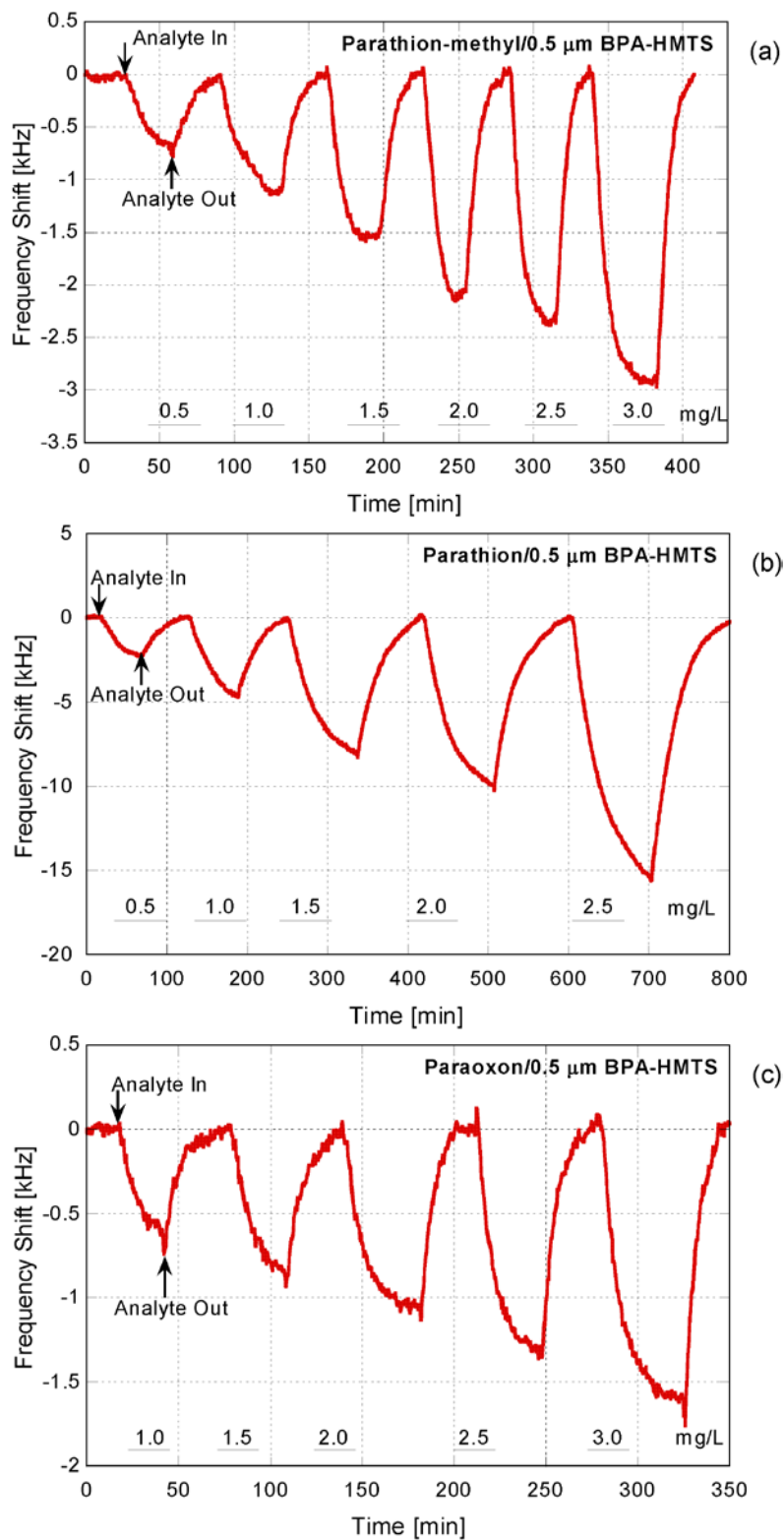
Figure 5.7: Measured frequency shifts in the detection of (a) 500 μg/L (ppb) to 3.0 mg/L (ppm) of parathion-methyl; (b) 500 μg/L (ppb) to 2.5 mg/L (ppm) of parathion; (c) 1 mg/L (ppm) to 3.0 mg/L (ppm) of paraoxon using 0.5 μm-thick BPA-HMTS on LiTaO$_3$ SH-SAW device.
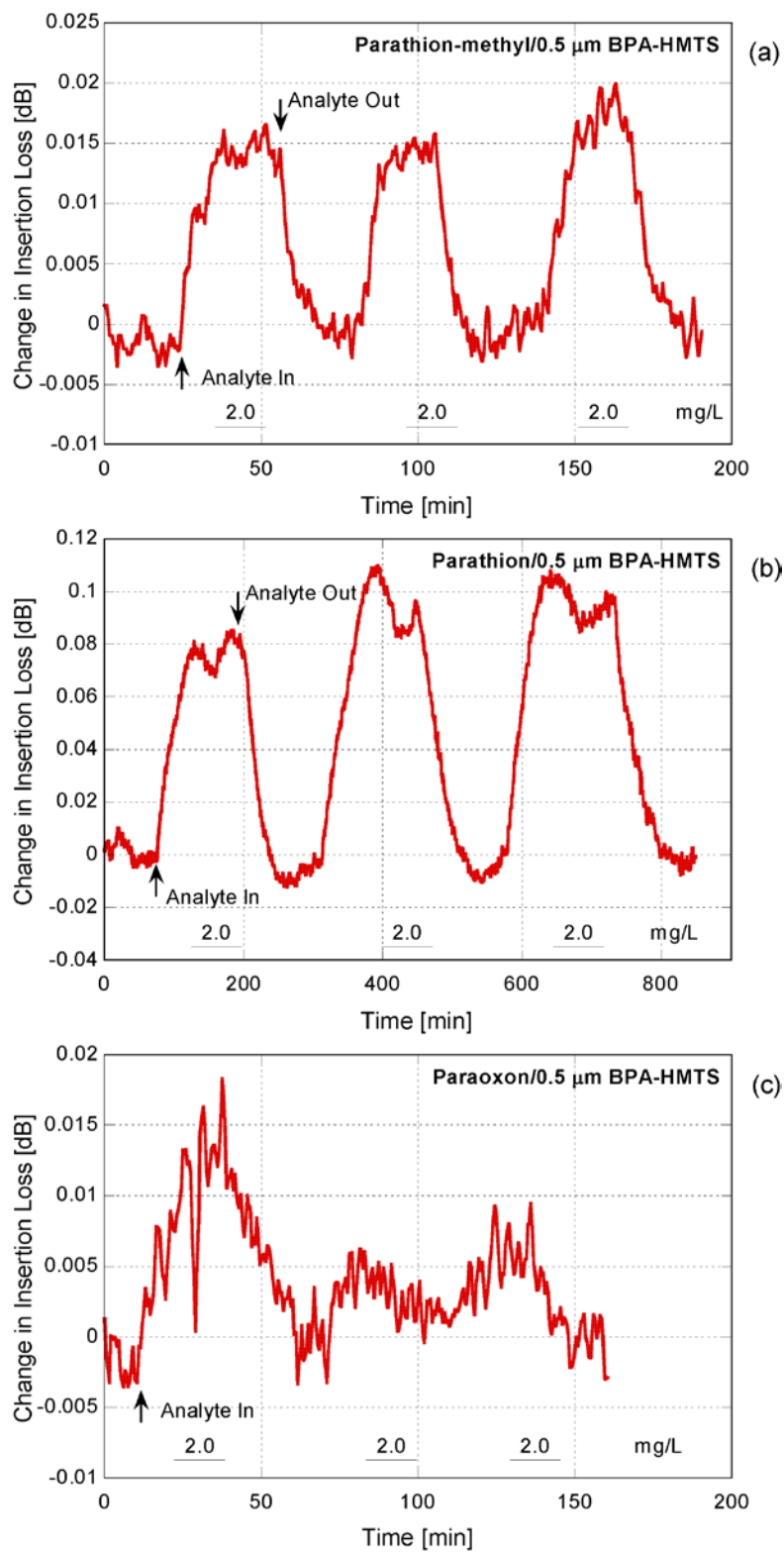
Figure 5.8: Measured change in insertion loss in the repeated detection of 2 mg/L of (a) parathion-methyl, (b) parathion, and (c) paraoxon using a 0.5 μm-thick BPA-HMTS layer on LiTaO₃ SH-SAW device.
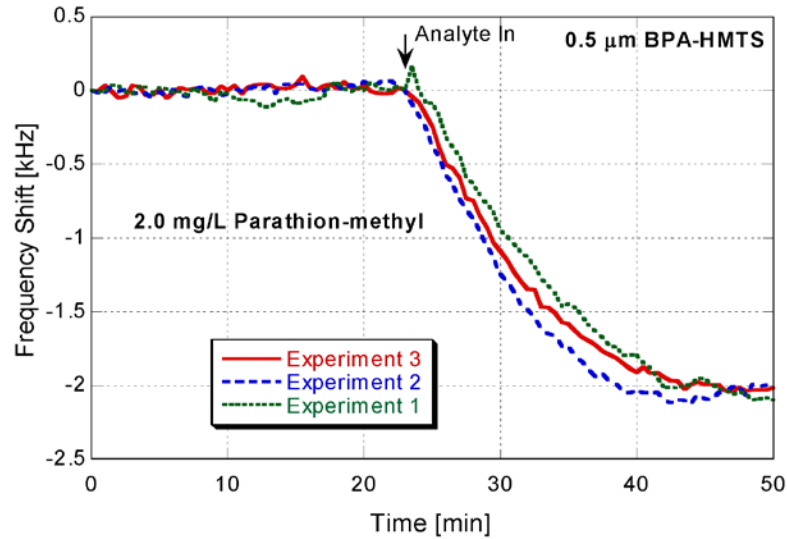
Figure 5.9: Measured frequency response for three independent experiments in the detection of 2.0 mg/L of parathion using a 0.5 μm-thick BPA-HMTS layer on LiTaO₃ SH-SAW device.

As discussed earlier, change in the guided SH-SAW response is due to changes in the film properties as a result of analyte sorption. Because the film is rigidly bonded to the substrate, it experiences translation and deformation under the influence of the traveling wave [90]. Translation motion produces a decrease in the SAW velocity that is proportional to the areal mass density contributed by the film- mass loading; film deformation produces energy storage (change in storage modulus, G') and power dissipation in the film (change in the loss modulus, G''), which change the phase velocity and attenuation, respectively [90]. In Figure 5.8, it is seen that the device loss increases as a result of the coating becoming more rubbery upon analyte absorption, i.e., G'' increases upon analyte absorption. This is in agreement with the positive change typically measured for the loss due to changes in the viscoelastic properties of the film upon analyte absorption [118] with the loss modulus effect on the attenuation being attributed to film plasticization or analyte induced softening and swelling [90;100].

In order to further understand and explain the sensor response, theoretical calculations were performed using equation 2.42. In the calculations, the density and thickness of the film is kept constant at 1.15 g/cm^3 (BPA-HMTS) and 0.5 μm, respectively; $v_2/\sqrt{P} = 0.226$ x $10^{-5}\sqrt{\omega}$ [(m/s)/$\sqrt{(W/m)}$][99], and the shear modulus is assumed to vary by a maximum of one order of magnitude upon exposure to 1 mg/L of analyte. Literature values are currently not available for the shear modulus at the operating frequency and thickness. Since BPA-HMTS is in the rubbery state at room temperature, simulation of the viscoelastic loading were performed using values in the range reported for rubbery polymers [36;90;99;119]. Figure 5.10 is a simulation of the sensor response for the case where the film properties are changed upon analyte sorption and the characteristics of the liquid are unchanged before and after perturbation. It is seen that the attenuation (loss change) gradually increases and the fractional velocity decreases for the region where the loss tangent, G''/G', is less than or equal to 0.4. This trend is in agreement with the measured response and confirms that the absorption of the analytes softens/plasticizes BPA-HMTS. Since the analytes (parathion-methyl, parathion, and paraoxon) have nearly identical mass and volume (see Table 4-2), one can say that the dominant contribution to the downward frequency shift is due to changes in the viscoelastic properties, specifically decrease in G', of the coating as a result of plasticization.
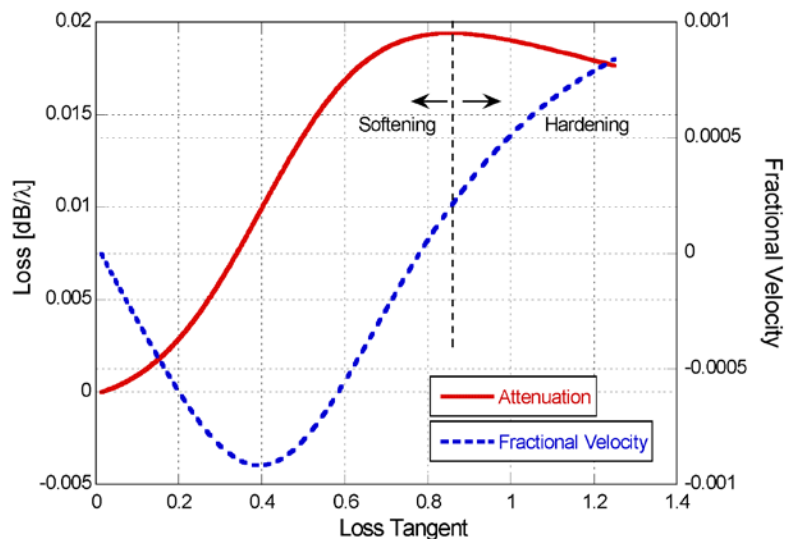
Figure 5.10: Calculated sensor responses as a function of loss tangent (G''/G') on the 3-layer geometry assuming the characteristics of the liquid are unchanged before and after perturbation. The polymer coating has a thickness of 0.5 μm and the liquid has a density of 997.5542 kg/m^3. G': 8 x 10^8 to 8 x 10^7 Pa; G'': 1 x 10^7 to 1 x 10^8 Pa.

5.5 Sensitivity, Partial Selectivity, and Limit of Detection

The coating, BPA-HMTS, synthesized in this work is partially selective and is sensitive to all the OPs, albeit to different levels. Because the viscoelastic contribution to the sensor response is significant, the sensitivity definition for gravimetric acoustic wave sensors will not be used here. Instead, the sensitivity (S) of the BPA-HMTS towards the analytes was evaluated using the relation $\Delta f/\Delta C$, where ΔC is the change in concentration and its value is given by the slope of the sensitivity curve. The sensitivity of BPA-HMTS towards the analytes is shown in Figure 5.11. It is noted that Δf is determined when the response has reached steady-state upon exposure to a given concentration of analyte and the error bar represents the standard deviation for three measurements. The small error bars is an indication of the stability of the coating in aqueous solutions since for each analyte/coating pair the measurements were performed with the coating immersed in

aqueous solution for at least 72 hours. Figure 5.12 compares the molar mass of the analytes to the sensitivity of BPA-HMTS towards the analytes. All values for a given analyte are normalized with respect to the corresponding value for paraoxon. Since the mass of the analytes are identical, the higher sensitivity exhibited by parathion suggests that it plasticizes the coating to a greater extent than the other analytes. For relatively low concentrations, the viscoelastic change/degree of plasticization and swelling is proportional to the amount of analyte absorbed by the coating. The amount of analyte absorbed depends on the polymer-liquid partition coefficient, which in turn depends on the analyte solubility parameters and the LSER coefficients for the polymer. For BPA-HMTS, the LSER coefficients (gas phase) are dictated by BPA (see Table 5-1). It is noted that these coefficients will be different in the liquid phase, because of the water solubility factor. Thus, care must be exercised in using this table. For a given polymer, these coefficients are constant, with the key primary coefficients of interest here being hydrogen-bond acidity, indicated by b. This coefficient describes the ability of the coating to interact with hydrogen-bond basic analytes. The solubility parameters for the analytes studied here are not available in the literature. However, the solubility of parathion-methyl and parathion in aqueous solution are 38 mg/L and 12.9 mg/L at 20 °C, respectively (see Table 4-2). From these values, one may hypothesize that the analyte with the lowest solubility in aqueous solution, in this case parathion, partitions into the coating to a greater extent (i.e., larger polymer-liquid partition coefficient) and hence more analyte being absorbed into the coating. This conclusion is in agreement with the trend observed for the detection of aromatic compounds (toluene, xylene, and ethylbenzene) in liquid [86]. Note that the ratio of the solubility of parathion-methyl to

parathion (~3) differs from how much more sensitive parathion (~6 times) is when

compared to parathion-methyl for the same thickness of BPA-HMTS (see Figure 5.11).

However, when concentration (C) is expressed as a percent of the saturation

concentration/solubility (C_{sat}) for a given analyte and frequency shift is divided by the

molecular weight/molar mass (M_w) of the analyte, the difference between the ratio of the

solubility of parathion-methyl to parathion (~3) and the ratio of their sensitive is smaller.

This is illustrated in Figure 5.13. In performing this conversion, the solubility values for

the analyte in water instead of water/methanol (data not available) are used. Furthermore,

it is assumed that the response is predominantly due to mass loading. Nevertheless,

Figure 5.13 does help us to understand the selectivity of BPA-HMTS in relation to the

number of analyte molecules absorbed and the thermodynamic activity of the analyte in

aqueous solution.
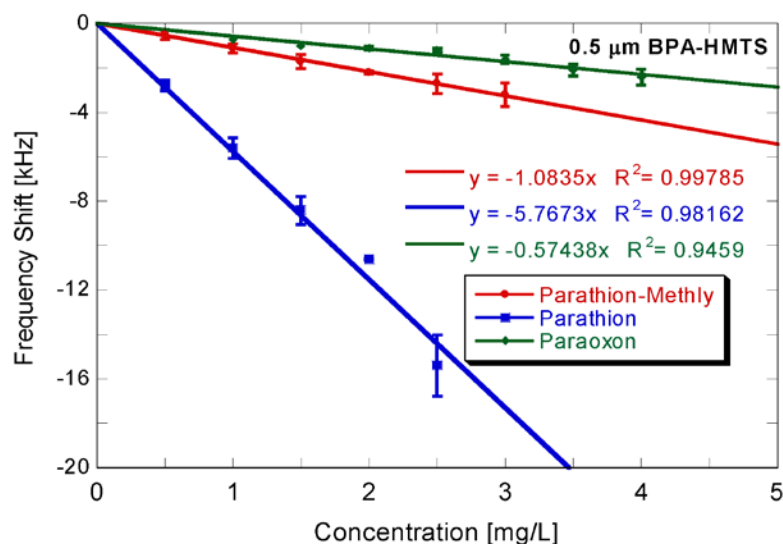
Figure 5.11: Sensitivity curve for the detection of parathion-methyl, parathion, and paraoxon in aqueous solution using a 0.5 µm-thick BPA-HMTS layer on LiTaO₃ SH-SAW device.
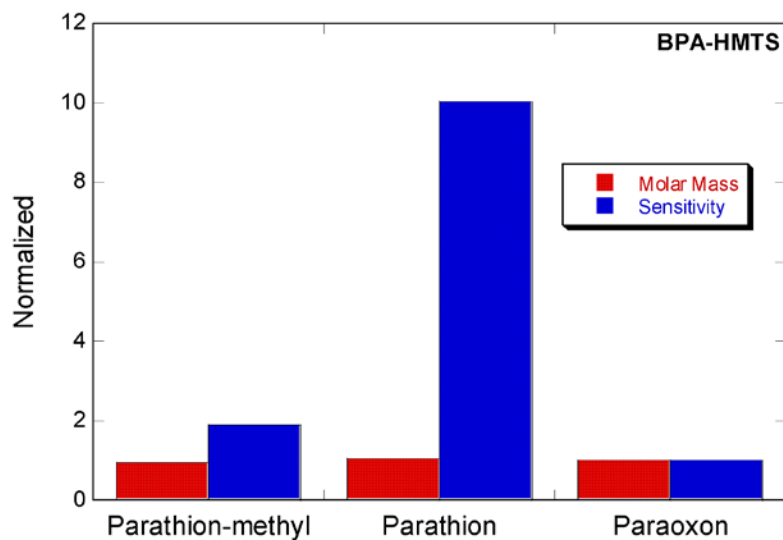
Figure 5.12: Comparison of molar mass of OPs to the sensitivity of 0.5 µm-thick BPA-coated in their detection. All values have been normalized with respect to the corresponding value for paraoxon.
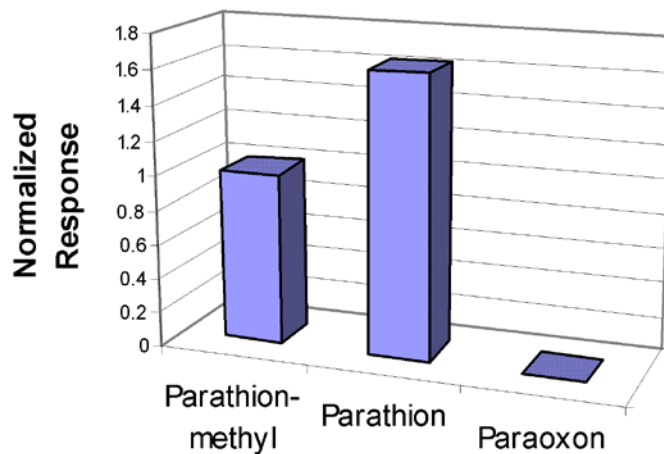
Figure 5.13: Comparison of the selectivity of 0.5 µm-thick BPA-HMTS coated SH-SAW device in the detection of OPs. All values have been normalized with respect to the corresponding value for parathion-methyl. Note that all three analytes have identical molar mass. Also, the solubility data is not available for paraoxon, hence computation was not performed for paraoxon.

Table 5-1: Linear solvation energy relationship (LSER) coefficients for BPA-HMTS in the gas phase [71]. It should be noted that although these coefficients will be different in water, it is hypothesized that the relative relationships presented here for gas will be the same for water. Thus, these values serve as a guide for understanding the nature of the analyte/coating interaction.

	c	*r*	*s*	*a*	*b*	*l*
BPA	-2.00	-0.92	2.24	2.79	**2.41**	0.975

Comparing the chemical structures (Figure 4.2), it is seen that the only difference between parathion-methyl and parathion is the alkyl substituents. The effect of the methyl group is to make the molecule more electrophilic/electronegative and hence more polar. Due to the polar nature of water, polar molecules are able to dissolve in water (i.e., "like dissolves like"), and hence the higher solubility of parathion-methyl. In other words, parathion-methyl prefers to be in aqueous solution as opposed to being in the coating. Similarly, the oxygen atom (a highly electronegative atom) in paraoxon makes it more soluble in water than parathion-methyl and parathion, respectively. It is noted that measurement of the analyte/coating partition coefficient using similar methods described in [100;120] will provide further insight into the nature of the analyte/coating interaction.

The limit of detection (LOD) of a chemical sensor is defined as the minimum measurable concentration that corresponds to a frequency shift no smaller than three times the root-mean-square noise level [36;118]. It is a function of both the sensitivity (S) and measurement noise (Δf_{noise}) and is given by [86]

$$LOD = \frac{3 \times \Delta f_{noise}}{S}.$$
(5.1)

The measurement noise is calculated by determining the root-mean-square of the signal in the reference solution. For the present measurements, the root-mean-square noise level for LiTaO$_3$ devices coated with 0.5 μm-thick BPA-HMTS is 0.04 kHz. Using Eq. (5.1), a limit of detection of 60 μg/L (ppb), 20 μg/L (ppb) and 100 μg/L (ppb) is estimated for parathion-methyl, parathion, and paraoxon respectively, when using a 0.5 μm-thick BPA-HMTS sensing layer. Note that concentrations as low as 500 μg/L (ppb) parathion have been measured in the present experiments. This concentration is significantly much lower than the typical concentrations found on agricultural produce ($\geq$ 10 ppm) [10]. It is also noted that these limits could not be achieved with PECH in previous work [89].

From Eq. (5.1), it is clear that the LOD can be improved by increasing the sensitivity and decreasing the signal noise. The signal depends on the device frequency of operation, coating stability in water, the flow system, and measurement system/circuit whereas the sensor sensitivity depends primarily on the frequency of operation and film thickness. In order to optimize the sensor performance, the effects of the frequency of operation and film thickness on sensitivity were studied. First, the thickness of the BPA-HMTS layer on LiTaO$_3$ SH-SAW device was decreased to 0.25 μm. In Figure 5.14, it is seen that for concentrations greater than 4 mg/L of parathion, the slope of the curve begins to change; for concentrations $\leq$ 4 mg/L of parathion, one can fit the data with a linear function having an R-squared value of 0.99. The value of 4 mg/L of parathion may be the concentration at which plasticization effect (hence viscoelastic loading) is significantly large and the Henry's law (region of linear behaviour with respect to analyte concentration) is no longer valid [121]. The observation that the fit does not pass through the origin is supported by the fact that for this thickness, 500 μg/L of parathion could not

be detected for the present non-optimized system. Next, the thickness of the BPA-HMTS

layer was varied from 0.25 μm to 1.23 μm.
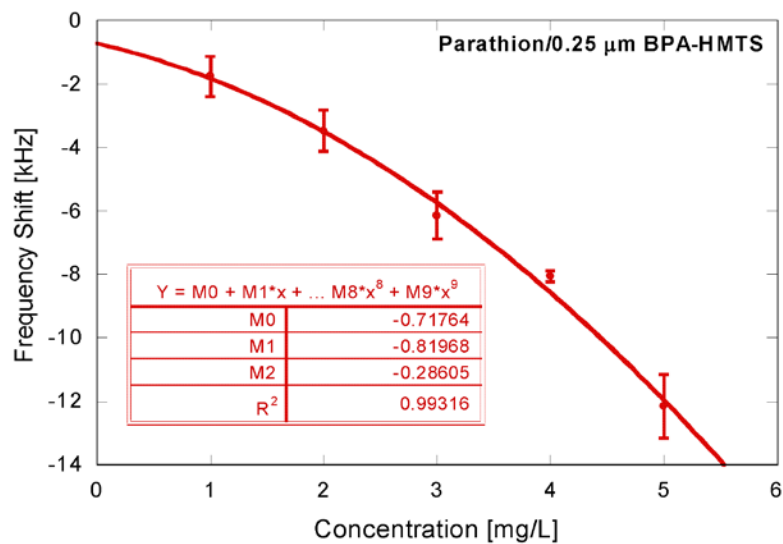
Figure 5.14: Sensitivity curve for the detection of parathion absorbed by 0.25 μm-thick BPA-HMTS layer on LiTaO$_3$ SH-SAW device.
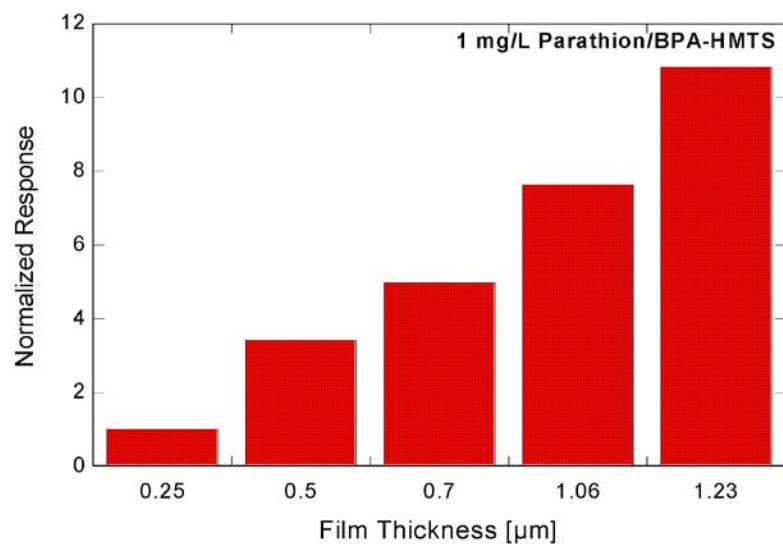
Figure 5.15: Effect of BPA-HMTS layer thickness on sensitivity of LiTaO$_3$ SH-SAW device.

In Figure 5.15, the frequency shifts upon exposure to 1 mg/L of parathion for different thicknesses of BPA-HMTS are normalized with respect to the frequency shift corresponding to 0.25 μm. It is noticed that the sensor sensitivity increases with increasing film thickness. This is due to the fact that the acoustic energy trapped to the surface increases with film thickness up to an optimum value [51;53]. Increasing acoustic energy at the surface makes the device more sensitive to surface perturbations. In addition, as the layer thickness increases, the amount of free volume increases. Consequently, the amount of analyte absorbed increases, leading to increased softening or plasticization. As will be discussed later, increasing film thickness also affects the sensor response time, another key design parameter.

Figure 5.16 shows the frequency shift for a Q155 device coated with 0.3 μm-thick BPA-HMTS on the propagation path and 1 mg/L of parathion. Even though the active sensing area and the film thickness are smaller when compared to the configuration used for LT103, Q155 exhibits about the same level of sensitivity for 1 mg/L of parathion. The high sensitivity is due to the fact that the acoustic energy at the surface is proportional to the operating frequency of the device. The high noise level is due to the fact that the deposition of 0.3 μm-thick BPA-HMTS on the propagation path results in a lossy system. It is noted that there are some key design challenges that have to be resolved before the full potential of Q155 can be realized. They include reproducible deposition of the polymer on the propagation path so that the propagating acoustic wave is not significantly distorted by the edge of the coating and minimizing the noise in the system; for the present measurements, the root-mean-square noise level is 0.16 kHz, four times higher than the measurements done with LT103 devices. As a result, the projected LOD

will be relatively higher. Nevertheless, the results demonstrate the potential of improving

the overall performance of the system by using a high-frequency device.
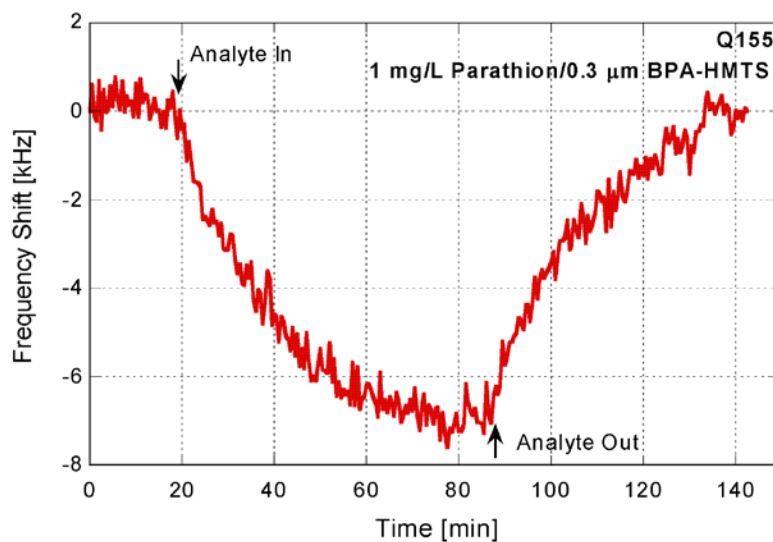
Figure 5.16: Measured frequency shift in the detection of 1 mg/L of parathion using 0.3μm-thick BPA-HMTS layer on the propagation path of the Q155 device.

5.6   Absorption Kinetics of Organophosphate Pesticides

As discussed in Chapter 3, the absorption process may be diffusion or penetration limited. Therefore, in order to correctly interpret absorption data, it is necessary to determine whether the transport of analyte through the polymer film is controlled by surface penetration or diffusion in the polymer network. This can be done by conducting studies at several film thicknesses or using an iterative process where key parameters are systematically changed until the proper relationship are found for the given experiment(s) [122]. Kinetic (study of molecular motion [36]) measurements for several BPA-HMTS thicknesses were performed in order to determine whether the effective absorption time constant (or simply absorption time constant) depends on surface penetration or bulk diffusion. In performing these measurements, the thickness of the polymer layer on LiTaO$_3$ was limited to less than 1.5 μm to avoid significantly attenuating the acoustic wave in liquid. Since the determination of the absorption time constant assumes a uniform and constant solution concentration of analyte, it was necessary to ensure that the ambient concentration in the flow-cell changes instantaneously upon switching samples. The flow rate was adjusted until a reasonable trade-off was found between the flow-rate and the resulting sensor noise. A flow rate of 0.7 mL/min was chosen for all measurements because it minimized the hydrodynamic coupling/sensor noise and ensured that the flow cell was completely flushed in less than a minute. It is noted that only five times the cell volume (0.134 mL) is required to completely flush the cell [36] and that the absorption time constants reported here were extracted using at least 10 minutes of data after analyte injection.

Normalized absorption curves for the detection of 1.0 mg/L of parathion using several thicknesses of BPA-HMTS are shown in Figure 5.17. Here, the frequency response has been normalized with respect to the steady-state value for each thickness. In this figure, it is very difficult to determine the rate-limiting step of the absorption process. However, plotting the data versus the square root of time ($\sqrt{t}$) will indicate which absorption model, Eq. (3.4b) or Eq. (3.6), should be used to explain the observed results. If the absorption process is diffusion limited, this plot yields a straight line that passes through the origin for the initial uptake [36;95]. In contrast, for a penetration limited absorption process, such a plot will yield a sigmoid or "S" shaped curved for the initial uptake. In Figure 5.18, it is seen that the absorption process here is limited by penetration and a linear variation with film thickness is expected. A log plot of the absorption time constant (τ_s) vs film thickness (h) shows a linear relationship, with the intercept equal to the reciprocal of the mass transfer coefficient ($1/\xi$), as shown in Figure 5.19a. It is noted that τ_s was extracted by fitting Eq. (3.4b) to the experimental data. The solution of the fit in Figure 5.19a yields a power function with the power close to one (see Figure 5.19b). The mass transfer coefficient for parathion/BPA-HMTS is extracted to be 2.1 x 10^{-8} cm/s.
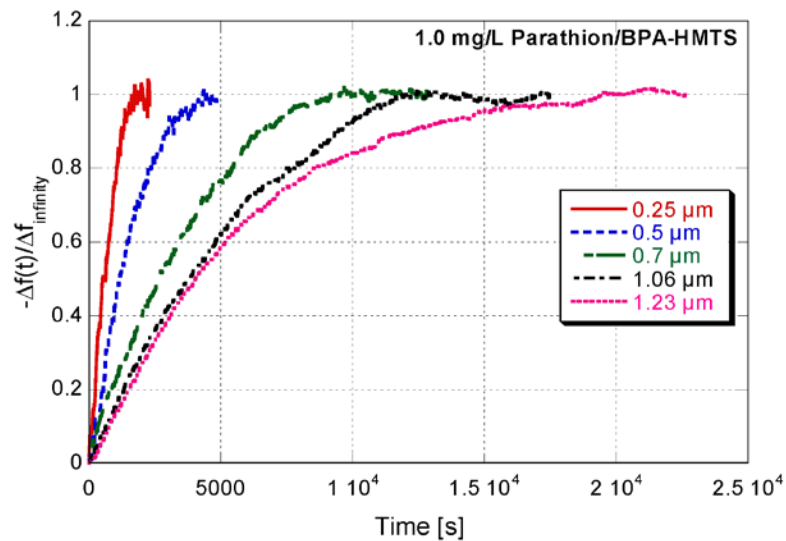
Figure 5.17: Absorption as a function of time during the detection of 1 mg/L (ppm) of parathion using varying thickness of BPA-HMTS (0.25 µm- 1.23 µm) layers on guided SH-SAW devices.
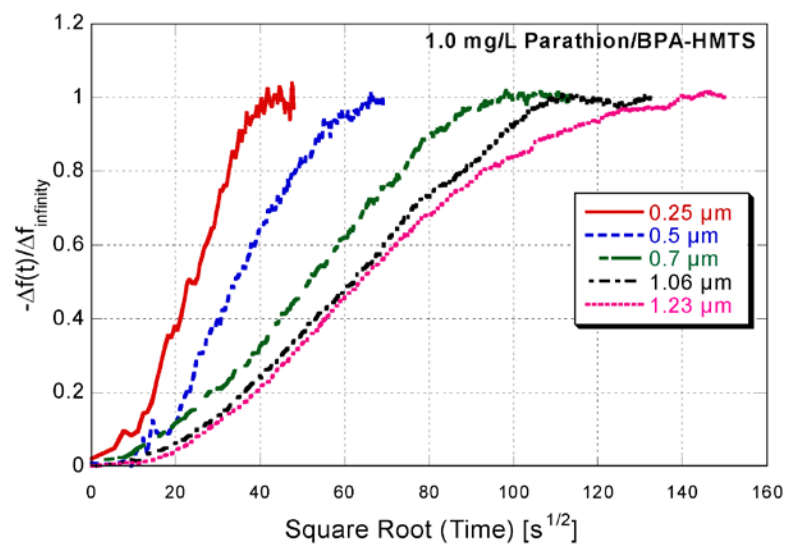
Figure 5.18: Absorption as a function of $\sqrt{t}$ during the detection of 1 mg/L (ppm) of parathion using varying thickness of BPA-HMTS (0.25 µm- 1.23 µm) layers on guided SH-SAW devices.
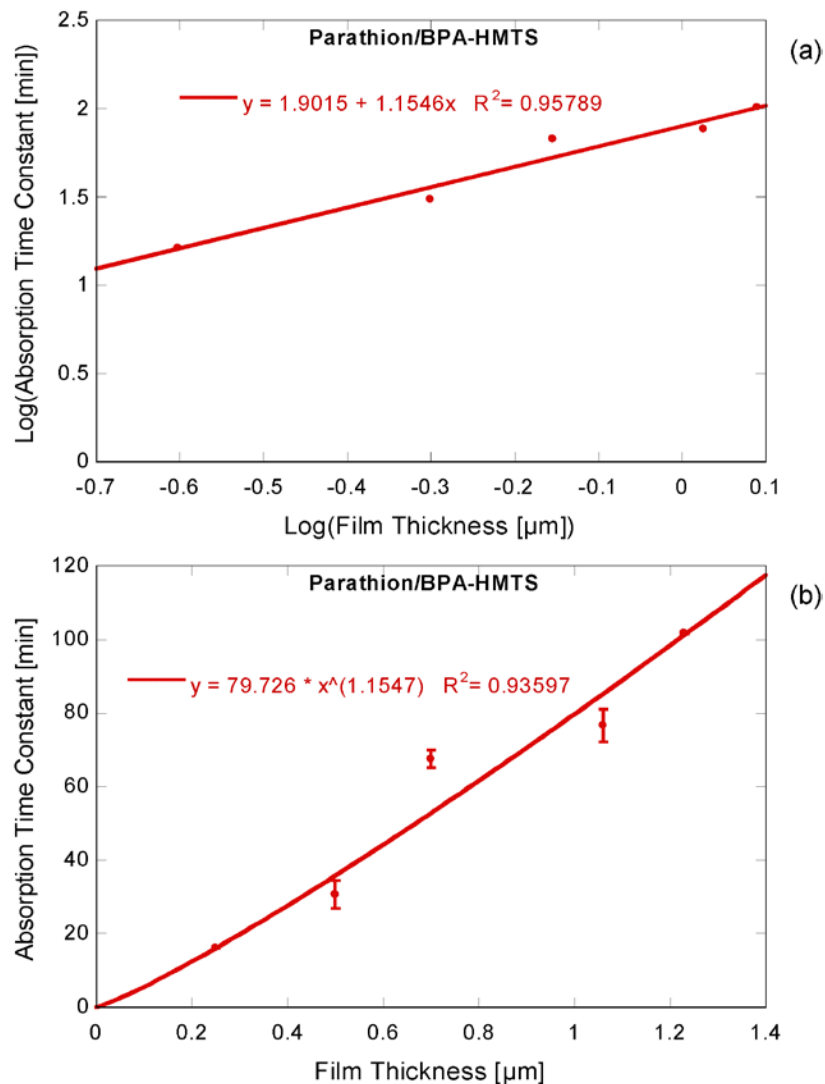
Figure 5.19: Relationship between absorption time constant and film thickness for the absorption of parathion by BPA-HMTS.

To determine whether τ_s is independent of analyte concentration, the effect of analyte concentration was investigated. The dependence of τ_s on analyte concentration for the three OPs studied here is shown in Figure 5.20. The averaged values for τ_s are about constant within the measured range. The statistical significance of the variation in averaged values for τ_s was tested by performing a one-way analysis of variance (ANOVA) (see Tables 5-2 to 5-4) on extracted values of τ_s for various ambient

concentrations of the analytes. The extracted values for τ_s are grouped based on the ambient concentration. The underlying assumption of ANOVA is that the observations are independent and the groups have the same variance. A significance level of 5% and a null hypothesis that τ_s is independent of concentration was used in this analysis. The *p*-values of 0.96, 0.91, and 0.23 for parathion-methyl, parathion, and paraoxon, respectively, suggest that within the measured ranges, τ_s is independent of ambient concentration. This implies that within the Henry's law region or for relatively low concentrations, the mass transfer coefficient is essentially constant. The low *p*-value for paraoxon compared to the other analytes is due to the scatter in its extracted τ_s .
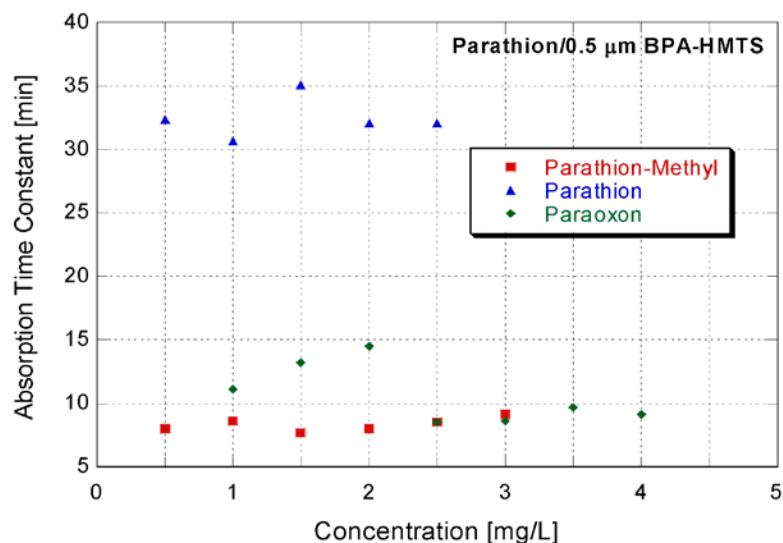
Figure 5.20: Absorption time constant as a function of ambient concentration. The time constant was extracted using the penetration model for absorption.

Table 5-2: ANOVA summary table for the absorption time constant extracted in the detection of 0.5 - 3.0 mg/L of parathion-methyl using a guided SH-SAW device (LiTaO₃)coated with 0.5 µm-thick BPA-HMTS layer. It is noted that the values for the absorption time constant, τ_s, is shown in Figure 5.20 and the significance value is set at the 5%.

Source of Variation	SS	df	MS	F	p-value	F_{crit}
Between groups	3.387	5	0.677	0.189	0.961	3.204
Within groups	39.436	11	3.585			
Total	42.823	16				

Table 5-3: ANOVA summary table for the absorption time constant extracted in the detection of 0.5 - 2.5 mg/L of parathion using a guided SH-SAW device (LiTaO₃) coated with 0.5 µm-thick BPA-HMTS layer. It is noted that the values for the absorption time constant, τ_s, is shown in Figure 5.20 and the significance value is set at the 5%.

Source of Variation	SS	df	MS	F	p-value	F_{crit}
Between groups	20.674	4	5.169	0.229	0.908	6.388
Within groups	90.095	4	22.524			
Total	110.769	8				

Table 5-4: ANOVA summary table for the absorption time constant extracted in the detection of 1.0 - 4.0 mg/L of paraoxon using a guided SH-SAW device (LiTaO₃) coated with 0.5 µm-thick BPA-HMTS layer. It is noted that the values for the absorption time constant, τ_s, is shown in Figure 5.20 and the significance value is set at the 5%.

Source of Variation	SS	df	MS	F	p-value	F_{crit}
Between groups	58.112	6	9.685	1.735	0.230	3.581
Within groups	44.662	8	5.583			
Total	102.774	14				

Figure 5.21 compares the volume of the OPs to the absorption time constant during detection using 0.5 μm-thick BPA-HMTS coated SH-SAW devices (LiTaO$_3$). It is seen that even though paraoxon is only 3.8% smaller (by volume) than parathion, its absorption time constant (~ 10.5 ± 2.1 minutes) is at least 50% faster than that of parathion (~ 32.5 ± 1.6 minutes). On the other hand, parathion-methyl, which is 9.5% smaller than paraoxon, exhibited about the same absorption time (~ 8.3 ± 0.5 minutes) as paraoxon. This transient response information can be used to improve analyte recognition (between parathion/paraoxon and parathion/parathion-methyl). A possible explanation for this difference in absorption time may be given by the degree of softening/plasticization. The absorption of parathion results in the highest degree of plasticization and thus it takes longer for the polymer to relax. Since the absorption process is non-fickian, one can say that the absorption time and polymer relaxation time are comparable [96]
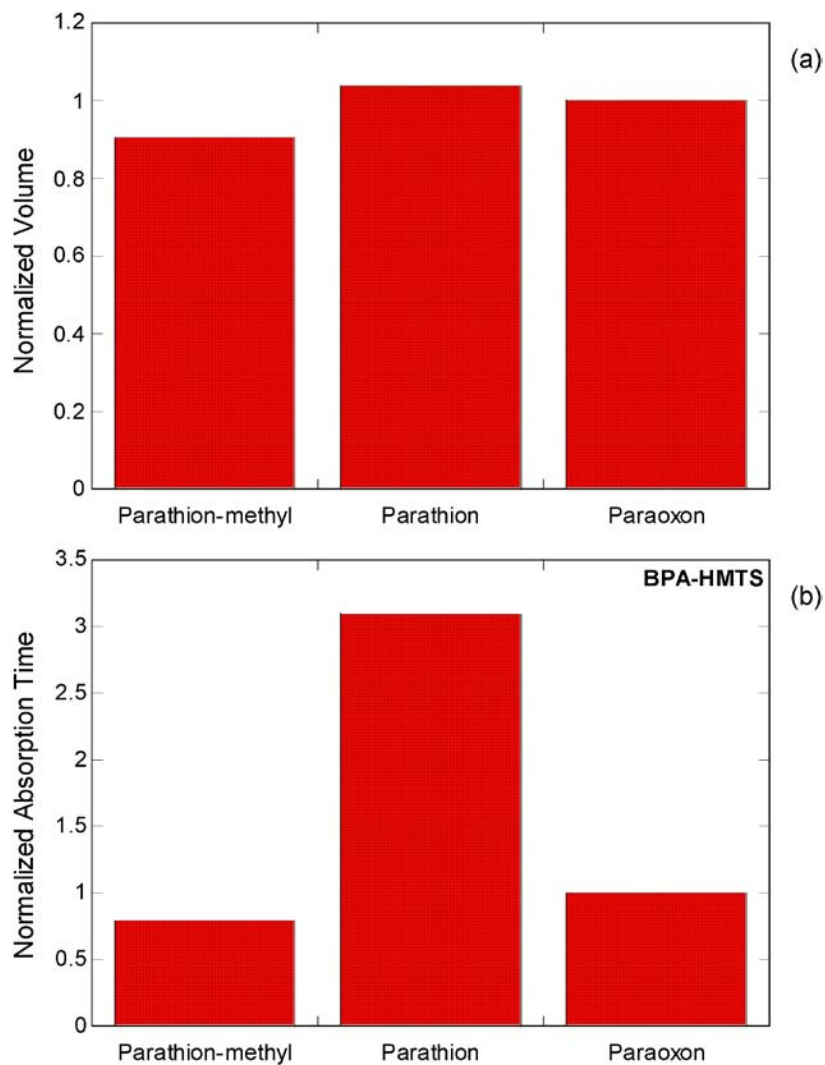
Figure 5.21: Comparison of (a) analyte volume to (b) absorption times during detection using 0.5 µm-thick BPA-HMTS coated SH-SAW devices (LiTaO₃). Note that all values have been normalized with respect to the corresponding value for paraoxon.

5.7 Comparison of Response Times for Different Coatings

Figure 5.22 compares the performance of BPA-HMTS to PECH. Here, the same thicknesses of the polymers were deposited on the LiTaO$_3$ SH-SAW device and exposed to 4 mg/L of parathion. Note that the sensor responses are allowed to run longer than necessary for the purpose of comparison. The sensor response time, t$_{90}$, is given by 2.3*absorption time. Comparing the glass transition temperature (T_g) for PECH (-25.5 °C) to the T_g for BPA-HMTS (4.95 °C), it is expected that PECH will be more rubbery at room temperature [74] and thus will exhibit a faster absorption process. However, from the measurements, it is observed that the sensor response time compared to PECH is decreased by at least 60% without loss of sensitivity for BPA-HMTS. The faster response time of BPA-HMTS is due to the inorganic part of the polymer i.e., HMTS. The porosity of HMTS increases the surface area-to-volume ratio. As a result, parathion is able to penetrate the surface of the coating rapidly and hence exhibit a faster absorption process. The sensitivity exhibited by BPA-HMTS is due to the organic part, i.e., BPA. BPA is a strong hydrogen-bond acidic coating and thus provides the medium for acid-base interactions with the strong hydrogen-bond basic analyte.
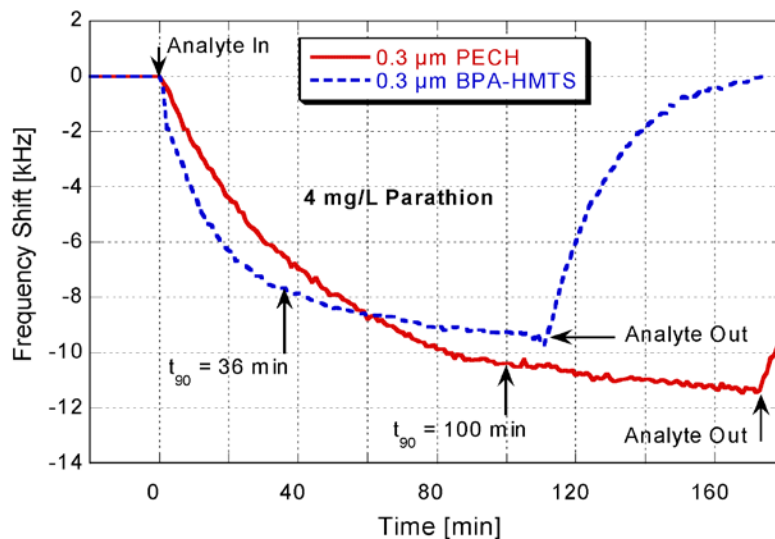
Figure 5.22: Measured frequency shift in the detection of 4 mg/L (ppm) parathion using 0.25 (~0.3) μm-thick PECH and BPA-HMTS on SH-SAW device (LiTaO$_3$). Note that t$_{90}$ = 2.3τ_s.

5.8 On-line Sensor Signal Processing

Rapid detection of contaminants such as volatile organic compounds and pesticides in water will allow real-time monitoring in aqueous environments. Reversible detection of OPs in the liquid phase has already been demonstrated using poly(epichlorohydrin) [PECH] and polyurethane as the sensing layer [79]. However, the response times were relatively long, on the order of hours. Several approaches have been investigated to achieve rapid detection of OPs in water. Initial studies of the response time revealed that it is possible to decrease the sensor response time by increasing temperature and/or decreasing film thickness. However, these approaches reduced device sensitivity. Here, a hybrid organic/inorganic chemically sensitive layer, [bisphenol A-hexamethyltrisiloxane (BPA-HMTS)], has been synthesized and investigated for the rapid detection and analysis of organophosphate pesticides. It is shown that, for the same coating thickness, a 60%

reduction in sensor response time is achieved without a significant reduction in sensitivity when compared with PECH (see Figure 5.22).

After physically achieving this in sensor response time, one can employ on-line sensor signal analysis in the form of the extended Kalman filter (EKF) during the detection process. This allows for the steady-state sensor response and absorption time constant to be extracted on-line well before equilibrium, thus further reducing the time required for analyte identification and quantification. In this section, the method used to perform on-line sensor signal processing and results will be discussed. This approach is based on the use of state-space methods and nonlinear estimation theory.

5.8.1 State-Space Model of Sensor Responses

In order to efficiently analyze the sensor signal, it is first necessary to model the time response of the sensor. It is first assumed that the rate of analyte absorption is proportional to the difference between the concentration of analyte in the coating at equilibrium, $\gamma_p C_{amb}$, and the concentration of analyte in the coating at time t, $C(t)$. This leads to a first-order absorption model given by:

$$\dot{C}(t) = \left(1/\tau_s\right)\left(\gamma_p C_{amb}(t) - C(t)\right), \quad \tau_s > 0 \qquad (5.2)$$

where $1/\tau_s$ represents the absorption rate coefficient, C_{amb} is the ambient analyte concentration, γ_p is the polymer-liquid partition coefficient, and $\dot{C}(t) = dC(t)/dt$. It is further assumed that within the Henry's law region (i.e., for relatively small concentration), the analyte-induced viscoelastic changes (storage and loss moduli) and mass loading are proportional to the concentration of analyte in the coating at constant

temperature. Following these assumptions, the observed sensor response (frequency shift and change in loss) at time t can be written as:

$$\Delta f(t) = g_1\left(\Delta m(t), \Delta G'(t)\right) = -aC(t), \tag{5.3a}$$

$$\Delta \alpha(t) = g_2\left(\Delta G''(t)\right) = bC(t), \tag{5.3b}$$

where a and b are parameters which are functions of the device, the analyte, and the medium properties. $\Delta m(t)$, $\Delta G'(t)$, $\Delta G''(t)$ are the change in mass, storage modulus, and loss modulus, respectively, at time t. It is possible to combine Eqs. (5.2) and (5.3) into a state-space format to describe the sensor response. The state equation and output equations are given by:

$$\dot{C}(t) = -\left(1/\tau_s\right)C(t) + \left(1/\tau_s\right)\gamma_p C_{amb}(t), \tag{5.4a}$$

$$\Delta f(t) = -aC(t), \tag{5.4b}$$

$$\Delta \alpha(t) = bC(t), \tag{5.4c}$$

where $C(t)$ is the state variable and $\Delta f(t)$ and $\Delta \alpha(t)$ are the outputs of the sensor representing the frequency shift and change in loss at time t. Using the above state-space description, it is possible to extract both transient and steady-state information from the sensor response. This information can be used to decrease the time required for analyte identification and quantification [123]. Furthermore, the use of transient information has been shown to improve analyte species recognition (or analyte identification) [124;125].

5.8.2 Sensor Signal Analysis

The extended Kalman Filter (EKF) will be used to analyze the sensor signal. The EKF is a state space based variable technique capable of on-line, real-time state estimation for nonlinear systems and measurement equations [126]. In this case, the EKF can be used to process all available measurement data to estimate the current value of the parameters of interest as well as the state variables. For computational simplicity in data processing, the state-space equations are reformulated in discrete time and are given by:

$$m_{k+1} = (1 - S_k)m_k + S_k u_k + v_k, \tag{5.5a}$$

$$S_{k+1} = S_k, \tag{5.5b}$$

$$a'_{k+1} = a'_k, \tag{5.5c}$$

$$\Delta f_k = a'_k m_k + w_k. \tag{5.5d}$$

One can rewrite the above equations in matrix form as:

$$\begin{bmatrix} m_{k+1} \\ S_{k+1} \\ a'_{k+1} \end{bmatrix} = \begin{bmatrix} 1-S_k & 0 & 0 \\ 0 & 1 & 0 \\ 0 & 0 & 1 \end{bmatrix} \begin{bmatrix} m_k \\ S_k \\ a'_k \end{bmatrix} + \begin{bmatrix} S_k \\ 0 \\ 0 \end{bmatrix} u_k + \begin{bmatrix} 1 \\ 0 \\ 0 \end{bmatrix} v_k$$

$$\Delta f_k = \begin{bmatrix} 0 & 0 & 1 \end{bmatrix} \begin{bmatrix} m_k \\ S_k \\ a'_k \end{bmatrix} + \begin{bmatrix} 1 \end{bmatrix} w_k \tag{5.6}$$

In Equations (5.5) and (5.6), m_k is the concentration (or amount) of absorbed analyte at $t = kT$, where T is the sampling rate, S_k is the absorption rate constant, and a'_k is the steady-state value for the sensor response. Note that S_k and a'_k have been augmented with the state vector in order to perform the estimation [127]. The ambient concentration with

respect to time is modeled as a step input with height C_{max} (i.e. the given concentration). The process noise, v_k, and measurement noise, w_k, are assumed to be uncorrelated white noise with zero means and covariances V and W, respectively. Also, the state and output equations have been normalized with respect to the ambient concentration and partition coefficient with the new variable defined as:

$$m_k = C_k / \gamma_p C_{\max} ,$$ (5.6a)

$$a'_k = a_k \gamma_p C_{\max} ,$$ (5.6b)

and

$$u_k = C_{amb,k} / C_{\max} .$$ (5.6c)

Here, the EKF is used to estimate the absorption rate constant and steady-state value for the sensor response. Once the uncertainty in the estimated parameters is sufficiently low, the parameters can be used for analyte identification and quantification. In general, this occurs well before the response has reached the steady-state, thus allowing for identification without waiting for the steady-state response. Furthermore, the absorption rate constant, which contains transient information and is a function of a class of analyte/coating pairs, can be used to improve analyte species recognition. It is noted that only the frequency response is used in the above analysis, and that the sensor loss response can be used in a similar manner but has been ignored here.

The EKF approach requires that initial values be specified to initialize the algorithm. Therefore, an appropriate choice of initial conditions is necessary to achieve convergence [128]. Because prior information about the system was not available, initial

values were determined by fitting the first few data points to an exponential function (Eq. 3.4b).

5.8.3   Estimation Results and Discussion

In section 5.2, it was seen that the sensor response time is relatively long for rapid detection of OPs in the liquid-phase using PECH. Two approaches (reducing film thickness and increasing temperature of operation) were initially investigated in an attempt to reduce the response times. In each case, a reduction in the response time was observed. However, the trade-off was a decrease in the sensor sensitivity. In Figure 5.21, it is shown that for the same film thickness, the response time for BPA-HMTS is significantly shorter (~ 60%) than for PECH without loss of sensitivity. In this sub-section, the EKF technique is applied on-line to sensor data to further improve the overall sensor performance i.e., reduce the time required for analyte identification and quantification.

Using the theory described above, the EKF is used to predict the entire sensor response as the data are being measured. Figure 5.23 shows the predicted responses using only part of the sensor output up to the time indicated in the figure caption. The predicted responses show good agreement with the measured responses. This demonstrates that the EKF is capable of predicting the entire response, both transient and steady-state, well before equilibrium is reached. It is shown that accurate estimation of the parameters (absorption constant $S \approx 1/\tau_s$ and the predicted steady-state value, a') is possible after a certain amount of data have been collected (e.g., $\tau_s = 10$ min for parathion-methyl and paraoxon). Thus, one does not have to wait for steady-state before a detection decision is

made. In Figures 5.29 and 5.21b, it is seen that parathion-methyl and paraoxon have almost identical absorption time constants but different sensitivities. Therefore, their steady-state value will be their distinguishing feature. Figure 5.24 indicates that using steady-state values alone to identify analytes can sometimes lead to incorrect classification. However, by estimating the time constants associated with the absorption process, it is possible to improve species recognition. It is important to note that this approach can highlight even minute differences in the absorption process of various analytes. Thus, it may be possible to implement a chemical sensor array with fewer coatings and devices. In addition to predicting the entire sensor response, the EKF technique provides two important sensor parameters, the steady-state value and the absorption time constant. It has been shown here that these parameters may be unique for a class of analyte/coating pairs, and thus can be used for identification and classification of analytes. Consequently, an additional 50% reduction in the time required for analyte quantification is possible while simultaneously improving recognition by processing the measured data on-line.
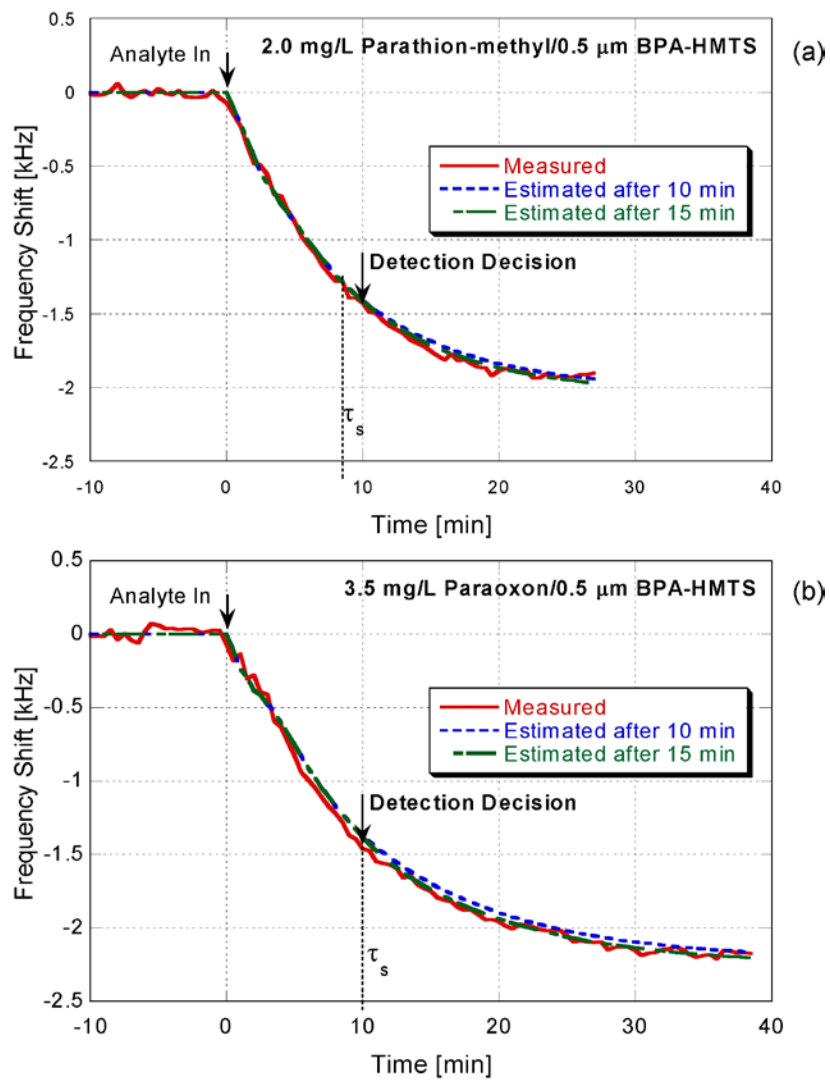
Figure 5.23: Estimated output obtained using an extended Kalman filter for the detection of (a) 2.0 mg/L (ppm) parathion-methyl and (b) 3.5 mg/L (ppm) paraoxon using 0.5 µm-thick BPA-HMTS on LiTaO₃ SH-SAW device. On-line predictions were done using the first 10 and 15 minutes of measured data. Absorption time (τ_s) and point of detection decision are shown.
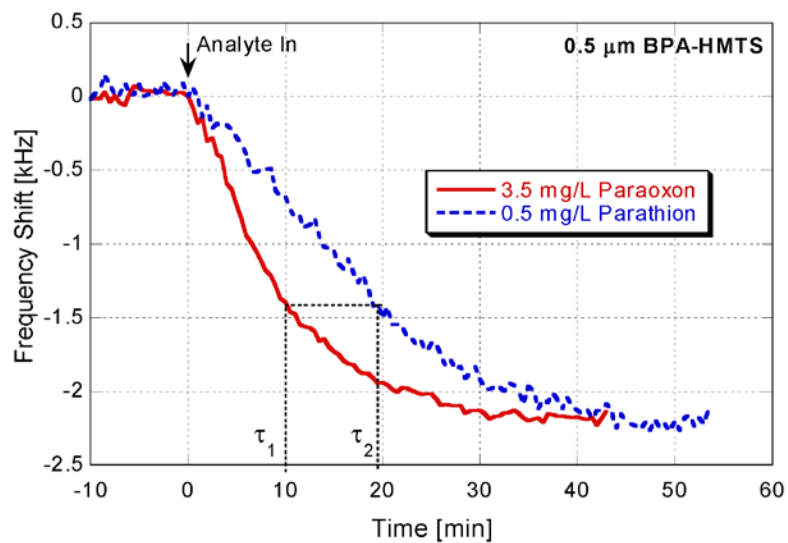
Figure 5.24: Sensor responses with similar steady-state values, but different absorption times. Increased selectivity is achieved using this difference in the absorption time (paraoxon (τ_1 = 10 min) and parathion (τ_2 = 20 min)).

6 SUMMARY, CONCLUSION, AND FUTURE WORK

6.1 Summary

The objective of this work was to develop a chemical sensor to allow for rapid on-line monitoring of organophosphate pesticides (OPs) in contaminated ground and waste water. In order to solve this problem, it is first necessary to develop and identify functionalized polymers for rapid and reversible analyte absorption of OPs with high sensitivity and improved selectivity. To this end, a hybrid organic/inorganic coating, BPA-HMTS, was synthesized and investigated for direct detection and analysis of OPs in aqueous solutions using guided SH-SAW devices. This investigation involved characterizing the coating (i.e., preparation techniques, water stability, aging, density, and glass transition temperature), analyzing the effect of coating thickness on sensor response time/rate of analyte absorption, and studying the effect of solution pH on analyte properties in aqueous solutions. Two possible types of analyte absorption processes were discussed, namely, absorption rate limited by penetration and absorption rate limited by diffusion. It was shown that under certain conditions, each absorption process can be described by a first-order differential equation. Furthermore, the viscoelastic properties of coating (polymeric) materials, the chemistry of organophosphate pesticides, and the rationale of the design of sensitive layers for detection of OPs in water were presented.

Experiments were performed to determine the suitability of bisphenol A-hexamethyltrisiloxane (dubbed BPA-HMTS) as the sensing and wave guiding layer for the detection of OPs in aqueous environments. The choice of the polymer layer is

important since it affects the key sensor performance criteria including sensitivity, selectivity, and response time. SH-SAW devices on 36° YX-LiTaO$_3$ with center frequency of 103 MHz and on 42.75° YX-Quartz (ST-90° X Quartz) with center frequency of 155 MHz were used in this work with the goal to determine the optimum operating conditions for rapid sensor response with high sensitivity. The devices were first prepared and then characterized using a vector network analyzer to determine the properties of the bare device. The devices were then spin-coated with BPA-HMTS and exposed to varying concentrations of target analytes (parathion-methyl, parathion, and paraoxon). The individual sensors were characterized by evaluating sensor properties of interest including reproducibility, sensitivity, selectivity, response time, and other relevant sensor parameters. These characterizations led to an understanding of the sensor response.

After characterizing the sensors, it was necessary to identify features that make it possible to deploy these sensors in the field. The two issues that are currently limiting the applicability of chemical sensors are sensor response time and array selectivity. Typically, only the steady-state response is used to identify and quantify analytes. In this work, novel sensor signal processing techniques based on nonlinear estimation theory were proposed and validated on experimental data. This required an accurate physics-based model of the sensor response to be developed. This model took into account added mass and viscoelastic changes, utilized state space techniques, and enabled nonlinear estimation theory (in the form of the Extended Kalman Filter (EKF)) to be used to extract transient information online to improve analyte recognition (i.e. selectivity) and reduce the time required for analyte identification and quantification. The EKF was

capable of accurately estimating the steady-state response in less than 40% of the time required for the sensor response to reach its steady-state.

6.2   Conclusion

A partially selective, water-stable, hybrid coating (BPA-HMTS) has been synthesized and characterized for rapid absorption of OPs. With this coating, under the same experimental conditions i.e., thickness, a 60% reduction in the sensor response time has been achieved over PECH without loss in sensitivity. Typically, in chemical sensor application it is desired that the coating have a low glass transition temperature i.e., the coating should be rubbery at or near the operating temperature to promote rapid analyte absorption. However, the results of this study indicate that this is not a sufficient condition for rapid analyte absorption. Rather, the porosity of the coating appears to be the key coating feature for rapid analyte absorption. The faster absorption exhibited by BPA-HMTS is rather due to the porosity of the siloxane (HMTS) backbone while the BPA provides the chemical sensitivity of the coating.

Kinetic studies of parathion absorption from aqueous solution into the BPA-HMTS coating show that the absorption process is rate limited by penetration. The mass transfer coefficient for parathion/BPA-HMTS is extracted to be 2.1×10^{-8} cm/s. It is expected that a similar study on the effect of film thickness on the absorption of parathion-methyl and paraoxon from aqueous solutions will also show that surface penetration is the rate limiting step for it absorption because of its structural similarity to parathion. For an absorption process that is penetration limited, the porosity of the coating affects the surface area-to-volume ratio. This in turn affects the absorption time. It is seen that even

though paraoxon is only 3.8% smaller (by volume) than parathion, its absorption time constant ($\sim 10.5 \pm 2.1$ minutes) is at least 50% faster than parathion ($\sim 32.5 \pm 1.6$ minutes). On the other hand, parathion-methyl, which is 9.5% smaller than paraoxon, exhibited about the same absorption time ($\sim 8.3 \pm 0.5$ minutes) as paraoxon. This transient information can be used to improve analyte recognition (between parathion/paraoxon and parathion/parathion-methyl). A possible explanation for this difference in absorption time may be given by the degree of softening/plasticization and the associated time required for polymer relaxation. Within the Henry's law region, it is seen that the absorption time is independent of concentration.

The coating exhibited different sensitivity levels towards the analytes. In fact, with respect to paraoxon, BPA-HMTS exhibited about twice and 10 times higher sensitivity towards parathion-methyl and parathion, respectively, even though the analytes have identical molar masses. This suggests that the coating has different partition coefficients for the analytes. An analysis of the solubility of the analytes in water indicates that the least soluble analyte, in this case parathion, will prefer to be in the coating. As a result, the amount of parathion absorbed by the coating is large in comparison to parathion-methyl and paraoxon. This results in greater plasticization leading to larger viscoelastic contribution to the frequency shift. This argument is supported by the larger change in loss observed for parathion. With the present non-optimized chemical sensor, a limit of detection of 60 µg/L (ppb), 20 µg/L (ppb) and 100 µg/L (ppb) is estimated for parathion-methyl, parathion, and paraoxon, respectively, when using a 0.5 µm-thick BPA-HMTS sensing layer. Concentrations as low as 500 µg/L (ppb) parathion have been measured.

This concentration is significantly much lower than the typical concentrations found on agricultural produce ($\geq$ 10 ppm).

To meet the need for rapid detection in liquid with high sensitivity and selectivity, the EKF was employed for on-line analysis of the sensor data during the detection process. To achieve the above, the sensor response was first represented by a state-space model. The model included all relevant contributions to the sensor response. Using on-line sensor signal processing allowed for a further reduction (at least 40%) in the time required for analyte identification and quantification, thus partially satisfying one of the design requirements for rapid chemical sensors. Furthermore, the technique can be used to extract the absorption time constant, allowing for class-based analyte classification. Nevertheless, a need still exits to continue to develop appropriate coatings that will reversibly and rapidly absorb OPs at room temperature with high selectivity so that the full capabilities of the EKF technique can be realized.

The investigated device that appears to be the best candidate for developing a chemical sensor for direct sensing in water is the 36° rotated Y-cut on $LiTaO_3$. This is an isolated orientation of the rotated Y-cuts that supports an SH-SAW wave. However, any slight deviation from this orientation, results in significant bulk wave generation. Because $LiTaO_3$ has a relatively high permittivity constant, both a coated IDT and coated propagation path on this device can be easily electrically isolated from the liquid. As a result, the coated IDT and the propagating wave do not experience any major electrical perturbation which could result in a distortion of the device response. For the present measurements, the root-mean-square noise level is 0.04 kHz; four times lower than the measurements done with devices fabricated on 42.75° rotated Y-cut in quartz. In terms of

sensitivity, limit of detection, and sensor response time, the 0.5 μm-thick BPA-HMTS on 36° YX-LiTaO$_3$ is the best sensor for direct sensing of OPs in the present work.

6.3 Future Work

The present work points to the need for more theoretical and experimental work. This work includes, but is not limited to, improvement in the coating performance (for higher sensitivity, improved selectivity, faster sensor response time, etc.), ruggedness characterization, coating array design, design and fabrication of higher frequency devices, investigation of new SH-SAW materials and orientations for sensor applications, and field testing of the chemical sensors. This section will discuss a few possible future research proposals.

1. Improving chemical sensitivity of the polymer coating

A un-fluorinated phenol structure (BPA) was used in the synthesis of the hybrid organic/inorganic acidic coating BPA-HMTS. This was due in part to the availability of 2,2'-diallylbisphenol A (BPA) commercially. However, there are other coatings with hydrogen bond acidity that may be used as the organic part of the hybrid coating. In designing coatings for hydrogen-bond basic analytes, a coating which provides maximum hydrogen-bond acidity, (b), with the minimum hydrogen-bond basicity, (a), or minimum dipolarity, (s), is desired. These features are characterised by the ratios b/a or b/s. From Table 6-1, it is seen that BPA is not the optimum hydrogen-bond acid coating. However, with this coating, concentrations as low as 500 μg/L of parathion have been measured in

water. Therefore, it is hypothesized that functionalizing HMTS with any of the two

coatings described below will lead to increased sensitivity.

Table 6-1: Comparison of linear solvation energy relationship (LSER) coefficients for potential hydrogen-bond acidic coating in the gas phase [71]. It should be noted that although these coefficients will be different in water, it is hypothesized that the relative relationships presented here for gas will be the same for water. Thus, these values serve as a guide for understanding the nature of the analyte/coating interaction.

	c	*r*	*s*	*a*	*b*	*l*	*b/a*	*b/s*
BPA	-2.00	-0.92	2.24	2.79	2.41	0.975	**0.86**	**1.08**
Fluorinated BPA	-0.58	-0.48	1.04	0.89	4.56	0.863	**5.12**	**4.38**
2,2-Bis(4-hydroxy-3-propylphenyl)hexafluoropropane	-1.21	-0.38	1.38	0.71	5.31	0.984	**7.48**	**3.85**

2. Designing higher frequency guided SH-SAW devices

High frequency implies that the acoustic energy is trapped closer to the sensing

surface, which makes the device more sensitive to mechanical perturbations.

Moreover, only a thinner coating (smaller h) is then needed for further energy

trapping. For a given crystal orientation that supports an SH-SAW wave, high

frequency devices can be achieved by reducing the operating wavelength (λ), since λ

= wave velocity/f. It is important to note that a high frequency shift is not a sufficient

requirement to achieve low limit of detection since the sensor resolution also depends

on the noise level.

3. Improving chemical selectivity of the polymer coating

For a given sensor platform, the chemically sensitive layer is arguably the most important component of the sensor platform. The BPA-HMTS coating used in this work is partially selective. Although improvement in selectivity is possible through the use of the transient information, for the analytes (parathion-methyl and paraoxon) which have similar transient behaviour, this is more challenging. However, if a molecularly imprinted polymer (MIP) that can be spin-coated on the device is developed, highly selective sensors will be possible. MIPs are of interests because they allow one to synthesize polymers with predetermined selectivity. Furthermore, they are reusable and unlike antibodies, are stable and have short preparation times. During the synthesis, the target or "print" molecule is present. After synthesis, the print molecule is removed to create a polymer that can be used as a selective binding medium for the print molecule. The challenge with this approach is the deposition of the MIP on the sensor platform so that there is good adhesion.

Combining proposals (1), (2), and (3) will enable the development of very sensitive and highly selective chemical sensors for organophosphate pesticides because the coating can be deposited on the sensor platform with the highest device sensitivity and lowest noise level.

4. Extraction of storage and loss moduli of the polymer coating

Sensor responses of the guided SH-SAW is the result of added mass and viscoelastic changes in the polymer. A comparison of the molar mass and frequency shift for the analytes studies in this work indicates that changes in the viscoelastic properties, shear storage and loss moduli, G' and G'', of the coating contribute significantly to the

sensor's response. Therefore, it is important to model and characterize the coating's viscoelastic properties during detection in liquid. This will require the S_{21} transmission response to be measured as a function of analyte concentration. The viscoelastic constants can then be extracted using the matrix method. Alternatively, a thickness shear mode (TSM) resonator and the Butteworth-Van dyke equivalent circuit model may be used.

5. Detection in binary and complex mixtures

In a field deployed sensor, detection and quantification of a particular organophosphate will be done, most likely, in the presence of other organophosphates and interferents. Therefore, it is necessary to conduct characterization studies for binary and complex mixtures of organophosphate. This will allow for models for competitive absorption to be developed and sensor signal/data processing techniques demonstrated in this work to be extended to the case of complex mixtures.

6. Designing hybrid sensor array

While polymer-coated SH-SAW chemical sensors have been shown to be very sensitive platform for direct sensing in water, no single sensor can identify all analytes. It is possible to build a sensor array using a single sensor platform but different coatings on the device to exploit particular physical interaction and applying pattern recognition algorithms to distinguish between analytes. The problem with this approach is that the data are correlated because the sensor platforms use the same transduction mechanism. As a result, the dimension of the feature space is increased without contributing significant additional information. However, it is hypothesized that the use of hybrid sensor arrays consisting of several different sensor technologies including MEMS

technology, acoustic wave technology, and optical technology will drastically improve analyte identification, quantification, and reduce the number of false alarm because the measurements will be truly orthogonal i.e., the data will be less correlated because each sensor platform is based on a different transduction principle. Designing a hybrid sensor array would make it possible to design experiments in order to test new applications for sensor arrays, test new signal processing techniques, new pattern recognition techniques, and new feature selection/extraction techniques.

7. Determine temperature characteristics for BPA-HMTS coated device

The temperature coefficient for the uncoated $36°$ YX-LiTaO$_3$ device is 32 ppm. However, the temperature characteristics of the BPA-HMTS coated $36°$ YX-LiTaO$_3$ device have not been determined. Performing this study may allow one to design the sensor so that it exhibits a zero or near-zero temperature coefficient of delay (TCD) as a function of coating thickness, or simply allow one to easily predict and correct for temperature variations.

8. Differentiate between mass loading and viscoelastic loading contributions to sensor response

The shear modulus for a given polymer is a function of frequency. However, mass loading as a result of analyte absorption is not a function of frequency. Therefore, designing and using multi-frequency devices may allow one to differentiate between added mass and viscoelastic changes to the sensor response.

REFERENCES

[1] US Environmental Protection Agency. What is a Pesticide? Available from: http://www.epa.gov/pesticides/about/index.htm . 8-4-2010. US Environmental Protection Agency. 8-4-2010.
Ref Type: Electronic Citation

[2] Food and Agriculture Organization of the United Nations. International Code of Conduct on the Distribution and Use of Pesticides. Available from: http://www.fao.org/WAICENT/FAOINFO/AGRICULT/AGP/AGPP/Pesticid/Code/Download/code.pdf . 2002. Food and Agriculture Organization of the United Nations. 8-4-2010.
Ref Type: Electronic Citation

[3] Levine, M. J., *Pesticides* Westport: Praeger Publishers, 2007.

[4] Schuman, S. H. and Simpson, W., "A clinical historical overview of pesticide health issues," *Occupational Medicine: State of the Art Reviews*, no. 12, pp. 203-207, 1997.

[5] Landrigan, P. J., Claudio, L., Markowitz, S. B., Berkowitz, G. S., Brenner, B. L., Romero, H., Wetmur, J. G., Matte, T. D., Gore, A. C., Godbold, J. H., and Wolff, M. S., "Pesticides and inner-city children: exposures, risks, and prevention," *Environmental Health Perspective*, vol. 107, no. 3, pp. 431-437, 1999.

[6] Gupta, R. C., *Toxicology of Organophosphate & Carbamate Compounds* Burlington: Elsevier Academic Press, 2006.

[7] Pimentel, D., Acquay, H., Biltonen, M., Rice, P., Silva, M., Nelson, J., Lipner, V., Giordano, S., Horowitz, A., and D'Amore, M., "Environmental and Economic Costs of Pesticide Use," *BioScience*, vol. 42, no. 10, pp. 750-760, 1992.

[8] Lobe, J. WHO Urges DDT for Malaria Control Strategies. Available from: http://www.commondreams.org/headlines06/0916-05.htm . 8-16-2006. Inter Press Service. 8-4-2010.
Ref Type: Electronic Citation

[9] American Bird Conservancy. Pesticide Profile - Ethyl parathion. Available from: http://www.abcbirds.org/abcprograms/policy/pesticides/Profiles/ethyl_parathion.html . 2007. 9-7-2010.
Ref Type: Electronic Citation

[10] Ragnarsdottir, K. V., "Environmental fate and toxicology of organophosphate pesticides," *Journal of the Geological Society*, vol. 157 pp. 859-876, 2000.

[11] US Environmental Protection Agency. Types of Pesticides. Available from: http://www.epa.gov/pesticides/about/types.htm . 1-29-2009. 8-5-2010.
Ref Type: Electronic Citation

[12] Eichelberger, J. W. and Lichtenberg, J. J., "Persistence of pesticides in river water," *Environmental Science & Technology*, vol. 5, no. 6, pp. 541-544, 1971.

[13] Abad, J. M., Pariente, F., Hern+índez, L., Abru+¦a, H. D., and Lorenzo, E., "Determination of Organophosphorus and Carbamate Pesticides Using a Piezoelectric Biosensor," *Analytical Chemistry*, vol. 70, no. 14, pp. 2848-2855, 1998.

[14] Daum, R. J., "Agricultural and Biocidal Applications of Organometallics," *Annals of the New York Academy of Sciences*, vol. 125, no. Industrial Synthesis and Applications of Organometallics, pp. 229-241, 1965.

[15] Proskocil, B. J., Bruun, D. A., Thompson, C. M., Fryer, A. D., and Lein, P. J., "Organophosphorus Pesticides Decrease M2 Mucarinic Receptor Function in Guinea Pig Airway Nevers via Indirect Mechanisms," *PLoS ONE*, vol. 5, no. 5: e10562, pp. 1-11, 2010.

[16] Gilden, R. C., Huffling, K., and Sattler, B., "Pesticides and Health Risks," *Journal of Obstetric, Gynecologic, & Neonatal Nursing*, vol. 39, no. 1, pp. 103-110, 2010.

[17] Kim, J. H., Stevens, R. C., Maccoss, M. J., Goodlett, D. R., Scherl, A., Richter, R. J., Suzuki, S. M., and Furlong, C. E., "Identification and characterization of biomarkers of organophosphorus exposures in humans," *Adv Exp Med Biol*, vol. 660 pp. 61-71, 2010.

[18] Weisenburger, D. D., "Human Health-Effects of Agrichemical Use," *Human Pathology*, vol. 24, no. 6, pp. 571-576, June1993.

[19] Whyatt, R. M., Camann, D. E., Kinney, P. L., Reyes, A., Ramirez, J., Dietrich, J., Diaz, D., Holmes, D., and Perera, F. P., "Residential pesticide use during pregnancy among a cohort of urban minority women," *Environmental Health Perspectives*, vol. 110, no. 5, pp. 507-514, May2002.

[20] Berkowitz, G. S., Obel, J., Deych, E., Lapinski, R., Godbold, J., Liu, Z. S., Landrigan, P. J., and Wolff, M. S., "Exposure to indoor pesticides during pregnancy in a multiethnic, urban cohort," *Environmental Health Perspectives*, vol. 111, no. 1, pp. 79-84, Jan.2003.

[21] Koch, D., Lu, C. S., Fisker-Andersen, J., Jolley, L., and Fenske, R. A., "Temporal association of children's pesticide exposure and agricultural

spraying: Report of a longitudinal biological monitoring study," *Environmental Health Perspectives*, vol. 110, no. 8, pp. 829-833, Aug.2002.

[22]   Loewenherz, C., Fenske, R. A., Simcox, N. J., Bellamy, G., and Kalman, D., "Biological monitoring of organophosphorus pesticide exposure among children of agricultural workers in central Washington State," *Environmental Health Perspectives*, vol. 105, no. 12, pp. 1344-1353, Dec.1997.

[23]   Quandt, S. A., Arcury, T. A., Rao, P., Snively, B. M., Camann, D. E., Doran, A. M., Yau, A. Y., Hoppin, J. A., and Jackson, D. S., "Agricultural and residential pesticides in wipe samples from farmworker family residences in North Carolina and Virginia," *Environmental Health Perspectives*, vol. 112, no. 3, pp. 382-387, Mar.2004.

[24]   Simonian, A. L., Rainina, E. I., and Wild, J. R., "A New Approach For Discriminative Detection of Organophosphate Neurotoxins in the Presence of Other Cholinesterase Inhibitors," *Analytical Letters*, vol. 30, no. 14, pp. 2453-2468, 1997.

[25]   Vergucht, S., de Voghel, S., Misson, C., Vrancken, C., Callebaut, K., Steurbaut, W., Pussemier, L., Marot, J., Maraite, H., and Vanhaecke, P. Health and environmental effects of pesticides and type 18 biocides (HEEPEBI). Available from: http://www.crphyto.be/fichiers/heepebi.pdf . 2006. 8-16-2010.
Ref Type: Electronic Citation

[26]   Pedrosa, V., Caetano, J., Machado, S., and Bertotti, M., "Determination of Parathion and Carbaryl Pesticides in Water and Food Samples Using a Self Assembled Monolayer /Acetylcholinesterase Electrochemical Biosensor," *Sensors*, vol. 8, no. 8, pp. 4600-4610, 2008.

[27]   US Environmental Protection Agency. Ground Water. Available from: http://water.epa.gov/type/groundwater/index.cfm . 3-31-2010. 8-14-2010.
Ref Type: Electronic Citation

[28]   US Environmental Protection Agency. Drinking Water Standards and Health Effects. Available from: http://water.epa.gov/lawsregs/guidance/sdwa/upload/2009_08_28_sdwa_fs_30a nn_standards_web.pdf . 2004. 8-13-2010.
Ref Type: Electronic Citation

[29]   Eskenazi, B., Bradman, A., and Castorina, R., "Exposures of children to organophosphate pesticides and their potential adverse health effects," *Environmental Health Perspectives*, vol. 107 pp. 409-419, June1999.

[30]   Dyro, F. M. Organophosphates. Available from: http://emedicine.medscape.com/article/1175139-overview . 2009. 8-14-2010.
Ref Type: Electronic Citation

[31] US Environmental Protection Agency. Drinking Water Contaminants. Available from: http://water.epa.gov/drink/contaminants/index.cfm . 6-2-2010. 8-13-2010. Ref Type: Electronic Citation

[32] Kolpin, D. W., Barbash, J. E., and Gilliom, R. J., "Occurrence of Pesticides in Shallow Groundwater of the United States:ΓÇë Initial Results from the National Water-Quality Assessment Program," *Environmental Science & Technology*, vol. 32, no. 5, pp. 558-566, Jan.1998.

[33] US Environmental Protection Agency. Drinking Water Monitoring, Compliance, and Enforcement. Available from: http://water.epa.gov/lawsregs/guidance/sdwa/upload/2009_08_28_sdwa_fs_30a nn_monitoring_web.pdf . 2004. 8-13-2010. Ref Type: Electronic Citation

[34] Dorozhkin, L. M. and Rozanov, I. A., "Acoustic Wave Chemical Sensors for Gases," *Analytical Chemistry*, vol. 56, no. 5, pp. 399-416, 2001.

[35] Grundler, P., *Chemical Sensors: An Introduction for Scientists and Engineers* Leipzig: Springer, 2007.

[36] Ballantine, D. S., White, R. M., Martin, S. J., Ricco, A. J., Frye, G. C., Zellers, E. T., and Wohltjen, H., *Acoustic Wave Sensors: Theory, Design and Physico-Chemical Applications* San Diego: Academic Press, 1997.

[37] Fraden, J., *Handbook of Modern Sensors: Physics, Designs and Applications* New York: Springer-Verlag Inc, 2004.

[38] National Research Council, *Expanding the Vision of Sensor Materials* Washington D.C.: National Academy Press, 1995, pp. 3.

[39] Drafts, B., "Acoustic wave technology sensors," *IEEE Trans.on Microwave Theory and Techniques*, vol. 49, no. 4, pp. 795-802, Apr.2001.

[40] Thompson, M. and Stone, D. C., *Surface-Launched Acoustic Wave Sensors: Chemical Sensing and Thin Film Characterization* New York: John Wiley & Sons, Inc., 1997.

[41] Campbell, C. K., *Surface Acoustic Wave Devices for Mobile and Wireless Applications* San Diego: Academic Press, 1998.

[42] Krishnamurthy, S., Atashbar, M. Z., and Bazuin, B. J., "Burst Transceiver Unit for Wireless Passive SAW Sensing System," *Instrumentation and Measurement, IEEE Transactions on*, vol. 58, no. 10, pp. 3746-3753, Oct.2009.

[43] Springer, A., Weigel, R., Pohl, A., and Seifert, F., "Wireless identification and sensing using surface acoustic wave devices," *Mechatronics*, vol. 9, no. 7, pp. 745-756, Oct.1999.

[44]   Vectron International. Wireless Food Probes Using Surface Acoustic Wave
        Technology. Available from:
        http://www.sengenuity.com/tech_ref/Wireless_Food_Probe.pdf . 7-19-2010. 7-
        19-2010.
        Ref Type: Electronic Citation

[45]   Gizeli, E., Bender, F., Rasmusson, A., Saha, K., Josse, F., and Cernosek, R.,
        "Sensitivity of the acoustic waveguide biosensor to protein binding as a function
        of the waveguide properties," *Biosensors & Bioelectronics*, vol. 18, no. 11, pp.
        1399-1406, Oct.2003.

[46]   Bjurstrom, J., Wingqvist, G., Yantchev, V., and Katardjiev, I., "3I-5 Design and
        Fabrication of Temperature Compensated Liquid FBAR Sensors," *Ultrasonics
        Symposium, 2006.IEEE*, pp. 898-901, 2006.

[47]   Nirschl, M., Rantala, A., Tukkiniemi, K., Auer, S., Hellgren, A. C., Pitzer, D.,
        Schreiter, M., and Vikholm-Lundin, I., "CMOS-Integrated Film Bulk Acoustic
        Resonators for Label-Free Biosensing," *Sensors*, vol. 10, no. 5, pp. 4180-4193,
        May2010.

[48]   Rey-Mermet, S., Lanz, R., and Muralt, P., "Bulk acoustic wave resonator
        operating at 8áGHz for gravimetric sensing of organic films," *Sensors and
        Actuators B: Chemical*, vol. 114, no. 2, pp. 681-686, Apr.2006.

[49]   Rey-Mermet, S., Lanz, R., and Muralt, P., "Bulk acoustic wave resonator
        operating at 8GHz for gravimetric sensing of organic films," *Sensors and
        Actuators B: Chemical*, vol. 114, no. 2, pp. 681-686, Apr.2006.

[50]   Josse, F. and Lee, D. L., "Analysis of the Excitation, Interaction, and Detection
        of Bulk and Surface Acoustic Waves on Piezoelectric Substrates," *Sonics and
        Ultrasonics, IEEE Transactions on*, vol. 29, no. 5, pp. 261-273, 1982.

[51]   Josse, F., Bender, F., and Cernosek, R. W., "Guided shear horizontal surface
        acoustic wave sensors for chemical and biochemical detection in liquids,"
        Analytical Chemistry, vol. 73, no. 24, pp. 5937-5944, Dec.2001.

[52]   Lee, D. L., "Analysis of Energy Trapping Effects for SH-Type Waves on
        Rotated Y-Cut Quartz," *IEEE Trans.on Sonics and Ultrasonics*, vol. 28, no. 5,
        pp. 330-341, 1981.

[53]   Mensah-Brown, A. K., Wenzel, M. J., Josse, F. J., and Yaz, E. E., "Near Real-
        Time Monitoring of Organophosphate Pesticides in the Aqueous-Phase Using
        SH-SAW Sensors Including Estimation-Based Signal Analysis," *Sensors
        Journal, IEEE*, vol. 9, no. 12, pp. 1817-1824, 2009.

[54]   Mensah-Brown, A. K., Mlambo, D., Josse, F., and Hossenlopp, J., "Rapid
        Detection of Organophosphates in Aqueous Solution Using a Hybrid

Organic/Inorganic Coating on SH-SAW Devices," *2010 IEEE International Frequency Control Symposium*, pp. 232-237, 2010.

[55] Ricco, A. J., Martin, S. J., and Zipperian, T. E., "Surface acoustic wave gas sensor based on film conductivity changes," *Sensors and Actuators*, vol. 8, no. 4, pp. 319-333, Dec.1985.

[56] Grate, J. W., Snow, A., Ballantine, D. S., Wohltjen, H., Abraham, M. H., McGill, R. A., and Sasson, P., "Determination of partition coefficients from surface acoustic wave vapor sensor responses and correlation with gas-liquid chromatographic partition coefficients," *Analytical Chemistry*, vol. 60, no. 9, pp. 869-875, May1988.

[57] Zimmermann, C., Rebiere, D., Dejous, C., Pistre, J., Chastaing, E., and Planade, R., "A love-wave gas sensor coated with functionalized polysiloxane for sensing organophosphorus compounds," *Sensors and Actuators B: Chemical*, vol. 76, no. 1-3, pp. 86-94, June2001.

[58] Bryant, A., Poirier, M., Riley, G., Lee, D. L., and Vetelino, J. F., "Gas detection using surface acoustic wave delay lines," *Sensors and Actuators*, vol. 4 pp. 105-111, 1983.

[59] D'Amico, A., Palma, A., and Verona, E., "Surface acoustic wave hydrogen sensor," *Sensors and Actuators*, vol. 3 pp. 31-39, 1982.

[60] Pinkham, W., Wark, M., Winters, S., French, L., Frankel, D. J., and Vetelino, J. F., "A lateral field excited acoustic wave pesticide sensor," *Ultrasonics Symposium, 2005 IEEE*, vol. 4 pp. 2279-2283, 2005.

[61] Zadaka, D., Nir, S., Radian, A., and Mishael, Y. G., "Atrazine removal from water by polycation-clay composites: Effect of dissolved organic matter and comparison to activated carbon," *Water Research*, vol. 43, no. 3, pp. 677-683, Feb.2009.

[62] Alizadeh, T., Ganjali, M. R., Nourozi, P., and Zare, M., "Multivariate optimization of molecularly imprinted polymer solid-phase extraction applied to parathion determination in different water samples," *Analytica Chimica Acta*, vol. 638, no. 2, pp. 154-161, Apr.2009.

[63] Zaromb, S. and Stetter, J. R., "Theoretical basis for identification and measurement of air contaminants using an array of sensors having partly overlapping selectivities," *Sensors and Actuators*, vol. 6, no. 4, pp. 225-243, Dec.1984.

[64] Nevada Nanotech Systems, I. Comprehensive Threat Detection Modules: Chemical-Explosive-Biopathogen. Available from: http://www.nevadanano.com/wp-content/uploads/file/NNTS_Technology_032309.pdf . 8-2-2010. 8-2-2010.

Ref Type: Electronic Citation

[65]   Gardner, J. W., "Detection of vapours and odours from a multisensor array using pattern recognition Part 1. Principal component and cluster analysis," *Sensors and Actuators B: Chemical*, vol. 4, no. 1-2, pp. 109-115, May1991.

[66]   Carey, W. P., Beebe, K. R., Kowalski, B. R., Illman, D. L., and Hirschfeld, T., "Selection of adsorbates for chemical sensor arrays by pattern recognition," *Analytical Chemistry*, vol. 58, no. 1, pp. 149-153, Jan.1986.

[67]   Carey, W. P., Beebe, K. R., Sanchez, E., Geladi, P., and Kowalski, B. R., "Chemometric analysis of multisensor arrays," *Sensors and Actuators*, vol. 9, no. 3, pp. 223-234, May1986.

[68]   Hong, H. K., Shin, H. W., Yun, D. H., Kim, S. R., Kwon, C. H., Lee, K., and Moriizumi, T., "Electronic nose system with micro gas sensor array," *Sensors and Actuators B: Chemical*, vol. 36, no. 1-3, pp. 338-341, Oct.1996.

[69]   Grate, J. W., "Acoustic wave microsensor arrays for vapor sensing," *Chemical Reviews*, vol. 100, no. 7, pp. 2627-2647, July2000.

[70]   Grate, J. W., Patrash, S. J., and Abraham, M. H., "Method for Estimating Polymer-Coated Acoustic-Wave Vapor Sensor Responses," *Analytical Chemistry*, vol. 67, no. 13, pp. 2162-2169, July1995.

[71]   Abraham, M. H., Hamerton, I., Rose, J. B., and Grate, J. W., "Hydrogen-Bonding. Part 18. Gas-Liquid-Chromatographic Measurements for the Design and Selection of Some Hydrogen-Bond Acidic Phases Suitable for Use As Coatings on Piezoelectric Sorption Detectors," *Journal of the Chemical Society-Perkin Transactions 2*, no. 9, pp. 1417-1423, Sept.1991.

[72]   Abraham, M. H., Andonianhaftvan, J., Whiting, G. S., Leo, A., and Taft, R. S., "Hydrogen-Bonding. Part 34. the Factors That Influence the Solubility of Gases and Vapors in Water at 298-K, and A New Method for Its Determination," *Journal of the Chemical Society-Perkin Transactions 2*, no. 8, pp. 1777-1791, Aug.1994.

[73]   Abraham, M. H., Andonianhaftvan, J., Du, C. M., Diart, V., Whiting, G. S., Grate, J. W., and Mcgill, R. A., "Hydrogen-Bonding. Part 29. Characterization of 14 Sorbent Coatings for Chemical Microsensors Using A New Solvation Equation," *Journal of the Chemical Society-Perkin Transactions 2*, no. 2, pp. 369-378, Feb.1995.

[74]   Grate, J. W. and Nelson, D. A., "Sorptive polymeric materials and photopatterned films for gas phase chemical microsensors," *Proceedings of the Ieee*, vol. 91, no. 6, pp. 881-889, June2003.

[75] Grate, J. W., "Hydrogen-bond acidic polymers for chemical vapor sensing," *Chemical Reviews*, vol. 108, no. 2, pp. 726-745, Feb.2008.

[76] Mcgill, R. A., Abraham, M. H., and Grate, J. W., "Choosing Polymer-Coatings for Chemical Sensors," *Chemtech*, vol. 24, no. 9, pp. 27-37, Sept.1994.

[77] Zimmermann, C., Mazein, P., Rebiere, D., Dejous, C., Pistre, J., and Planade, R., "Detection of GB and DMMP vapors by love wave acoustic sensors using strong acidic fluoride polymers," *Ieee Sensors Journal*, vol. 4, no. 4, pp. 479-488, Aug.2004.

[78] Wenzel, M. J., "Polymer-Coated and Polymer-Base Microcantilever Chemical Sensors: Analysis and Sensor Signal Processing." Dissertation (Ph.D.) -- Marquette University, 2009.

[79] Mensah-Brown, A., Wenzel, M. J., Josse, F., Yaz, E., and Sadik, O., "Liquid-Phase Detection of Organophosphate Pesticides Using Guided SH-SAW Sensor," *Sensors, 2007 IEEE*, pp. 1420-1423, Oct.2007.

[80] Muezzinoglu, M. K., Vergara, A., Huerta, R., Rulkov, N., Rabinovich, M. I., Selverston, A., and Abarbanel, H. D. I., "Acceleration of chemo-sensory information processing using transient features," *Sensors and Actuators B: Chemical*, vol. 137, no. 2, pp. 507-512, Apr.2009.

[81] Bender, F., Cernosek, R. W., and Josse, F., "Love-wave biosensors using cross-linked polymer waveguides on LiTaO$_{3\ substrates}$," *Electronics Letters*, vol. 36, no. 19, pp. 1672-1673, Sept.2000.

[82] Gizeli, E., "Study of the sensitivity of the acoustic waveguide sensor," *Analytical Chemistry*, vol. 72, no. 24, pp. 5967-5972, Dec.2000.

[83] Zhou, Tingting, "Theoretical Modeling of Acoustic Waves in Layered Structure Chemical Sensors and Biosensors." Thesis (M.S.) -- Marquette University, 1992.

[84] Matthews, H., *Surface Wave Filters: Design, Construction, and Use* John Wiley & Sons, 1977, pp. 7.

[85] White, R. M., "Surface elastic waves," *Proc.of the IEEE*, vol. 58, no. 8, pp. 1238-1276, 1970.

[86] Li, Z. H, "Guided Shear-Horizontal Surface Acoustic Wave (SH-SAW) Chemical Sensors for Detection of Organic Contaminants in Aqueous Environments." Dissertation (Ph.D.) -- Marquette University, 2005.

[87] Auld, B. A., *Acoustic Fields and Waves in Solids*, 2nd ed. Malabar, FL: Krieger, 1990.

[88] Adler, E. L., "Matrix-Methods Applied to Acoustic-Waves in Multilayers," *IEEE Trans.on Ultrasonics Ferroelectrics and Frequency Control*, vol. 37, no. 6, pp. 485-490, Nov.1990.

[89] Mensah-Brown, A. K., "Detection of organophosphates in the liquid-phase using guided SH-SAW sensors." Thesis (M.S.) -- Marquette University, 2007.

[90] Martin, S. J., Frye, G. C., and Senturia, S. D., "Dynamics and Response of Polymer-Coated Surface Acoustic Wave Devices: Effect of Viscoelastic Properties and Film Resonance," *Analytical Chemistry*, vol. 66, no. 14, pp. 2201-2219, May2002.

[91] Ferry, J. D., *Viscoelastic Properties of Polymers*, 3rd ed. New York: John Wiley & Sons, 1980.

[92] Ricco, A. J., Staton, A. W., Crooks, R. M., and Kim, T., "Single-monolayer insitu modulus measurements using a SAW device Photocrosslinking of a diacetylenic thiol-based monolayer," *Faraday Discuss.*, vol. 107 pp. 247-258, 1997.

[93] Martin, S. J. and Frye, G. C., "Surface Acoustic-Wave Response to Changes in Viscoelastic Film Properties," *Applied Physics Letters*, vol. 57, no. 18, pp. 1867-1869, Oct.1990.

[94] Flugge, W., *Viscoelasticity*, 2nd ed. New York: Springer-Verlag, 1975, pp. 23.

[95] Nielsen, T. B. and Hansen, C. M., "Significance of surface resistance in absorption by polymers," *Industrial & Engineering Chemistry Research*, vol. 44, no. 11, pp. 3959-3965, May2005.

[96] Crank, J., *The Mathematics of Diffusion*, 2nd Edition ed. Clarendon: Oxford University Press, 1979.

[97] Topart, P. and Josowicz, M., "Transient Effects in the Interaction Between Polypyrrole and Methanol Vapor," *Journal of Physical Chemistry*, vol. 96, no. 21, pp. 8662-8666, Oct.1992.

[98] Grate, J. W. and Zellers, E. T., "The fractional free volume of the sorbed vapor in modeling the viscoelastic contribution to polymer-coated surface acoustic wave vapor sensor responses," *Analytical Chemistry*, vol. 72, no. 13, pp. 2861-2868, July2000.

[99] Kondoh, J., Shiokawa, S., Rapp, M., and Stier, S., "Simulation of viscoelastic effects of polymer coatings on surface acoustic wave gas sensor under consideration of film thickness," *Japanese Journal of Applied Physics Part 1-Regular Papers Short Notes & Review Papers*, vol. 37, no. 5B, pp. 2842-2848, May1998.

[100]   Grate, J. W., Klusty, M., Mcgill, R. A., Abraham, M. H., Whiting, G., and Andonianhaftvan, J., "The Predominant Role of Swelling-Induced Modulus Changes of the Sorbent Phase in Determining the Responses of Polymer-Coated Surface Acoustic-Wave Vapor Sensors," *Analytical Chemistry*, vol. 64, no. 6, pp. 610-624, Mar.1992.

[101]   Ahuja, A., James, D. L., and Narayan, R., "Dynamic behavior of ultra-thin polymer films deposited on surface acoustical wave devices," *Sensors and Actuators A: Physical*, vol. 72, no. 3, pp. 234-241, Feb.1999.

[102]   Bartley, D. L. and Dominguez, D. D., "Elastic effects of polymer coatings on surface acoustic waves," *Analytical Chemistry*, vol. 62, no. 15, pp. 1649-1656, Aug.1990.

[103]   Ruzicka, J. H., Thomson, J., and Wheals, B. B., "The gas chromatographic determination of organophosphorus pesticides," *Journal of Chromatography*, vol. 31 pp. 37-47, 1967.

[104]   Gass, T. E., "Geothermal Heat Pumps," *Geothermal Resouce Council Bullentin*, vol. 11, no. 11, pp. 3-8, 1982.

[105]   Cowart, R. P., Bonner, F. L., and Epps, E. A., "Rate of hydrolysis of seven organophosphate pesticides," *Bulletin of Environmental Contamination and Toxicology*, vol. 6, no. 3, pp. 231-234, May1971.

[106]   Menon, A., Zhou, R. N., and Josse, F., "Coated-quartz crystal resonator (QCR) sensors for on-line detection of organic contaminants in water," *IEEE Trans.on Ultrasonics, Ferroelectrics, and Frequency Control*, vol. 45, no. 5, pp. 1416-1426, Sept.1998.

[107]   Grate, J. W., Kaganove, S. N., Patrash, S. J., Craig, R., and Bliss, M., "Hybrid Organic/Inorganic Copolymers with Strongly Hydrogen-Bond Acidic Properties for Acoustic Wave and Optical Sensors," *Chemistry of Materials*, vol. 9, no. 5, pp. 1201-1207, May1997.

[108]   Grate, J. W. and Nelson, D. A. Polymers for Chemical Sensors Using Hydrosilylation Chemistry. Available from: http://www.pnl.gov/main/publications/external/technical_reports/PNNL-13556.pdf . 2001. 8-2-2008.
        Ref Type: Electronic Citation

[109]   Grate, J. W. and Abraham, M. H., "Solubility interactions and the design of chemically selective sorbent coatings for chemical sensors and arrays," *Sensors and Actuators B: Chemical*, vol. 3, no. 2, pp. 85-111, Feb.1991.

[110]   Mensah-Brown, A., Josse, F., Wenzel, M. J., Yaz, E., and Schneider, S., "Rapid detection of organophosphate pesticides in aqueous environment using a

polysiloxane coated SH-SAW device," *Sensors, 2008 IEEE*, pp. 1540-1543, 2008.

[111] Lide, D. R., *CRC Handbook of Chemistry and Physics*, 90 ed. CRC Press, 2010, pp. 8-110-8-113.

[112] Fest, C. and Schmidt, K. J., *The chemistry of organophosphorus pesticides* New York: Springer-Verlag, 1973.

[113] Ku, Y. and Chang, J. L., "Effect of Solution pH on the Hydrolysis and Photolysis of Diazinon in Aqueous Solution," *Water, Air, and Soil Pollution*, vol. 108 pp. 445-456, 1998.

[114] Fisher, S. R. Ground water quality in Kentucky: pH. Available from: http://kgs.uky.edu/kgsweb/olops/pub/kgs/ic06_12.pdf . 6-9-2010. 6-9-2010. Ref Type: Electronic Citation

[115] Zhonghui, L., Jones, Y., Hossenlopp, J., Cernosek, R., and Josse, F., "Chemical liquid-phase detection using guided SH-SAW: theoretical simulation and experiments," *2003 IEEE International Frequency Control Symposium and PDA Exhibition Jointly with the 17th European Frequency and Time Forum*, pp. 918-926, 2003.

[116] Brewer Science. Spin Coating Theory. Available from: http://www.brewerscience.com/products/cee-benchtop-products/cee-technical-information/spin-coater-theory/#scpt1 . 2010. 8-11-2010. Ref Type: Electronic Citation

[117] Wenzel, M. J., Mensah-Brown, A. K., Josse, F., and Yaz, E. E., "Online Drift Compensation for Chemical Sensors Using Estimation Theory," *Sensors Journal, IEEE*, vol. DOI: 10.1109/JSEN.2010.2055236 2010.

[118] Li, Z. H., Jones, Y., Hossenlopp, J., Cernosek, R., and Josse, F., "Analysis of liquid-phase chemical detection using guided shear horizontal-surface acoustic wave sensors," *Analytical Chemistry*, vol. 77, no. 14, pp. 4595-4603, July2005.

[119] Martin, S. J. and Frye, G. C., "Polymer film characterization using quartz resonators," *1991 IEEE Ultrasonics Symposium*, pp. 393-398, 1991.

[120] Urbanczyk, A., Staniewski, J., and Szymanowski, J., "Abraham model in gas chromatography of phenol pollutants," *Analytica Chimica Acta*, vol. 466, no. 1, pp. 151-159, 2002.

[121] Hierlemann, A., Ricco, A. J., Bodenhofer, K., and Gopel, W., "Effective Use of Molecular Recognition in Gas Sensing: Results from Acoustic Wave and in Situ FT-IR Measurements," *Analytical Chemistry*, vol. 71, no. 15, pp. 3022-3035, June1999.

[122] Hansen, C. M., "The significance of the surface condition in solutions to the diffusion equation: explaining "anomalous" sigmoidal, Case II, and Super Case II absorption behavior," *European Polymer Journal*, vol. 46, no. 4, pp. 651-662, Apr.2010.

[123] Wenzel, M. J., Josse, F., Yaz, E., Heinrich, S. M., and Datskos, P. G., "Rapid Detection of Analytes with Improved Selectivity Using Coated Microcantilever Chemical Sensors and Estimation Theory," *Sensors, 2007 IEEE*, pp. 91-94, 2007.

[124] Albert, K. J., Lewis, N. S., Schauer, C. L., Sotzing, G. A., Stitzel, S. E., Vaid, T. P., and Walt, D. R., "Cross-Reactive Chemical Sensor Arrays," *Chemical Reviews*, vol. 100, no. 7, pp. 2595-2626, June2000.

[125] Di Nucci, C., Fort, A., Rocchi, S., Tondi, L., Vignoli, V., Di Francesco, F., and Santos, M. B. S., "A measurement system for odor classification based on the dynamic response of QCM sensors," *Instrumentation and Measurement, IEEE Transactions on*, vol. 52, no. 4, pp. 1079-1086, 2003.

[126] Maybeck, P. S., *Stochastic Models, Estimation, and Controls* New York: Academic Press, 1979.

[127] Ljung, L., "Asymptotic behavior of the extended Kalman filter as a parameter estimator for linear systems," *Automatic Control, IEEE Transactions on*, vol. 24, no. 1, pp. 36-50, 1979.

[128] Reif, K., Gunther, S., Yaz, E., and Unbehauen, R., "Stochastic stability of the discrete-time extended Kalman filter," *Automatic Control, IEEE Transactions on*, vol. 44, no. 4, pp. 714-728, 1999.

APPENDIX A: DSC TRACE FOR BPA-HMTS

The glass transition temperature, T_g, for BPA-HMTS is reported as the inflection point in the DSC trace. The sample (1 mg) was heated at a rate of 5 °C/min in the temperature range -80 °C to 120 °C.